NASA CONTRACTOR REPORT

NASA CR-2368

NASA CR-2368

NUMERICAL CALCULATIONS OF VELOCITY AND PRESSURE DISTRIBUTION AROUND OSCILLATING AIRFOILS

by Theodore Bratanow, Akin Ecer, and Michael Kobiske

Prepared by
UNIVERSITY OF WISCONSIN-MILWAUKEE
Milwaukee, Wis.
for Langley Research Center

NATIONAL AERONAUTICS AND SPACE ADMINISTRATION • WASHINGTON, D. C. • FEBRUARY 1974

1. Report No.	2. Government Accession No.	3. Recipient's Catalog No.
NASA CR-2368		

4. Title and Subtitle	5. Report Date
NUMERICAL CALCULATIONS OF VELOCITY AND PRESSURE DISTRIBUTION AROUND OSCILLATING AIRFOILS	FEBRUARY 1974
	6. Performing Organization Code

7. Author(s)	8. Performing Organization Report No.
THEODORE BRATANOW, AKIN ECER, AND MICHAEL KOBISKE	
	10. Work Unit No.

9. Performing Organization Name and Address	11. Contract or Grant No.
UNIVERSITY OF WISCONSIN - MILWAUKEE MILWAUKEE, WI	NGR 50-007-001
	13. Type of Report and Period Covered
12. Sponsoring Agency Name and Address	CONTRACTOR REPORT
NATIONAL AERONAUTICS AND SPACE ADMINISTRATION WASHINGTON, D.C. 20546	14. Sponsoring Agency Code

15. Supplementary Notes

TOPICAL REPORT

16. Abstract

AN ANALYTICAL PROCEDURE BASED ON THE NAVIER-STOKES EQUATIONS WAS DEVELOPED FOR ANALYZING AND REPRESENTING PROPERTIES OF UNSTEADY VISCOUS FLOW AROUND OSCILLATING OBSTACLES. A VARIATIONAL FORMULATION OF THE VORTICITY TRANSPORT EQUATION WAS DISCRETIZED IN FINITE ELEMENT FORM AND INTEGRATED NUMERICALLY. AT EACH TIME STEP OF THE NUMERICAL INTEGRATION, THE VELOCITY FIELD AROUND THE OBSTACLE WAS DETERMINED FOR THE INSTANTANEOUS VORTICITY DISTRIBUTION FROM THE FINITE ELEMENT SOLUTION OF POISSON'S EQUATION. THE TIME-DEPENDENT BOUNDARY CONDITIONS AROUND THE OSCILLATING OBSTACLE WERE INTRODUCED AS EXTERNAL CONSTRAINTS, USING THE LAGRANGIAN MULTIPLIER TECHNIQUE, AT EACH TIME STEP OF THE NUMERICAL INTEGRATION. THE PROCEDURE WAS THEN APPLIED FOR DETERMINING PRESSURES AROUND OBSTACLES OSCILLATING IN UNSTEADY FLOW. THE OBTAINED RESULTS FOR A CYLINDER AND AN AIRFOIL WERE ILLUSTRATED IN THE FORM OF STREAMLINES AND VORTICITY AND PRESSURE DISTRIBUTIONS.

17. Key Words (Suggested by Author(s))	18. Distribution Statement
FINITE ELEMENT ANALYSIS NAVIER-STOKES EQUATIONS UNSTEADY FLOW	UNCLASSIFIED - UNLIMITED Cat. 01

19. Security Classif. (of this report)	20. Security Classif. (of this page)	21. No. of Pages	22. Price*
UNCLASSIFIED	UNCLASSIFIED	84	$3.75

*For sale by the National Technical Information Service, Springfield, Virginia 22151

CONTENTS

ILLUSTRATIONS

NUMERICAL CALCULATIONS OF VELOCITY AND PRESSURE DISTRIBUTION AROUND OSCILLATING AIRFOILS

Theodore Bratanow,* Akin Ecer,**
and Michael Kobiske†
University of Wisconsin-Milwaukee

SUMMARY

An analytical procedure based on the Navier-Stokes equations was developed for analyzing and representing properties of unsteady viscous flow around oscillating obstacles. A variational formulation of the vorticity transport equation was discretized in finite element form and integrated numerically. At each time step of the numerical integration, the velocity field around the obstacle was determined for the instantaneous vorticity distribution from the finite element solution of Poisson's equation. The time-dependent boundary conditions around the oscillating obstacle were introduced as external constraints, using the Lagrangian Multiplier Technique, at each time step of the numerical integration. The procedure was then applied for determining pressures around obstacles oscillating in unsteady flow. The obtained results for a cylinder and an airfoil were illustrated in the form of streamlines and vorticity and pressure distributions.

INTRODUCTION

The objectives of the investigation were to develop a method for analysis of general, unsteady, viscous and incompressible flow around an oscillating obstacle of arbitrary shape and to determine the velocity and pressure distribution around this obstacle. Using the finite element method, a numerical procedure was developed and tested by investigating first the unsteady flow past a stationary circular cylinder. This method was then applied to analyze the flow around stationary and pitching airfoils. The velocity and pressure distributions around these obstacles were determined. The method of analysis considers the viscous effects of the boundary layer and the overall flow characteristics in a unified mathematical frame.

Unsteady flow around a circular cylinder has been analyzed by several investigators [1,2,3,4,5]. In most cases, however, the numerical procedure was developed specifically to suit the geometry of a stationary obstacle. The problem of moving obstacles was analyzed only for a circular cylinder oscillating around its longitudinal axis [4], where the instantaneous geometry of the obstacle remains the same. A review of existing studies of unsteady,

---

* Professor, ** Assistant Professor, † Research Assistant, Department of Mechanics, College of Engineering and Applied Science.

viscous flow showed discrepancies in the results between analyses and experiments. In the case of a circular cylinder, the experimental results for the surface pressure distribution do not agree with theoretical results [3, 6,7]. Similar discrepancies are observed for the drag coefficients and the points of separation.

SYMBOLS

A area of a finite element, in.^{2} (m^2)

$\underline{A}$ rectangular matrix defined in Eq. (B1)

$\overline{A}$ general differential operator

$\underline{b}$ rectangular matrix representing the boundary conditions on the obstacle

$\underline{b}^*$ rectangular matrix containing matrix $\underline{b}$, $\underline{b}^* = (\underline{b}\ \underline{0})$

$\underline{B}$ row vector defining the variation of vorticity, pressure and velocities over an element

$\underline{c}$ rectangular matrix defining the free stream boundary conditions

$\underline{C}$ row vector defining the variation of stream functions over an element

$\underline{d}$ column vector specifying the stream function values on the free stream boundary

$\underline{e}$ column vector specifying the vorticity on the obstacle's boundary

f $f(x,y)$ - arbitrary function constrained by boundary conditions

F $F(x,y,\lambda_i)$ - arbitrary function with Lagrange multipliers as defined in Eq. (27)

$\underline{F}$ inverse of matrix $\underline{S}^*$

$\underline{h}$ column vector defined in Eqs. (49), (57), and (65)

$\underline{h}^*$ column vector containing vector $\underline{h}$, $\underline{h}^* = (\underline{h}\ \underline{d})$

$\underline{I}$ identity matrix

$\underline{J}$ rectangular matrix defined in Eq. (B6)

k constant members in Eqs. (B5) and (B9)

$\underline{K}$ row vectors representing the stream function's partial derivatives with respect to the area coordinates

$\underline{M}$ $\underline{M}(u,v,\omega)$ - nonlinear term in the vorticity transport equation, $M = u \frac{\partial}{\partial x} + v \frac{\partial}{\partial y}$

$\underline{0}$ null matrix

p local static pressure, lbf/in.^{2} (N/m^2)

$\underline{p}$ column vector representing the pressure values at the nodal points of an element, lbf/in.^{2} (N/m^2)

$\overline{\underline{p}}$ column vector representing the pressure values at the nodes of the entire grid, lbf/in.^{2} (N/m^2)

$\overline{\underline{p}}^*$ column vector containing vector $\overline{\underline{p}}$ and the Lagrange multipliers, $\overline{\underline{p}}^* = (\overline{\underline{p}}\ \underline{\delta}_{cp})$

$\underline{P}$ symmetric matrix defined in Eq. (65)

$\underline{P}^*$ symmetric matrix containing matrix $\underline{P}$ and the free stream boundary conditions

$\underline{q}$ column vector resulting from the multiplication of column $\underline{h}^*$ by a symmetric inverse

Q $Q(x,y)$, $Q = 2\left[\frac{\partial u}{\partial y}\frac{\partial v}{\partial x} - \frac{\partial u}{\partial x}\frac{\partial v}{\partial y}\right]$

$\underline{Q}$ column vector in Eq. (40)

$\underline{r}$ rectangular matrix resulting from the multiplication of matrix $\underline{b}^*$ by a symmetric inverse

$\underline{S}$ symmetric matrix defined by Eq. (49)

$\underline{S}^*$ symmetric matrix containing matrix $\underline{S}$ and the free stream boundary conditions

t time, sec.

$\underline{T}$ square transformation matrix defined in Eq. (B7)

u,v,w velocity components, in./sec. (m/sec.)

$\underline{u},\underline{v}$ velocity vectors, in./sec. (m/sec.)

V volume of a fluid element, in.^{3} (m^3)

$\underline{W}$ symmetric matrix defined by Eq. (57)

$\underline{W}^*$ symmetric matrix containing matrix $\underline{W}$ and the free stream boundary conditions

x,y,z coordinate directions

X,Y body forces in the x and y directions respectively, lbf (N)

$\underline{\nabla}$ del operator, $\underline{\nabla} = \underline{i}\frac{\partial}{\partial x} + \underline{j}\frac{\partial}{\partial y}$

∇^2 Laplace operator, $\nabla^2 = \frac{\partial^2}{\partial x^2} + \frac{\partial^2}{\partial y^2}$

ξ,η tangential and radial coordinate directions respectively

$\underline{\delta}$ column vector representing the Lagrange multiplier

$\underline{Y}$ column vector representing the second derivatives of the stream function at the nodal points of an element

Γ length of the perimeter of area A, in. (m)

λ Lagrange multiplier

ν kinematic viscosity coefficient, $in.^2/sec.$ ($m^2/sec.$)

ρ density of the fluid, $lbm/in.^3$ (kg/m^3)

ϕ constant members of the matrix in Eq. (B6)

$\underline{\phi}$ $\underline{\phi}(x,y)$ - boundary conditions of an arbitrary function

Φ general quadratic functional for variational formulations

ψ $\psi(x,y)$ - stream function defined in Eq. (6), $in.^2/sec.$ ($m^2/sec.$)

$\underline{\psi}$ column vector representing stream function and velocity values at the nodal points of an element

$\overline{\underline{\psi}}$ column vector representing the stream function and velocity values at the nodes of the entire grid

$\overline{\underline{\psi}}^*$ column vector containing vector $\overline{\underline{\psi}}$ and the Lagrange multipliers, $\overline{\underline{\psi}}^* = (\overline{\underline{\psi}}\ \underline{\delta}_{cs})$

θ angle between the horizontal line and the line normal to the surface of the obstacle

ω vorticity at a point, sec.$^{-1}$

$\underline{\omega}$ vorticity vector, sec.$^{-1}$

$\dot{\underline{\omega}}$ column vector representing the time derivative of vorticity at the nodes of the entire grid, sec.$^{-2}$

$\dot{\underline{\omega}}^*$ column vector containing vector $\dot{\underline{\omega}}$ and the Lagrange multipliers, $\dot{\underline{\omega}}^* = (\dot{\underline{\omega}}\ \underline{\delta}_{cw})$

ζ area coordinate, in. (m)

Subscripts

b obstacle

c free stream

i i-th boundary condition

m m-th node

n n-th node

o at time t_o

p pressure

s stream function

v total volume

w vorticity

x,y derivative with respect to x or y respectively

ξ tangential direction

η normal direction

Superscripts

m,n,p variable powers

t transpose

MATHEMATICAL ANALYSIS

The mathematical analysis of the two-dimensional unsteady viscous flow around an obstacle of arbitrary shape will be described. The variational formulation of the problem is based on the most general form of the Navier-Stokes equations. The finite element method was applied for the discrete representation of the governing equations. The equations from which velocity and pressure distributions were calculated, were derived using the principle of conservation of mass and the balance of momentum in terms of stream functions and vorticities. The boundary conditions applied for the solution of these equations will also be described.

Equations of Motion

The governing differential equations of motion for the analysis of two-dimensional unsteady flow of incompressible viscous fluids can be written as follows [8]:

$$\frac{\partial u}{\partial t} + u\frac{\partial u}{\partial x} + v\frac{\partial u}{\partial y} = \frac{1}{\rho}X - \frac{1}{\rho}\frac{\partial p}{\partial x} + \nu\left[\frac{\partial^2 u}{\partial x^2} + \frac{\partial^2 u}{\partial y^2}\right] \tag{1}$$

$$\frac{\partial v}{\partial t} + u\frac{\partial v}{\partial x} + v\frac{\partial v}{\partial y} = \frac{1}{\rho}Y - \frac{1}{\rho}\frac{\partial p}{\partial y} + \nu\left[\frac{\partial^2 v}{\partial x^2} + \frac{\partial^2 v}{\partial y^2}\right] \tag{2}$$

$$\frac{\partial u}{\partial x} + \frac{\partial v}{\partial y} = 0 \tag{3}$$

Eqs. (1) and (2) are the Navier-Stokes equations and Eq. (3) is the continuity condition for incompressible fluids.

Stream function and vorticity formulation - The vorticity and pressure distributions can be obtained from a simultaneous solution of Eqs. (1), (2) and (3). Although a direct solution of these equations is possible, the equation of continuity can be included in the formulation in a more natural manner using the concept of stream functions and vorticities. The stream functions can be defined in such a way that they satisfy the equation of continuity. The system of Eqs. (1), (2) and (3) can then be reduced to two equations in terms of vorticities and stream functions. The vorticity is defined as [8]:

$$\underline{\omega} = \underline{\nabla} \times \underline{u} \tag{4}$$

In the case of two-dimensional flow only one component of the vorticity exists and it is perpendicular to the plane of the flow:

$$\omega = \frac{\partial v}{\partial x} - \frac{\partial u}{\partial y} \tag{5}$$

The stream functions are defined for the two-dimensional case as follows:

$$u = \frac{\partial \psi}{\partial y} \qquad v = -\frac{\partial \psi}{\partial x} \tag{6}$$

Substituting Eq. (6) into Eq. (3), the continuity equation is automatically satisfied. From Eq. (5) the vorticity can be written in terms of the stream functions as follows:

$$\omega = -\nabla^2 \psi \tag{7}$$

Vorticity transport equation - Vorticity is a measure of the angular momentum of the fluid particles in motion. Eqs. (1), (2) and (3) can be combined and using Eqs. (4), (5) and (6), the vorticity transport equation or the Helmholtz equation is obtained as follows [8]:

$$\frac{\partial \omega}{\partial t} + u \frac{\partial \omega}{\partial x} + v \frac{\partial \omega}{\partial y} = \nu \left[\frac{\partial^2 \omega}{\partial x^2} + \frac{\partial^2 \omega}{\partial y^2} \right] \tag{8}$$

According to this equation, the time derivative of the vorticity in space, which consists of local and convective terms, is equal to the rate of dissipation of the viscous terms.

Using Eq. (7), Eq. (8) can be converted into another equation with a single variable in terms of the stream functions as follows:

$$\frac{\partial \nabla^2 \psi}{\partial t} + \frac{\partial \psi}{\partial y} \frac{\partial \nabla^2 \psi}{\partial x} - \frac{\partial \psi}{\partial x} \frac{\partial \nabla^2 \psi}{\partial y} = \nu \nabla^4 \psi \tag{9}$$

The left-hand side of the equation again contains local and convective inertia terms, while the right-hand side describes the viscous dissipation. When the fluid motion is slow, the viscous forces are considerably greater than the convective inertia terms. Neglecting the convective inertia terms, the equations of motion become linear with respect to velocity and describe the creeping motion of a viscous fluid.

At high Reynolds numbers the inertia forces are more important in comparison with the viscous forces. In this case, the viscous forces can not be neglected because, although they are small in magnitude, they change the basic characteristics of the equations. If the viscous terms are neglected, the complete set of boundary conditions is not necessary for a unique solution of the problem. This corresponds to the Euler's equation for an ideal

fluid. A unique solution of Euler's equation is obtained by using a boundary condition specifying zero normal velocity at the boundary. However, the condition for zero tangential velocity is not satisfied. Therefore, the boundary layer is still important at higher Reynolds numbers although the changes from the ideal fluid conditions occur only in a small region around the obstacle. In the conducted analysis, the Navier-Stokes equations were kept in the complete form for the cases of different Reynolds numbers and the boundary layer effects were considered.

Equation for pressures - The pressures can be calculated from another equation, which can be derived again from the Navier-Stokes equations. Using Eqs. (1), (2) and (3), the pressure distribution is expressed in terms of the velocity distribution as follows [9]:

$$\frac{\partial^2 p}{\partial x^2} + \frac{\partial^2 p}{\partial y^2} = - \rho Q \tag{10}$$

where

$$Q = 2 \left[\frac{\partial u}{\partial y} \frac{\partial v}{\partial x} - \frac{\partial u}{\partial x} \frac{\partial v}{\partial y} \right] \tag{11}$$

According to Eq. (10), the instantaneous pressure distribution can be determined for a particular velocity distribution. On the other hand, pressures are not required for the determination of the velocity distribution.

Boundary Conditions

The boundary conditions for stream functions, vorticities and pressures around the obstacle and the free stream boundary conditions can be described as follows:

Boundary conditions for stream functions - For the solution of Poisson's equation, Eq. (7), two types of boundary conditions were considered: Dirichlet type boundary conditions, specifying the stream functions, and Neumann type boundary conditions, specifying the normal slope of the stream functions. These two types of conditions can be summarized as follows [11]:

ψ = prescribed for free stream flow on the outer rectangular boundary

$\frac{\partial \psi}{\partial x}$ = zero on the outer rectangular boundary

$\frac{\partial \psi}{\partial y}$ = free stream velocity on the outer rectangular boundary

ψ = constant on the obstacle boundary

$\frac{\partial \psi}{\partial \xi}$ = zero on the obstacle boundary (see figure 4)

Boundary conditions for vorticity - The conditions for the free stream boundary can be defined according to Kelvin's theorem. A closed boundary in the free stream will have zero vorticity along the boundary line. On the other hand, the vorticity at the obstacle boundary can be defined in terms of the normal derivative of the tangential velocity only.

ω = zero on the outer rectangular boundary

$\omega = \frac{\partial u_\xi}{\partial \eta}$ on the obstacle boundary

Boundary conditions for pressures - The boundary conditions for pressures can be defined by specifying the static pressure at the free stream boundary and specifying the fluid pressure around the solid boundary.

p = zero on the outer rectangular boundary

$\frac{\partial p}{\partial \eta}$ = zero on the obstacle boundary

Variational Formulation of Navier-Stokes Equations

A variational method was applied for the solution of Eqs. (7), (8) and (10). The solution of the following partial differential equation

$$\bar{A}\,\psi = \omega \tag{12}$$

was sought, under a set of boundary conditions, where $\bar{A}$ represents the differential operator. The solution of Eq. (12) can be calculated by minimizing the quadratic functional

$$-2\,\Phi = \int_A \left(\psi\,\bar{A}\,\psi - 2\,\psi\,\omega\right) dA \tag{13}$$

with respect to solution functions that satisfy the boundary conditions.

Stream function equation - The variational formulation of the Poisson's equation is the well-known Dirichlet's problem [10]. As applied to the Poisson equation, Eq. (7), Eq. (13) becomes

$$2\,\Phi = \int_A \left(\psi\,\nabla^2\psi + 2\,\psi\,\omega\right) dA \tag{14}$$

The first term of the integral in Eq. (14) can be rewritten using Green's theorem as

$$\int_A \psi \nabla^2\psi \, dA = - \int_A \left[\left(\frac{\partial\psi}{\partial x}\right)^2 + \left(\frac{\partial\psi}{\partial y}\right)^2\right] dA + \int_\Gamma \psi \frac{\partial\psi}{\partial\eta} \, d\Gamma \qquad (15)$$

The last integral in Eq. (15) vanishes because of the applied boundary conditions. One of the boundary conditions for Eq. (7) states that the normal derivative $\partial\psi/\partial x$ is zero on the rectangular boundary. Thus, the value of the integral is identically zero on the vertical sides of the rectangle. On the upper and lower sides, the stream functions have constant magnitudes but alternating signs. Thus, their sum is equal to zero. After the application of Green's theorem, Eq. (7) can be written as

$$\Phi = \frac{1}{2} \int_A \left[\left(\frac{\partial\psi}{\partial x}\right)^2 + \left(\frac{\partial\psi}{\partial y}\right)^2\right] dA - \int_A \omega \psi \, dA \qquad (16)$$

The solution of Eq. (7) can now be obtained by minimizing the functional Φ in Eq. (16). The stream functions and the velocity distribution can be obtained from this formulation for a given set of vorticities.

Equation for pressures - The variational formulation of the equation for pressures, Eq. (10), is again a Dirichlet type of problem. A similar procedure is followed for the variational formulation of the Poisson's equation for pressures, Eq. (10). The contour integral in Eq. (15) vanishes again, since the pressure is identically zero on the outer boundary. The resulting variational functional is

$$\Phi = \frac{1}{2} \int_A \left[\left(\frac{\partial p}{\partial x}\right)^2 + \left(\frac{\partial p}{\partial y}\right)^2\right] dA - \rho \int_A Q \, p \, dA \qquad (17)$$

The parameter Q in Eq. (17) is defined for a particular distribution of the velocity.

Vorticity transport equation - For the finite element representation of the vorticity transport equation, Eq. (8), a variational formulation of this differential equation was developed. However, for this case, an exact variational formulation does not exist due to the nonlinear terms on the left-hand side of Eq. (8). The right-hand side is in the form of Poisson's equation and can be written in a variational form corresponding to Dirichlet's problem. The solution of the right-hand side of Eq. (8) can be obtained by minimizing a functional Φ_1, given as

$$\Phi_1 = \frac{\nu}{2} \int_A \left[\left(\frac{\partial \omega}{\partial x} \right)^2 + \left(\frac{\partial \omega}{\partial y} \right)^2 \right] dA \tag{18}$$

The local time derivative of the vorticity term in Eq. (8) can be formulated in variational form using Hamilton's principle. The discretized form of the vorticity transport equation can then be written in matrix form as

$$\frac{\partial \underline{\omega}}{\partial t} = \underline{M}\ \underline{\omega} \tag{19}$$

where the matrix $\underline{M}$ is a nonlinear function of velocity and vorticity distributions. The solution of Eq. (19) can be obtained by minimizing the functional Φ_2, given as

$$\Phi_2 = \int_A \left[\frac{d}{dt} \left(\underline{\omega}^t \underline{\omega} \right) - \underline{\omega}^t \underline{M}\ \underline{\omega} \right] dA \tag{20}$$

The matrix $\underline{M}$ in Eq. (19) can be derived from a perturbation analysis of the vorticity transport equation. From a Taylor series expansion of the velocities in terms of the vorticities, the velocity distribution at time t_o can be written as

$$\underline{u} = \underline{u}_o + \left(\frac{\partial \underline{u}}{\partial \underline{\omega}} \right)_o (\Delta \underline{\omega}) + \left(\frac{\partial^2 \underline{u}}{\partial \underline{\omega}^2} \right)_o \frac{(\Delta \underline{\omega})^2}{2!} + \ldots \tag{21}$$

Once the instantaneous derivatives of the velocities with respect to vorticities are determined, the matrix $\underline{M}$ can be calculated for any desired accuracy. From the equation of continuity and the definition of vorticity

$$\nabla \cdot \underline{u} = 0 \qquad \nabla \times \underline{u} = \underline{\omega} \tag{22}$$

the derivatives of velocities with respect to vorticities can be calculated as

$$\underline{\nabla} \cdot \frac{\partial \underline{u}}{\partial \underline{\omega}} = 0 \qquad \underline{\nabla} \times \frac{\partial \underline{u}}{\partial \underline{\omega}} = \underline{I} \tag{23}$$

The solutions of the systems of equations in Eq. (23) are similar to the solution of Eq. (7) except for a right-hand side consisting of unit vorticities at each nodal point of the finite element grid. Considering that the velocity distribution is not very sensitive to the incremental changes in the vorticity distribution, only the first terms in the Taylor series can be employed in the analysis. The variational formulation of the vorticity

transport equation can then be written as follows:

$$\Phi = \int_A \omega \frac{\partial \omega}{\partial t} \, dA + \frac{1}{2} \int_A u\omega \frac{\partial \omega}{\partial x} \, dA + \frac{1}{2} \int_A v\omega \frac{\partial \omega}{\partial y} \, dA$$

$$+ \frac{\nu}{2} \int_A \left[\left(\frac{\partial \omega}{\partial x} \right)^2 + \left(\frac{\partial \omega}{\partial y} \right)^2 \right] dA \qquad (24)$$

The local time derivatives of the vorticities can be calculated by minimizing Eq. (24).

Lagrange Multipliers

The variational formulation of the governing differential equations derived above does not include the boundary conditions. The time dependent boundary conditions can be introduced in a simple fashion which then becomes one of the main advantages of the variational method. The Lagrangian multiplier technique was used for this purpose. Accordingly, the boundary conditions are added to the variational formulation as additional constraint conditions. The method of solution will now be summarized.

Considering a variational functional of the form

$$f(x,y) \qquad (25)$$

where the boundary conditions are excluded and that

$$\underline{\phi}_i(x,y) = 0 \qquad (26)$$

is a set of boundary conditions, the solution of the differential equations satisfying the boundary conditions is sought through another functional

$$F(x,y,\lambda_i) = f(x,y) + \sum \lambda_i \underline{\phi}_i(x,y) \qquad (27)$$

where λ_i is the Lagrange multiplier. The solution can be obtained by minimizing $F(x,y,\lambda_i)$ with respect to x, y and λ_i, as

$$\frac{\partial F}{\partial x} = 0 \qquad \frac{\partial F}{\partial y} = 0 \qquad \frac{\partial F}{\partial \lambda_i} = 0 \qquad (28)$$

In the case of a quadratic functional, a system of linear algebraic equations are obtained. The application of the Lagrange multiplier technique

produces a constrained minimum of the functional, which satisfies the boundary conditions.

New boundary conditions can be included using the Lagrangian multiplier technique by defining only the additional constraint equations at each time step. In this problem the obstacle boundary conditions change at each step of the numerical integration, depending on the position and the motion of the obstacle. For a stationary obstacle, the Poisson's equation is solved only for changing terms on the right-hand side of Eq. (7). The boundary conditions at the free stream boundary do not change with time. The application of the Lagrangian multiplier technique reduces the computational cost of the solution considerably.

THE NUMERICAL SOLUTION OF THE GOVERNING EQUATIONS

When the variational formulation of the governing differential equations is completed, they can be discretized in finite element form. The resulting discrete systems consist of linear algebraic equations and a matrix differential equation. The details of the discretization and the application of the finite element method is summarized in this section. The solutions of the systems of equations are analyzed and the corresponding boundary conditions are discussed.

Discretization of the Equations of Motion

Following the basic discretization procedure of the finite element analysis, the obstacle and the surrounding continuum were represented by triangular finite elements. The finite element gridwork for the analysis of flow around a cylinder is shown in figure 1. In this case the objective of the particular triangulation was to represent most accurately, the boundary layer effects around the cylinder. However, in general, it is not necessary to describe the obstacle boundary with nodal points. For example, the gridwork in figure 2 was used for the analysis of the flow around a moving airfoil, where the position of the airfoil changed at each time step.

Stream function equation - The variation of the stream functions over a triangular element was approximated by a third-order polynomial, which can uniquely be determined from the values of the stream functions and velocities at the nodes of the triangles. The stream function at any point of the triangle can then be written as

$$\psi = \underline{C}\,\underline{A}\,\underline{\psi} \tag{29}$$

where $\underline{A}$ is a rectangular matrix describing the approximation functions as shown in Eq. (B1) of Appendix B. $\underline{C}$ is a row vector formed by the area coordinates of a point and $\underline{\psi}$ is another vector formed by the nodal velocities and the stream functions of the finite element:

$$\underline{C} = \begin{bmatrix} \zeta_1^3 & \zeta_2^3 & \zeta_3^3 & \zeta_1^2\zeta_2 & \zeta_1^2\zeta_3 & \zeta_2^2\zeta_3 & \zeta_2^2\zeta_1 & \zeta_3^2\zeta_1 & \zeta_3^2\zeta_2 & \zeta_1\zeta_2\zeta_3 \end{bmatrix} \quad (30)$$

$$\psi^t = \begin{bmatrix} \psi_1 & \frac{\partial\psi_1}{\partial x} & \frac{\partial\psi_1}{\partial y} & \psi_2 & \frac{\partial\psi_2}{\partial x} & \frac{\partial\psi_2}{\partial y} & \psi_3 & \frac{\partial\psi_3}{\partial x} & \frac{\partial\psi_3}{\partial y} \end{bmatrix} \quad (31)$$

The area coordinates ζ_i in Eq. (30) are described in detail in Appendix A [11].

Vorticities, on the other hand, were considered to vary linearly over a triangular element and can be defined as follows:

$$\omega = \begin{bmatrix} \zeta_1 & \zeta_2 & \zeta_3 \end{bmatrix} \begin{bmatrix} \omega_1 \\ \omega_2 \\ \omega_3 \end{bmatrix} = \underline{B}\,\underline{\omega} \quad (32)$$

Eqs. (29) and (32) can be substituted in Eq. (16) to obtain a discrete variational functional as follows:

$$\Phi = \frac{1}{2} \int_A \underline{\psi}^t \left[\underline{A}^t \underline{C}_x^t \underline{C}_x \underline{A} + \underline{A}^t \underline{C}_y^t \underline{C}_y \underline{A} \right] \underline{\psi}\, dA - \int_A \underline{\psi}^t \left[\underline{A}^t \underline{C}^t \underline{B} \right] \underline{\omega}\, dA \quad (33)$$

In this case the integration domain A indicates an integration over the area of the triangular element and a summation of the terms at each node from all neighboring elements.

The solution of Eq. (7) can be obtained by minimizing the variational functional in Eq. (33) with respect to ω_i. After setting the first derivative of Φ in Eq. (33) equal to zero, a system of linear algebraic equations is obtained as follows:

$$\int_A \left[\underline{A}^t \underline{C}_x^t \underline{C}_x \underline{A} + \underline{A}^t \underline{C}_y^t \underline{C}_y \underline{A} \right] dA\, \underline{\psi} = \int_A \left[\underline{A}^t \underline{C}^t \underline{B} \right] dA\, \underline{\omega} \quad (34)$$

where matrix $\underline{A}$ is constant for each triangle. Integrating and adding the $\underline{C}_x^t \underline{C}_x$ and $\underline{C}_y^t \underline{C}_y$ terms in Eq. (34), a square matrix is obtained for each of the triangular elements. The matrix $\underline{C}^t \underline{B}$ is also constant for each triangular element. Each of the matrices in Eq. (34) is given in Appendix B.

Vorticity transport equation - In the solution of the vorticity transport equation, the variation of velocities over each finite element was approximated linearly as

$$u = \begin{bmatrix} \zeta_1 & \zeta_2 & \zeta_3 \end{bmatrix} \begin{bmatrix} u_1 \\ u_2 \\ u_3 \end{bmatrix} = \underline{B}\,\underline{u} \tag{35}$$

$$v = \begin{bmatrix} \zeta_1 & \zeta_2 & \zeta_3 \end{bmatrix} \begin{bmatrix} v_1 \\ v_2 \\ v_3 \end{bmatrix} = \underline{B}\,\underline{v} \tag{36}$$

Substituting Eqs.(32), (35) and (36) into the variational form of the vorticity transport equation, Eq. (24), the following discrete functional was obtained:

$$\Phi = \int_A \underline{\omega}^t \underline{B}^t \underline{B}\, \frac{\partial \underline{\omega}}{\partial t}\, dA + \frac{1}{2} \int_A \left\{ \nu\, \underline{\omega}^t \left[\underline{B}_x^t \underline{B}_x + \underline{B}_y^t \underline{B}_y \right] \underline{\omega} + \underline{\omega}^t \underline{B}^t \underline{B}\, \underline{u}\, \underline{B}_x \underline{\omega} + \underline{\omega}^t \underline{B}^t \underline{B}\, \underline{v}\, \underline{B}_y\, \underline{\omega} \right\} dA \tag{37}$$

The functional Φ in Eq. (37) was then minimized by differentiating with respect to $\underline{\omega}$. The resulting system of ordinary differential equations with respect to time was written in matrix form as

$$\int_A \underline{B}^t \underline{B}\, dA\, \frac{\partial \underline{\omega}}{\partial t} = - \int_A \left\{ \nu \left[\underline{B}_x^t \underline{B}_x + \underline{B}_y^t \underline{B}_y \right] + \underline{B}^t \underline{B}\, \underline{u}\, \underline{B}_x + \underline{B}^t \underline{B}\, \underline{v}\, \underline{B}_y \right\} dA\, \underline{\omega} \tag{38}$$

The velocity distribution obtained from the solution of Eq. (34) together with the instantaneous vorticity distribution is used to calculate the time derivative of the vorticity distribution. The coefficient matrix of the left-hand side of the equation does not change with respect to time. The right-hand side of the equation is calculated at each time step of the numerical integration. Each of the matrices in Eq. (38) is given in Appendix B.

Equation for pressures - The pressures were also assumed to vary linearly over a finite element and were defined as follows:

$$p = \begin{bmatrix} \zeta_1 & \zeta_2 & \zeta_3 \end{bmatrix} \begin{bmatrix} p_1 \\ p_2 \\ p_3 \end{bmatrix} = \underline{B}\ \underline{p} \tag{39}$$

Repeating the same analytical procedure, a variational functional was obtained by substituting Eqs. (35), (36) and (39) into Eq. (17) to obtain:

$$\Phi = \frac{1}{2} \int_A \underline{p}^t \left[\underline{B}_x^t \underline{B}_x + \underline{B}_y^t \underline{B}_y \right] \underline{p}\ dA - \rho \int_A \underline{Q}\ \underline{B}\ \underline{p}\ dA \tag{40}$$

By minimizing the functional in Eq. (40) with respect to nodal pressures, the resulting system of algebraic equations can be written as

$$\int_A \left[\underline{B}_x^t \underline{B}_x + \underline{B}_y^t \underline{B}_y \right] dA\ \underline{p} = \rho \int_A \underline{Q}\ \underline{B}\ dA \tag{41}$$

The right-hand side of Eq. (41) can be calculated in terms of the variation of velocities over the finite element from Eq. (11)

$$Q = -2 \left[\left(\frac{\partial^2 \psi}{\partial x \partial y} \right)^2 - \frac{\partial^2 \psi}{\partial x^2} \frac{\partial^2 \psi}{\partial y^2} \right] \tag{42}$$

The second derivatives of the stream functions in Eq. (42) can be calculated from the definition of $\underline{\psi}$ for a finite element in Eq. (29). By taking derivatives of the stream functions in Eq. (29), the second derivatives can be written in discrete form as

$$\underline{\gamma} = \underline{J}\ \underline{K} \tag{43}$$

where $\underline{J}$ is a rectangular matrix as shown in Appendix B. The nodal values and the derivatives of stream functions, in terms of area coordinates, can be defined in Eqs. (44) and (45) respectively.

$$\underline{\gamma}^t = \begin{bmatrix} \psi_{xx1} & \psi_{yy1} & 2\psi_{xy1} & \psi_{xx2} & \psi_{yy2} & 2\psi_{xy2} & \psi_{xx3} & \psi_{yy3} & 2\psi_{xy3} \end{bmatrix} \tag{44}$$

$$\underline{K}^t = \begin{bmatrix} \frac{\partial^2 \psi}{\partial \zeta_1^2} & \frac{\partial^2 \psi}{\partial \zeta_2^2} & \frac{\partial^2 \psi}{\partial \zeta_3^2} & \frac{\partial^2 \psi}{\partial \zeta_1 \partial \zeta_2} & \frac{\partial^2 \psi}{\partial \zeta_2 \partial \zeta_3} & \frac{\partial^2 \psi}{\partial \zeta_1 \partial \zeta_3} \end{bmatrix} \tag{45}$$

Substituting Eq. (45) into Eq. (43), the second derivatives of the stream functions can be obtained for each element in terms of nodal stream functions as follows:

$$\underline{\gamma} = \underline{T}\,\underline{\psi} \tag{46}$$

Matrix $\underline{T}$ is obtained from matrix $\underline{J}$ in Eq. (B6) and matrix $\underline{C}\,\underline{A}$ in Eq. (29). The resultant matrix $\underline{T}$ for each finite element is given in Appendix B. After the vector $\underline{Q}$ in Eq. (41) is defined, the final result of the integral on the right-hand side of Eq. (41) was calculated as shown in Appendix B.

Solution of the System of Equations

For the numerical solution of the governing equations, each of the Eqs. (34), (38) and (41) was written in matrix form including the boundary conditions. A similar procedure was used for all three equations and the programming was carried out in a uniform manner.

Stream function solution - The boundary conditions for the solution of stream functions in Eq. (34) were included as external constraints in matrix form as follows:

$$\underline{c}_s^t\,\underline{\bar{\psi}} = \underline{d}_s \tag{47}$$

for the free stream boundary and

$$\underline{b}_s^t\,\underline{\bar{\psi}} = 0 \tag{48}$$

for the obstacle. Eqs. (47) and (48) can be combined with Eq. (34) to obtain

$$\begin{bmatrix} \underline{S} & \underline{c}_s & \underline{b}_s \\ \underline{c}_s^t & \underline{0} & \underline{0} \\ \underline{b}_s^t & \underline{0} & \underline{0} \end{bmatrix} \begin{bmatrix} \underline{\bar{\psi}} \\ \underline{\delta}_{cs} \\ \underline{\delta}_{bs} \end{bmatrix} = \begin{bmatrix} \underline{h}_s \\ \underline{d}_s \\ \underline{0} \end{bmatrix} \tag{49}$$

In Eq. (49), the $\underline{S}$, $\underline{c}_s$ and $\underline{d}_s$ matrices are constant while $\underline{b}_s$ depends on the position and the shape of the obstacle. Separating the time-dependent portion, Eq. (49) can be written as

$$\begin{bmatrix} \underline{S}^* & \underline{b}_s^* \\ \underline{b}_s^{*t} & \underline{0} \end{bmatrix} \begin{bmatrix} \overline{\underline{\psi}}^* \\ \underline{\delta}_{bs} \end{bmatrix} = \begin{bmatrix} \underline{h}_s^* \\ \underline{0} \end{bmatrix} \tag{50}$$

where

$$\underline{S}^* = \begin{bmatrix} \underline{S} & \underline{c}_s \\ \underline{c}_s^t & \underline{0} \end{bmatrix} \quad \underline{b}_s^* = \begin{bmatrix} \underline{b}_s \\ \underline{0} \end{bmatrix} \quad \underline{h}_s^* = \begin{bmatrix} \underline{h}_s \\ \underline{d}_s \end{bmatrix} \quad \overline{\underline{\psi}}^* = \begin{bmatrix} \overline{\underline{\psi}} \\ \underline{\delta}_{cs} \end{bmatrix} \tag{51}$$

In this case, $\underline{\delta}_{bs}$ is a column vector representing the Lagrange multipliers corresponding to the obstacle's boundary conditions. In the case of the moving obstacle, matrix $\underline{b}_s^*$ is defined at each step of the numerical integration. Eq. (50) can be solved to obtain $\overline{\underline{\psi}}^*$ as

$$\overline{\underline{\psi}}^* = \underline{q}_s - \underline{r}_s \, (\underline{b}_s^{*t} \, \underline{r}_s)^{-1} \, (\underline{b}_s^{*t} \, \underline{q}_s) \tag{52}$$

where

$$\underline{q}_s = \underline{S}^{*-1} \, \underline{h}_s^* \tag{53}$$

$$\underline{r}_s = \underline{S}^{*-1} \, \underline{b}_s^* \tag{54}$$

$\underline{S}^*$ matrix is a constant for a particular grid system and has to be inverted only once. Different types of obstacles can be defined by specifying the $\underline{b}_s$ vector. Computational efforts are thus reduced considerably.

Vorticity solution - The boundary condition for the vorticities can be written in matrix form as

$$\underline{c}_w^t \, \dot{\underline{\omega}} = \underline{0} \tag{55}$$

on the free stream boundary and

$$\underline{b}_w^t \, \dot{\underline{\omega}} = \underline{e}_w \tag{56}$$

on the obstacle boundary.

The total system of equations for the solution of the vorticity vector is then

$$\begin{bmatrix} \underline{W} & \underline{c}_w & \underline{b}_w \\ \underline{c}_w^t & \underline{0} & \underline{0} \\ \underline{b}_w^t & \underline{0} & \underline{0} \end{bmatrix} \begin{bmatrix} \dot{\underline{\omega}} \\ \underline{\delta}_{cw} \\ \underline{\delta}_{bw} \end{bmatrix} = \begin{bmatrix} \underline{h}_w \\ \underline{0} \\ \underline{e}_w \end{bmatrix} \tag{57}$$

In this case $\underline{W}$ and $\underline{c}_w$ matrices are again constant and can be combined as

$$\begin{bmatrix} \underline{W}^* & \underline{b}_w^* \\ \underline{b}_w^{*t} & \underline{0} \end{bmatrix} \begin{bmatrix} \dot{\underline{\omega}}^* \\ \underline{\delta}_{bw} \end{bmatrix} = \begin{bmatrix} \underline{h}_w^* \\ \underline{e}_w \end{bmatrix} \tag{58}$$

where

$$\underline{W}^* = \begin{bmatrix} \underline{W} & \underline{c}_w \\ \underline{c}_w^t & \underline{0} \end{bmatrix} \quad \underline{b}_w^* = \begin{bmatrix} \underline{b}_w \\ \underline{0} \end{bmatrix} \quad \underline{h}_w^* = \begin{bmatrix} \underline{h}_w \\ \underline{0} \end{bmatrix} \quad \dot{\underline{\omega}}^* = \begin{bmatrix} \dot{\underline{\omega}} \\ \underline{\delta}_{cw} \end{bmatrix} \tag{59}$$

The time derivative of the vorticities can be calculated from Eq. (58) as

$$\dot{\underline{\omega}}^* = \underline{q}_w - \underline{r}_w \left(\underline{b}_w^{*t} \underline{r}_w\right)^{-1} \left(\underline{b}_w^{*t} \underline{q}_w - \underline{e}_w\right) \tag{60}$$

where

$$\underline{q}_w = \underline{W}^{*-1} \underline{h}_w^* \tag{61}$$

$$\underline{r}_w = \underline{W}^{*-1} \underline{b}_w^* \tag{62}$$

Matrix $\underline{W}^*$ is again constant for a particular grid system and matrix $\underline{b}_w$ is defined for a particular obstacle shape.

Solution for pressures - The boundary conditions for pressure are

$$\underline{c}_p^t \underline{\bar{p}} = \underline{0} \tag{63}$$

at the free stream boundary and

$$\underline{b}_p^t \, \bar{\underline{p}} = \underline{0} \tag{64}$$

on the obstacle. The total system of equations for obtaining pressures can be written as

$$\begin{bmatrix} \underline{P} & \underline{c}_p & \underline{b}_p \\ \underline{c}_p^t & \underline{0} & \underline{0} \\ \underline{b}_p^t & \underline{0} & \underline{0} \end{bmatrix} \begin{bmatrix} \bar{\underline{p}} \\ \underline{\delta}_{cp} \\ \underline{\delta}_{bp} \end{bmatrix} = \begin{bmatrix} \underline{h}_p \\ \underline{0} \\ \underline{0} \end{bmatrix} \tag{65}$$

Combining matrices $\underline{P}$ and $\underline{c}_p$

$$\begin{bmatrix} \underline{P}^* & \underline{b}_p^* \\ \underline{b}_p^{*t} & \underline{0} \end{bmatrix} \begin{bmatrix} \bar{\underline{p}}^* \\ \underline{\delta}_{bp} \end{bmatrix} = \begin{bmatrix} \underline{h}_p^* \\ \underline{0} \end{bmatrix} \tag{66}$$

where

$$\underline{P}^* = \begin{bmatrix} \underline{P} & \underline{c}_p \\ \underline{c}_p^t & \underline{0} \end{bmatrix} \quad \underline{b}_p^* = \begin{bmatrix} \underline{b}_p \\ \underline{0} \end{bmatrix} \quad \underline{h}_p^* = \begin{bmatrix} \underline{h}_p \\ \underline{0} \end{bmatrix} \quad \bar{\underline{p}}^* = \begin{bmatrix} \bar{\underline{p}} \\ \underline{\delta}_{cp} \end{bmatrix} \tag{67}$$

The solution of Eq. (66) for $\bar{\underline{p}}^*$is

$$\bar{\underline{p}}^* = \underline{q}_p - \underline{r}_p \, (\underline{b}_p^{*t} \, \underline{r}_p)^{-1} \, (\underline{b}_p^{*t} \, \underline{q}_p) \tag{68}$$

where

$$\underline{q}_p = \underline{P}^{*-1} \, \underline{h}_p^* \tag{69}$$

$$\underline{r}_p = \underline{P}^{*-1} \, \underline{b}_p^* \tag{70}$$

Matrix $\underline{P}^*$ is assembled and inverted only once for a specified finite element gridwork.

Detailed Analysis of the Boundary Conditions

The assembly of the matrices corresponding to the boundary conditions can now be described in further detail. The governing equations have to be defined in a discrete form suitable for computer applications.

Stream function analysis - The $\underline{c}_s$ matrix in Eq. (47) represents the boundary conditions applied at the free stream boundary. The stream functions and the velocities at the free stream are described depending on the geometry and flow conditions. Vector $\underline{d}_s$ represents the obstacle boundary conditions as described on page 8.

Matrix $\underline{b}_s$ of Eq. (48) has two parts; the first half specifies constant stream functions on the obstacle and the second half makes the tangential velocity on the obstacle equal to zero. The first half of the matrix consists of terms for the nodes with equal values of stream functions

$$\psi_m - \psi_n = 0 \tag{71}$$

The second half of matrix $\underline{b}_s$ specifies that the tangential velocities are equal to zero again at specific points on the obstacle boundary. The tangential velocity u_ξ was defined from figure 4 in terms of the horizontal and vertical velocities as

$$u_\xi = - u \sin \theta + v \cos \theta \tag{72}$$

The angle θ is defined by the obstacle geometry and can be included into the matrix formulation of the boundary conditions as follows:

$$u_\xi = - \left[\underline{C}_y \underline{A} \sin \theta + \underline{C}_x \underline{A} \cos \theta \right] \underline{\psi} \tag{73}$$

The discrete coefficients of Eq. (73) were put in matrix form as shown in Appendix B.

Vorticity analysis - The equations specifying zero values of vorticities at the free stream boundary were assembled in matrix form. The components of the $\underline{c}_w$ matrix were defined at points on the free stream boundary. As defined in Eq. (72), the tangential component of the velocity was calculated again in terms of the nodal velocities and stream functions. Then matrix $\underline{b}_w$ contains the area coordinates of each of the points of the obstacle. Column vector $\underline{e}_w$ is defined at each point by:

$$\underline{e}_w = \frac{\frac{\partial u_\xi}{\partial n} - \omega}{\Delta t} \tag{74}$$

where ω is obtained from Eq. (32) and u_ξ from Eq. (73). Substituting Eq. (6) into Eq. (72) and taking derivatives with respect to η, the normal gradient of the tangential velocity can be written as

$$\frac{\partial u_\xi}{\partial \eta} = -\left[\psi_{xy} \sin 2\theta + \psi_{xx} \cos^2\theta + \psi_{yy} \sin^2\theta\right] \tag{75}$$

The second derivative of stream functions has already been presented in Eq. (46).

Analysis for pressure - Matrix $\underline{c}_p$ of Eq. (63), specifying zero pressure conditions, is identical to matrix $\underline{c}_w$ for the vorticity boundary conditions. In Eq. (64) matrix $\underline{b}_p$ is formed to satisfy the boundary conditions on the obstacle surface by specifying that the normal gradient of the pressure is equal to zero. For the angle θ calculated previously in Eq. (72), the normal gradient of pressure is

$$\frac{\partial p}{\partial \eta} = \frac{\partial p}{\partial y} \cos\theta - \frac{\partial p}{\partial x} \sin\theta \tag{76}$$

Using the discrete finite element representation of the pressures, Eq. (76) can be written as

$$\frac{\partial p}{\partial \eta} = \left[\underline{B}_y \cos\theta - \underline{B}_x \sin\theta\right] \underline{p} \tag{77}$$

Each of the three terms in Eq. (77), defining the boundary conditions at one point, is inserted into the system of equations corresponding to the nodes of the surrounding triangle.

DISCUSSION AND RESULTS

The analytical procedure was tested by calculating first the unsteady viscous flow past a circular cylinder. The procedure was then applied for the analysis of flow around an airfoil. The obtained results and some of the difficulties related to the initial and boundary conditions will now be described. Accuracy and stability of the solution and the numerical integration technique, along with convergence rates and computer time, will also be discussed.

Initial and Boundary Conditions

The boundary conditions were employed in a discretized form. Several alternatives for satisfying the boundary conditions on the obstacle surface

were tested using different discretized constraint equations. This investigation was carried out to decide which set of constraint equations yielded the best accuracy.

For the stream functions, the obstacle boundary conditions were defined by specifying that the tangential velocities are equal to zero and that the stream functions are equal to each other at several points on the obstacle boundary. The same boundary conditions were also defined by specifying that the horizontal and vertical velocities are equal to zero at the same points. The number and positions of the points at which the boundary conditions are specified were tested and compared. It was found that the direct application of zero tangential velocity condition was as accurate as specifying that both horizontal and vertical velocities are equal to zero.

For the analysis of vorticities, the boundary conditions were defined by setting the vorticity equal to the normal derivative of the tangential velocity at the obstacle boundary. The accuracy of the boundary conditions was tested by imposing an additional boundary condition at the leading edge of the cylinder and the airfoil at zero angle of attack. When the vorticity was artificially set equal to zero at the leading edge, the obtained results from the numerical integration were close to the results obtained without this additional condition.

Another important feature of the developed procedure is the description of the initial vorticity distribution. At the beginning of the numerical integration, the vorticity distribution was assumed to be equal to zero for the entire velocity field. With advancing time, vorticities develop on the obstacle surface due to the vorticity boundary conditions and then diffuse throughout the flow region. In the initial stages, the disturbances introduced by these boundary conditions are quite high in magnitude. These disturbances cause instability in the numerical integration of the vorticity transport equation. To eliminate this problem, an underrelaxation factor was applied for the first few steps of the numerical integration. A small percentage of the vorticities, generated at the obstacle surface, was included in the equations. Once these vorticities diffused away from the obstacle boundaries, the underrelaxation factor was removed and the integration was continued with the full value of the surface vorticity distribution.

Another computational difficulty encountered during the solution was related to the position of the points representing the obstacle on the finite element gridwork. Singularities develop in the solution routine, when the nodes describing the obstacle are concentrated in any one finite element triangle. This problem is a result of the number of boundary conditions specified in each finite element. Since the stream functions vary as a third order polynomial, up to three boundary conditions can be specified in each triangle. However, since there are two boundary conditions applied to each obstacle node in the stream function analysis, only one obstacle node can be placed in a single triangle. Similarly, since vorticities and pressures vary linearly over each finite element and only one type of boundary condition is applied in the solution, again only one node can be considered for each triangle. If more than one node is specified in a triangle, singularities arise

in the matrices shown in Eqs. (51), (59) and (67). A similar problem occurs if a boundary condition is duplicated. For example, if the vertical and tangential velocities are specified as the boundary conditions, these two conditions may be equivalent at some points on the obstacle.

Efficiency of the Method of Solution

The systems of linear algebraic equations, Eqs. (49), (57) and (65), were solved by direct inversion of the coefficient matrices shown in Eqs. (52), (60) and (68). Since three unknowns are considered at each node of the gridwork for the stream function solution, the order of the largest matrix is equal to three times the total number of nodes plus the number of boundary conditions at the free stream. Although the resulting matrix is relatively large, it is well-conditioned and the inverse of this matrix was obtained quite accurately by the method of partitioning. The accuracy of the results was checked from the symmetric properties of the flow around a circular cylinder.

For a UNIVAC 1108 computer with 65K core storage, the computation time needed to invert the largest matrix (458 x 458) was slightly over 12 minutes. A significant portion of this time was used up in transferring data between the low speed drum and the high speed core. This was necessary because the core was able to hold only one-fourth of the total matrix at any one time.

Since the major portion of the system of equations was solved by the inversion of matrices S*, W*, and P*, only the constraint equations representing the obstacle's boundary conditions were solved at each step of the numerical integration. The computer time needed for the solution of several sample problems, presented in this analysis, is summarized below:

Re	Δt	No. Time Steps	Comp. Time
40	1.00	110	7.5 min.
1000	0.10	120	8.5 min.
10000	0.01	300	15.5 min.

Again, most of the time used by the computer was for the transfer of data from drum storage to core storage.

An important source of numerical errors in the analysis was due to the numerical integration procedure. The accuracy and stability of the integration was checked by comparing results from different integration techniques and different integration time steps. Three different numerical integration routines were tested, and the results were found to be quite accurate. The time increment employed for each of these integration methods was proportional to the inverse of the Reynolds number. At higher Reynolds numbers, although it required more steps to reach a steady state, the total number of steps corresponded to a shorter real time, due to the convection terms.

Figure 5 shows the convergence to a steady state with different time increments.

Discussion of Results

The results shown in figures 6 through 23 include contour plots of stream functions and vorticity and pressure distributions around a stationary circular cylinder and a stationary and oscillating airfoil.

The sequence of streamline plots in figures 6, 9 and 11 shows the development of the wake behind a cylinder. As time advances, the wake region becomes larger, as does the angle at which the flow separates. Streamlines around a stationary airfoil are shown in figure 15. At the beginning of the integration, the flow is attached to the airfoil. As time advances, vorticities are generated, forcing the flow away from the surface of the airfoil. This process continues until the vorticities have moved past the airfoil into its wake. It should be noted that these results remain symmetric throughout the entire integration time sequence, which is one indication of the accuracy and stability of the solution. At higher Reynolds numbers, unsymmetrical results are also obtained.

The plots of the vorticity distribution shown in figures 7, 10, 12, 16 and 18 also show symmetric results. The flow around an airfoil, stationary or oscillating, is shown in figures 20 and 22, respectively. Since the initial vorticity distribution was assumed to be zero, the first few plots show the vorticities located near the obstacle. The following plots show the diffusion of the vorticities in the surrounding area.

The pressure contours, or isobars, are shown in figures 8, 13, 17, 19, 21 and 23. The highest pressure is at the leading edge of the cylinder and the airfoil. The surface pressure distribution in figure 14 shows that the pressure decreases towards the trailing edge until reverse flow occurs. In this region, the pressure is of an unsteady nature.

Conclusions

The advantages of the developed mathematical procedure will now be summarized. The analysis of the fluid flow around any arbitrarily shaped obstacle can be facilitated by specifying a series of points on the boundary of the obstacle. The solution routines of the analytical procedure are efficient. Since the time-dependent boundary conditions were kept separately, the remaining portion of the system of equations, which amounts to the bulk of computations, was assembled in matrix form and inverted only once. The velocity distribution was calculated directly at each time step, without using iteration. The major portion of the computational cost involved in the analysis was due to core-to-drum transfers of data. Further programming efforts to minimize the data handling costs can decrease the computational cost considerably.

The illustrated results give a good indication of the type of flow problems for which the method can be applied. The cylinder problem was analyzed for testing the method. Numerous solutions for the cylinder already exist. The obtained results were compared and good correlation was achieved. A refined evaluation of the method and the accuracy of the obtained results can be achieved through a more rigorous error analysis. The numerical errors can be related to the physical problem in terms of the flow characteristics, the obstacle shape and the finite element representation of the problem; such as the finite element gridwork and numerical integration technique. The use of higher order finite elements can also lead to an improvement of the present method.

APPENDIX A

AREA COORDINATES

Definition

Area coordinates are useful for integration of polynomials over an area [12, 13]. In this analysis, area coordinates were employed to approximate a variational functional to be integrated over a finite element region.

Using area coordinates, the position of a point P inside the triangle in figure A1 can be specified in terms of the ratio of the area of the subtriangles to the area of the triangle. The ratios for A_1, A_2, A_3 are defined as:

$$\zeta_1 = \frac{A_1}{A} \qquad \zeta_2 = \frac{A_2}{A} \qquad \zeta_3 = \frac{A_3}{A} \tag{A1}$$

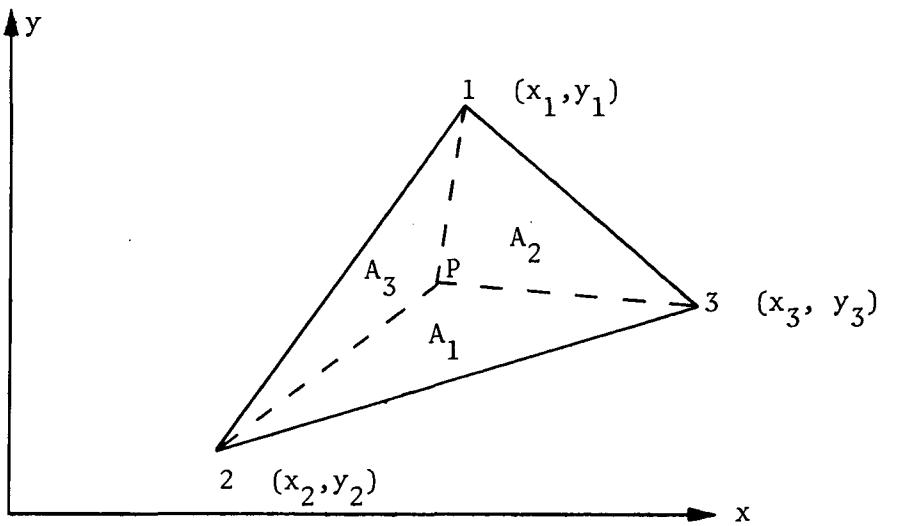

Figure A1. Area coordinate definition for arbitrary point P.

The ζ_m's are defined as area coordinates. The three area coordinates are also related by the expression

$$\zeta_1 + \zeta_2 + \zeta_3 = 1 \tag{A2}$$

The area coordinates can be written in terms of rectangular coordinates by satisfying the conditions at the nodes and using Eq. (A2) as

$$\begin{bmatrix} x \\ y \\ 1 \end{bmatrix} = \begin{bmatrix} x_1 & x_2 & x_3 \\ y_1 & y_2 & y_3 \\ 1 & 1 & 1 \end{bmatrix} \begin{bmatrix} \zeta_1 \\ \zeta_2 \\ \zeta_3 \end{bmatrix} \tag{A3}$$

Inversion of the square matrix in Eq. (A3) leads to the definition of area coordinates in terms of the rectangular coordinates:

$$\underline{B}^t = \begin{bmatrix} \zeta_1 \\ \zeta_2 \\ \zeta_3 \end{bmatrix} = \frac{1}{2A} \begin{bmatrix} y_{23} & x_{32} & x_2y_3 - x_3y_2 \\ y_{31} & x_{13} & x_3y_1 - x_1y_3 \\ y_{12} & x_{21} & x_1y_2 - x_2y_1 \end{bmatrix} \begin{bmatrix} x \\ y \\ 1 \end{bmatrix} \tag{A4}$$

where

$$x_{mn} = x_m - x_n \qquad y_{mn} = y_m - y_n \tag{A5}$$

Differentiation of Area Coordinates

The derivatives of the area coordinates in x and y directions can be calculated using Eq. (A4) as

$$\underline{B}_x^t = \begin{bmatrix} \frac{\partial \zeta_1}{\partial x} \\ \frac{\partial \zeta_2}{\partial x} \\ \frac{\partial \zeta_3}{\partial x} \end{bmatrix} = \frac{1}{2A} \begin{bmatrix} y_{23} \\ y_{31} \\ y_{12} \end{bmatrix} \tag{A6}$$

$$\underline{B}_y^t = \begin{bmatrix} \frac{\partial \zeta_1}{\partial y} \\ \frac{\partial \zeta_2}{\partial y} \\ \frac{\partial \zeta_3}{\partial y} \end{bmatrix} = \frac{1}{2A} \begin{bmatrix} x_{32} \\ x_{13} \\ x_{21} \end{bmatrix} \tag{A7}$$

Integration of the Area Coordinates

The simplicity of the integration of polynomials in terms of area coordinates is one of the important advantages of area coordinates. In general form the integral can be written as [12]:

$$\int_A \zeta_1^m \, \zeta_2^n \, \zeta_3^p \, dA = 2A \, \frac{m! \; n! \; p!}{(m+n+p+2)!} \tag{A8}$$

Eq. (A8) was used extensively in deriving the matrices in Appendix B.

APPENDIX B

FINITE ELEMENT MATRICES

$$A = \begin{bmatrix}
1 & 0 & 0 & 0 & 0 & 0 & 0 & 0 & 0 \\
0 & 0 & 0 & 1 & 0 & 0 & 0 & 0 & 0 \\
0 & 0 & 0 & 0 & 0 & 0 & 1 & 0 & 0 \\
3 & x_{21} & -y_{12} & 0 & 0 & 0 & 0 & 0 & 0 \\
3 & -x_{13} & y_{31} & 0 & 0 & 0 & 0 & 0 & 0 \\
0 & 0 & 0 & 3 & x_{32} & -y_{23} & 0 & 0 & 0 \\
0 & 0 & 0 & 3 & -x_{21} & y_{12} & 0 & 0 & 0 \\
0 & 0 & 0 & 0 & 0 & 0 & 3 & x_{13} & -y_{31} \\
0 & 0 & 0 & 0 & 0 & 0 & 3 & -x_{32} & y_{23} \\
2 & -\frac{3}{2}x_1 & -\frac{3}{2}y_1 & 2 & -\frac{3}{2}x_2 & -\frac{3}{2}y_2 & 2 & -\frac{3}{2}x_3 & -\frac{3}{2}y_3
\end{bmatrix} \quad \text{(B1)}$$

where:

$$x_{mn} = x_m - x_n$$

$$y_{mn} = y_m - y_n$$

$$\int_A \left(\frac{c^t c}{\underline{x}\,\underline{x}} + \frac{c^t c}{\underline{y}\,\underline{y}} \right) dA = \frac{1}{720\,A}$$

$108\,x_{32}^2$ $108\,y_{23}^2$	$18x_{13}x_{32}$ $18y_{31}y_{23}$	$18x_{21}x_{32}$ $18y_{12}y_{23}$	$18x_{32}(x_{13}-x_{21})$ $18y_{23}(y_{31}-y_{12})$	$18x_{32}(x_{21}-x_{13})$ $18y_{23}(y_{12}-y_{31})$	$-6\,x_{32}^2$ $-6\,y_{23}^2$	$6x_{32}(2x_{13}-x_{21})$ $6y_{23}(2y_{31}-y_{12})$	$6x_{32}(2x_{21}-x_{13})$ $6y_{23}(2y_{12}-y_{31})$	$-6\,x_{32}^2$ $-6\,y_{23}^2$	$-6\,x_{32}^2$ $-6\,y_{23}^2$
	$108\,x_{13}^2$ $108\,y_{31}^2$	$18x_{13}x_{21}$ $18y_{31}y_{12}$	$6x_{13}(2x_{32}-x_{21})$ $6y_{31}(2y_{23}-y_{12})$	$-6\,x_{13}^2$ $-6\,y_{31}^2$	$18x_{13}(x_{21}-x_{32})$ $18y_{31}(y_{12}-y_{23})$	$18x_{13}(x_{32}-x_{21})$ $18y_{31}(y_{23}-y_{12})$	$-6\,x_{13}^2$ $-6\,y_{31}^2$	$6x_{13}(2x_{21}-x_{32})$ $6y_{31}(2y_{12}-y_{23})$	$-6\,x_{13}^2$ $-6\,y_{31}^2$
		$108\,x_{21}^2$ $108\,y_{12}^2$	$-6\,x_{21}^2$ $-6\,y_{12}^2$	$6x_{21}(2x_{32}-x_{13})$ $6y_{12}(2y_{23}-y_{31})$	$6x_{21}(2x_{13}-x_{32})$ $6y_{12}(2y_{31}-y_{23})$	$-6\,x_{21}^2$ $-6\,y_{12}^2$	$18x_{21}(x_{32}-x_{13})$ $18y_{12}(y_{23}-y_{31})$	$18x_{21}(x_{13}-x_{32})$ $18y_{12}(y_{31}-y_{23})$	$-6\,x_{21}^2$ $-6\,y_{12}^2$
			$8x_{32}^2-12x_{13}x_{21}$ $8y_{23}^2-12y_{31}y_{12}$	$12x_{21}x_{13}-2x_{32}^2$ $12y_{12}y_{31}-2y_{23}^2$	$2x_{32}x_{13}+6x_{21}x_{32}$ $2y_{23}y_{31}+6y_{12}y_{23}$	$6x_{21}^2-2x_{13}x_{32}$ $6y_{12}^2-2y_{31}y_{23}$	$2x_{21}x_{32}+6x_{13}x_{21}$ $2y_{12}y_{23}+6y_{31}y_{12}$	$4x_{32}x_{21}$ $4y_{23}y_{12}$	$2x_{32}(x_{21}-x_{13})$ $2y_{23}(y_{12}-y_{31})$
				$8x_{32}^2-12x_{21}x_{13}$ $8y_{23}^2-12y_{12}y_{31}$	$4x_{32}x_{13}$ $4y_{23}y_{31}$	$2x_{32}x_{13}+6x_{21}x_{13}$ $2y_{23}y_{31}+6y_{12}y_{31}$	$6x_{13}^2-2x_{21}x_{32}$ $6y_{31}^2-2y_{12}y_{23}$	$2x_{21}x_{32}+6x_{32}x_{13}$ $2y_{12}y_{23}+6y_{23}y_{31}$	$2x_{32}(x_{13}-x_{21})$ $2y_{23}(y_{31}-y_{12})$
					$8x_{13}^2-12x_{32}x_{21}$ $8y_{31}^2-12y_{23}y_{12}$	$12x_{21}x_{32}-2x_{13}^2$ $12y_{12}y_{23}-2y_{31}^2$	$2x_{21}x_{13}+6x_{13}x_{32}$ $2y_{12}y_{31}+6y_{31}y_{23}$	$6x_{32}^2-2x_{13}x_{21}$ $6y_{23}^2-2y_{31}y_{12}$	$2x_{13}(x_{32}-x_{21})$ $2y_{31}(y_{23}-y_{12})$
						$8x_{13}^2-12x_{32}x_{21}$ $8y_{31}^2-12y_{23}y_{12}$	$4x_{21}x_{13}$ $4y_{12}y_{31}$	$2x_{21}x_{13}+6x_{21}x_{32}$ $2y_{12}y_{31}+6y_{12}y_{23}$	$2x_{13}(x_{21}-x_{32})$ $2y_{31}(y_{12}-y_{23})$
							$8x_{21}^2-12x_{32}x_{13}$ $8y_{12}^2-12y_{23}y_{31}$	$12x_{32}x_{13}-2x_{21}^2$ $12y_{23}y_{31}-2y_{12}^2$	$2x_{21}(x_{13}-x_{32})$ $2y_{12}(y_{31}-y_{23})$
								$8x_{21}^2-12x_{13}x_{32}$ $8y_{12}^2-12y_{31}y_{23}$	$2x_{21}(x_{32}-x_{13})$ $2y_{12}(y_{23}-y_{31})$
									$-2(x_{32}x_{21}+x_{13}x_{32}$ $+x_{21}x_{13}+y_{23}y_{12}$ $+y_{31}y_{23}+y_{12}y_{31})$

Symmetric

(B2)

$$\int_A \underline{C}^t \underline{B}\, dA = \frac{A}{180} \begin{bmatrix} 12 & 3 & 3 \\ 3 & 12 & 3 \\ 3 & 3 & 12 \\ 3 & 2 & 1 \\ 3 & 1 & 2 \\ 1 & 3 & 2 \\ 2 & 3 & 1 \\ 2 & 1 & 3 \\ 1 & 2 & 3 \\ 1 & 1 & 1 \end{bmatrix} \tag{B3}$$

$$\int_A \underline{B}^t \underline{B}\, dA = \frac{A}{12} \begin{bmatrix} 2 & 1 & 1 \\ 1 & 2 & 1 \\ 1 & 1 & 2 \end{bmatrix} \tag{B4}$$

$$\int_A \left\{ \nu \left[\underline{B}_x^t \underline{B}_x + \underline{B}_y^t \underline{B}_y \right] + \underline{B}^t \underline{B}\, \underline{u}\, \underline{B}_x + \underline{B}^t \underline{B}\, \underline{v}\, \underline{B}_y \right\} dA$$

$$= \frac{k_d}{24} \begin{bmatrix} 2u_1 + u_2 + u_3 \\ u_1 + 2u_2 + u_3 \\ u_1 + u_2 + 2u_3 \end{bmatrix} + \frac{\nu k_d}{4A} \begin{bmatrix} y_{23} \\ y_{31} \\ y_{12} \end{bmatrix} + \frac{k_e}{24} \begin{bmatrix} 2v_1 + v_2 + v_3 \\ v_1 + 2v_2 + v_3 \\ v_1 + v_2 + 2v_3 \end{bmatrix} + \frac{\nu k_e}{4A} \begin{bmatrix} x_{32} \\ x_{13} \\ x_{21} \end{bmatrix}$$

(B5)

where

$$k_d = -\left(y_{23}\, \omega_1 + y_{31}\, \omega_2 + y_{12}\, \omega_3 \right)$$

$$k_e = -\left(x_{32}\, \omega_1 + x_{13}\, \omega_2 + x_{21}\, \omega_3 \right)$$

$$\underline{J} = \frac{1}{4A^2} \begin{bmatrix} y_{23}^2 & y_{31}^2 & y_{12}^2 & 2y_{31}y_{23} & 2y_{31}y_{12} & 2y_{23}y_{12} \\ x_{32}^2 & x_{13}^2 & x_{21}^2 & 2x_{13}x_{32} & 2x_{13}x_{21} & 2x_{32}x_{21} \\ 2x_{32}y_{23} & 2x_{13}y_{31} & 2x_{21}y_{12} & 2\phi_3 & 2\phi_1 & 2\phi_2 \end{bmatrix}$$

(B6)

where

$$\phi_1 = x_{13}\, y_{12} + x_{21}\, y_{31}$$

$$\phi_2 = x_{32}\, y_{12} + x_{21}\, y_{23}$$

$$\phi_3 = x_{32}\, y_{31} + x_{13}\, y_{23}$$

$$\underline{T} = \frac{1}{4A^2}$$

$-4y_{23}^2-2y_{12}^2$ $-2y_{31}^2$	$8\,A\,y_{23}$ $-3y_{31}y_{12}x_1$	$-3y_{31}y_{12}y_1$	$6y_{31}^2$ $+4y_{31}y_{12}$	$-2y_{31}^2x_{21}$ $-3y_{31}y_{12}x_2$	$2y_{31}^2y_{12}$ $-3y_{31}y_{12}y_2$	$6y_{12}^2$ $+4y_{31}y_{12}$	$2y_{12}^2x_{13}$ $-3y_{31}y_{12}x_3$	$-2y_{12}^2y_{31}$ $-3y_{31}y_{12}y_3$
$-4x_{32}^2-2x_{13}^2$ $-2x_{21}^2$	$-3x_{13}x_{21}x_1$	$8\,A\,x_{32}$ $-3x_{13}x_{21}y_1$	$6x_{13}^2$ $+4x_{13}x_{21}$	$-2x_{13}^2x_{21}$ $-3x_{13}x_{21}x_2$	$2x_{13}^2y_{12}$ $-3x_{13}x_{21}y_2$	$6x_{21}^2$ $+4x_{13}x_{21}$	$2x_{21}^2x_{13}$ $-3x_{13}x_{21}x_3$	$-2x_{21}^2y_{31}$ $-3x_{13}x_{21}y_3$
$-8x_{32}y_{23}-4x_{21}y_{12}$ $-4x_{13}y_{31}$	$8\,A\,x_{32}$ $-3\phi_1x_1$	$8\,A\,y_{23}$ $-3\phi_1y_1$	$12x_{13}y_{31}$ $+4\,\phi_1$	$-4x_{13}y_{31}x_{21}$ $-3x_2\phi_1$	$4x_{13}y_{31}y_{12}$ $-3y_2\phi_1$	$12x_{21}y_{12}$ $+4\,\phi_1$	$4x_{21}y_{12}x_{13}$ $-3x_3\phi_1$	$-4x_{21}y_{12}y_{31}$ $-3y_3\phi_1$
$6y_{23}^2$ $+4y_{23}y_{12}$	$2y_{23}^2x_{21}$ $-3y_{23}y_{12}x_1$	$-2y_{23}^2y_{12}$ $-3y_{23}y_{12}y_1$	$-4y_{31}^2-2y_{23}^2$ $-2y_{12}^2$	$8\,A\,y_{31}$ $-3y_{23}y_{12}x_2$	$-3y_{23}y_{12}y_2$	$6y_{12}^2$ $+4y_{23}y_{12}$	$-2y_{12}^2x_{32}$ $-3y_{23}y_{12}x_3$	$2y_{12}^2y_{23}$ $-3y_{23}y_{12}y_3$
$6x_{32}^2$ $+4x_{32}x_{21}$	$2x_{32}^2x_{21}$ $-3x_{32}x_{21}x_1$	$-2x_{32}^2y_{12}$ $-3x_{32}x_{21}y_1$	$-4x_{13}^2-2x_{21}^2$ $-2x_{32}^2$	$-3x_{32}x_{21}x_2$	$8\,A\,x_{13}$ $-3x_{32}x_{21}y_2$	$6x_{21}^2$ $+4x_{32}x_{21}$	$-2x_{21}^2x_{32}$ $-3x_{32}x_{21}x_3$	$2x_{21}^2y_{23}$ $-3x_{32}x_{21}y_3$
$12x_{32}y_{23}$ $+4\,\phi_2$	$4x_{32}y_{23}x_{21}$ $-3x_1\phi_2$	$-4x_{32}y_{23}y_{12}$ $-3y_1\phi_2$	$-8x_{13}y_{31}-4x_{21}y_{12}$ $-4x_{32}y_{23}$	$8\,A\,x_{13}$ $-3x_2\phi_2$	$8\,A\,y_{31}$ $-3y_2\phi_2$	$12x_{21}y_{12}$ $+4\,\phi_2$	$-4x_{21}y_{12}x_{32}$ $-3x_3\phi_2$	$4x_{21}y_{12}y_{23}$ $-3y_3\phi_2$
$6y_{23}^2$ $+4y_{31}y_{23}$	$-2y_{23}^2x_{13}$ $-3y_{31}y_{23}x_1$	$2y_{23}^2y_{31}$ $-3y_{31}y_{23}y_1$	$6y_{31}^2$ $+4y_{31}y_{23}$	$2y_{31}^2x_{32}$ $-3y_{31}y_{23}x_2$	$-2y_{31}^2y_{23}$ $-3y_{31}y_{23}y_2$	$-4y_{12}^2-2y_{31}^2$ $-2y_{23}^2$	$8\,A\,y_{12}$ $-3y_{31}y_{23}x_3$	$-3y_{31}y_{23}y_3$
$6x_{32}^2$ $+4x_{13}x_{32}$	$-2x_{32}^2x_{13}$ $-3x_{13}x_{32}x_1$	$2x_{32}^2y_{31}$ $-3x_{13}x_{32}y_1$	$6x_{13}^2$ $+4x_{13}x_{32}$	$2x_{13}^2x_{32}$ $-3x_{13}x_{32}x_2$	$-2x_{13}^2y_{23}$ $-3x_{13}x_{32}y_2$	$-4x_{21}^2-2x_{32}^2$ $-2x_{13}^2$	$-3x_{13}x_{32}x_3$	$8\,A\,x_{21}$ $-3x_{13}x_{32}y_3$
$12x_{32}y_{23}$ $+4\,\phi_3$	$-4x_{32}y_{23}x_{13}$ $-3x_1\phi_3$	$4x_{32}y_{23}y_{31}$ $-3y_1\phi_3$	$12x_{13}y_{31}$ $+4\,\phi_3$	$4x_{13}y_{31}x_{32}$ $-3x_2\phi_3$	$-4x_{13}y_{31}y_{23}$ $-3y_2\phi_3$	$-8x_{21}y_{12}-4x_{13}y_{31}$ $-4x_{32}y_{23}$	$8\,A\,x_{21}$ $-3x_3\phi_3$	$8\,A\,y_{12}$ $-3y_3\phi_3$

(B7)

$$\int_A \underline{Q}\,\underline{B}\,dA = -\frac{\rho A}{30}\begin{bmatrix} 6 & 2 & 2 & 2 & 2 & 1 \\ 2 & 6 & 2 & 2 & 1 & 2 \\ 2 & 2 & 6 & 1 & 2 & 2 \end{bmatrix}\begin{bmatrix} \psi^2_{xy_1} - \psi_{xx_1}\psi_{yy_1} \\ \psi^2_{xy_2} - \psi_{xx_2}\psi_{yy_2} \\ \psi^2_{xy_3} - \psi_{xx_3}\psi_{yy_3} \\ 2\psi_{xy_1}\psi_{xy_2} - \psi_{xx_1}\psi_{yy_2} - \psi_{xx_2}\psi_{yy_1} \\ 2\psi_{xy_1}\psi_{xy_3} - \psi_{xx_1}\psi_{yy_3} - \psi_{xx_3}\psi_{yy_1} \\ 2\psi_{xy_2}\psi_{xy_3} - \psi_{xx_2}\psi_{yy_3} - \psi_{xx_3}\psi_{yy_2} \end{bmatrix} \tag{B8}$$

$$\underline{C}_y \, \underline{A} \sin\theta + \underline{C}_x \, \underline{A} \cos\theta =$$

$$\frac{1}{2A}\begin{bmatrix} 6\,\zeta_1\,x_{32}\,(1-\zeta_1) + 2\,k_f \\ 2\,\zeta_1\,x_{32}\,(k_h-x_1) - 1.5\,x_1 k_f \\ 2\,\zeta_1\,x_{32}\,(k_j-y_1) + 2\,A\,\zeta_1^2 - 1.5\,y_1 k_f \\ 6\,\zeta_2\,x_{13}\,(1-\zeta_2) + 2\,k_f \\ 2\,\zeta_2\,x_{13}\,(k_h-x_2) - 1.5\,x_2 k_f \\ 2\,\zeta_2\,x_{13}\,(k_j-y_2) + 2\,A\,\zeta_2^2 - 1.5\,y_2 k_f \\ 6\,\zeta_3\,x_{21}\,(1-\zeta_3) + 2\,k_f \\ 2\,\zeta_3\,x_{21}\,(k_h-x_3) - 1.5\,x_3 k_f \\ 2\,\zeta_3\,x_{21}\,(k_j-y_3) + 2\,A\,\zeta_3^2 - 1.5\,y_3 k_f \end{bmatrix} \sin\theta + \frac{1}{2A}\begin{bmatrix} 6\,\zeta_1\,y_{23}\,(1-\zeta_1) + 2\,k_g \\ 2\,\zeta_1\,y_{23}\,(k_h-x_1) + 2\,A\,\zeta_1^2 - 1.5\,x_1 k_g \\ 2\,\zeta_1\,y_{23}\,(k_j-y_1) - 1.5\,y_1 k_g \\ 6\,\zeta_2\,y_{31}\,(1-\zeta_2) + 2\,k_g \\ 2\,\zeta_2\,y_{31}\,(k_h-x_2) + 2\,A\,\zeta_2^2 - 1.5\,x_2 k_g \\ 2\,\zeta_2\,y_{31}\,(k_j-y_2) - 1.5\,y_2 k_g \\ 6\,\zeta_3\,y_{12}\,(1-\zeta_3) + 2\,k_g \\ 2\,\zeta_3\,y_{12}\,(k_h-x_3) + 2\,A\,\zeta_3^2 - 1.5\,x_3 k_g \\ 2\,\zeta_3\,y_{12}\,(k_j-y_3) - 1.5\,y_3 k_g \end{bmatrix} \cos\theta \qquad \text{(B9)}$$

where:

$$k_f = \zeta_2\zeta_3 x_{32} + \zeta_1\zeta_3 x_{13} + \zeta_1\zeta_2 x_{21}$$

$$k_g = \zeta_2\zeta_3 y_{23} + \zeta_1\zeta_3 y_{31} + \zeta_1\zeta_2 y_{12}$$

$$k_h = \zeta_1 x_1 + \zeta_2 x_2 + \zeta_3 x_3$$

$$k_j = \zeta_1 y_1 + \zeta_2 y_2 + \zeta_3 y_3$$

$$\int_A \left[\underline{B}_x^t \underline{B}_x + \underline{B}_y^t \underline{B}_y \right] dA = \frac{1}{4A} \begin{bmatrix} x_{32} \\ x_{13} \\ x_{21} \end{bmatrix} \begin{bmatrix} x_{32} & x_{13} & x_{21} \end{bmatrix} + \frac{1}{4A} \begin{bmatrix} y_{23} \\ y_{31} \\ y_{12} \end{bmatrix} \begin{bmatrix} y_{23} & y_{31} & y_{12} \end{bmatrix} \quad \text{(B10)}$$

APPENDIX C

FLOW CHARTS

Several computer programs were prepared in obtaining the presented results. The first step of the numerical procedure was to determine the matrices describing stream functions, vorticities and pressure distributions for the finite element mesh without the obstacle; the square matrices $\underline{S}^*$, $\underline{W}^*$ and $\underline{P}^*$ shown in Eqs. (51), (59) and (67) were assembled and inverted. Since these matrices remain constant, they were inverted only once and then stored for use in the solution program. After these matrices were inverted, the matrices representing the boundary conditions in Eqs. (52), (60) and (68) were added to give the final solution. The overall procedure is summarized in figure C1.

The matrices defining the finite element mesh were assembled from individual element matrices. These individual matrices were derived from Eqs. (B2), (B4) and (B10) for stream functions, vorticities and pressures respectively. It should be noted that the order of the element matrix for stream functions was three times larger than those for either vorticities or pressures, since at each node there were three unknowns; stream function and two velocities. For the final matrices $\underline{S}^*$, $\underline{W}^*$ and $\underline{P}^*$, the order of the latter two was equal to the number of nodes in the finite element mesh, while the order of $\underline{S}^*$ was three times larger. Since the entire matrix $\underline{S}^*$ could not be stored in the computer at one time, it was assembled one quadrant at a time and stored on magnetic tape as shown in figure C2. The smaller matrices, for vorticity and pressure, were assembled at the same time in conjunction with the free stream boundary conditions, as shown in figures C3 and C4 respectively.

After the matrices were inverted and stored on tape, the solution was obtained using another computer program. This program sets up the matrices for the obstacle boundary conditions and the column vectors corresponding to the right-hand sides of Eqs. (49), (57) and (65), and then calculates the velocity, pressure and vorticity distributions. These distributions can be plotted and their development with respect to time can be recorded at any time instant. The flow chart for this final program is given in figure C6.

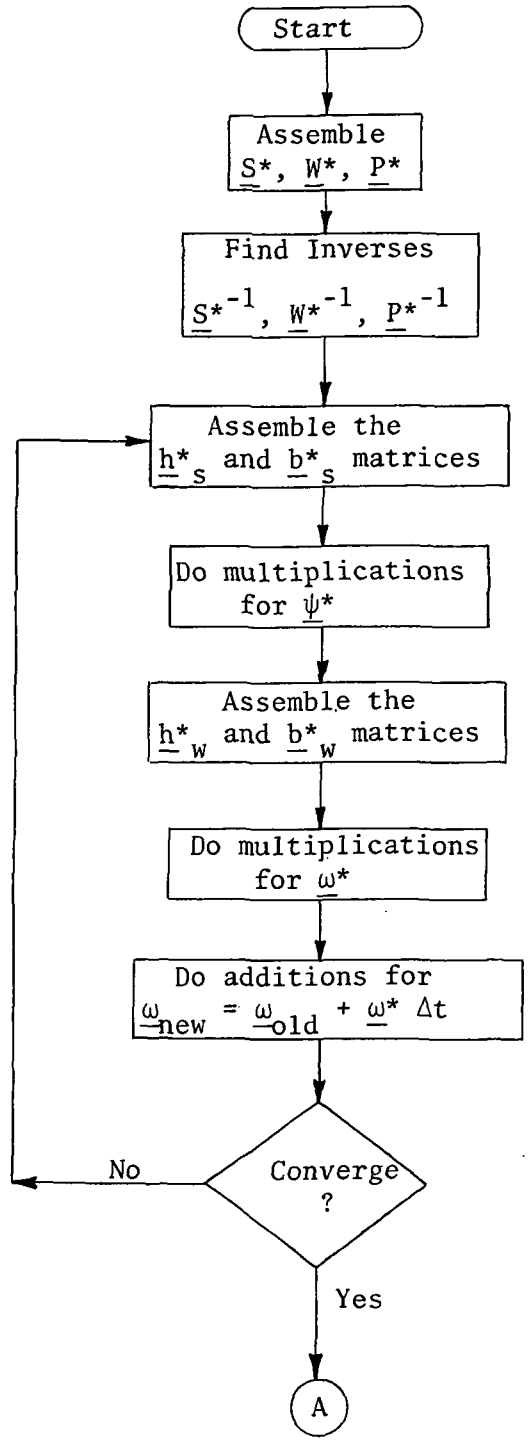

Fig. C1. Overall procedure for the computer solution.

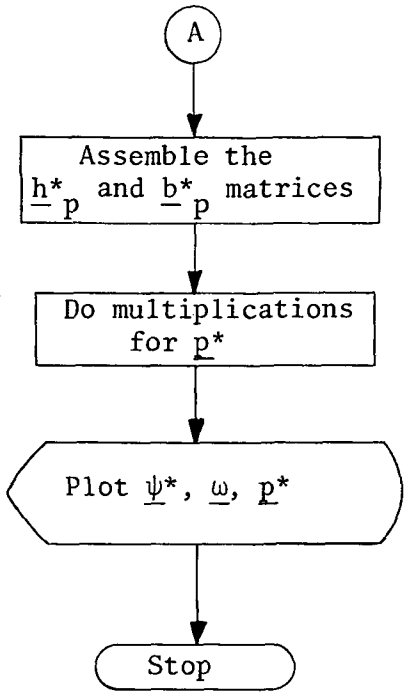

Fig. C1. Continued.

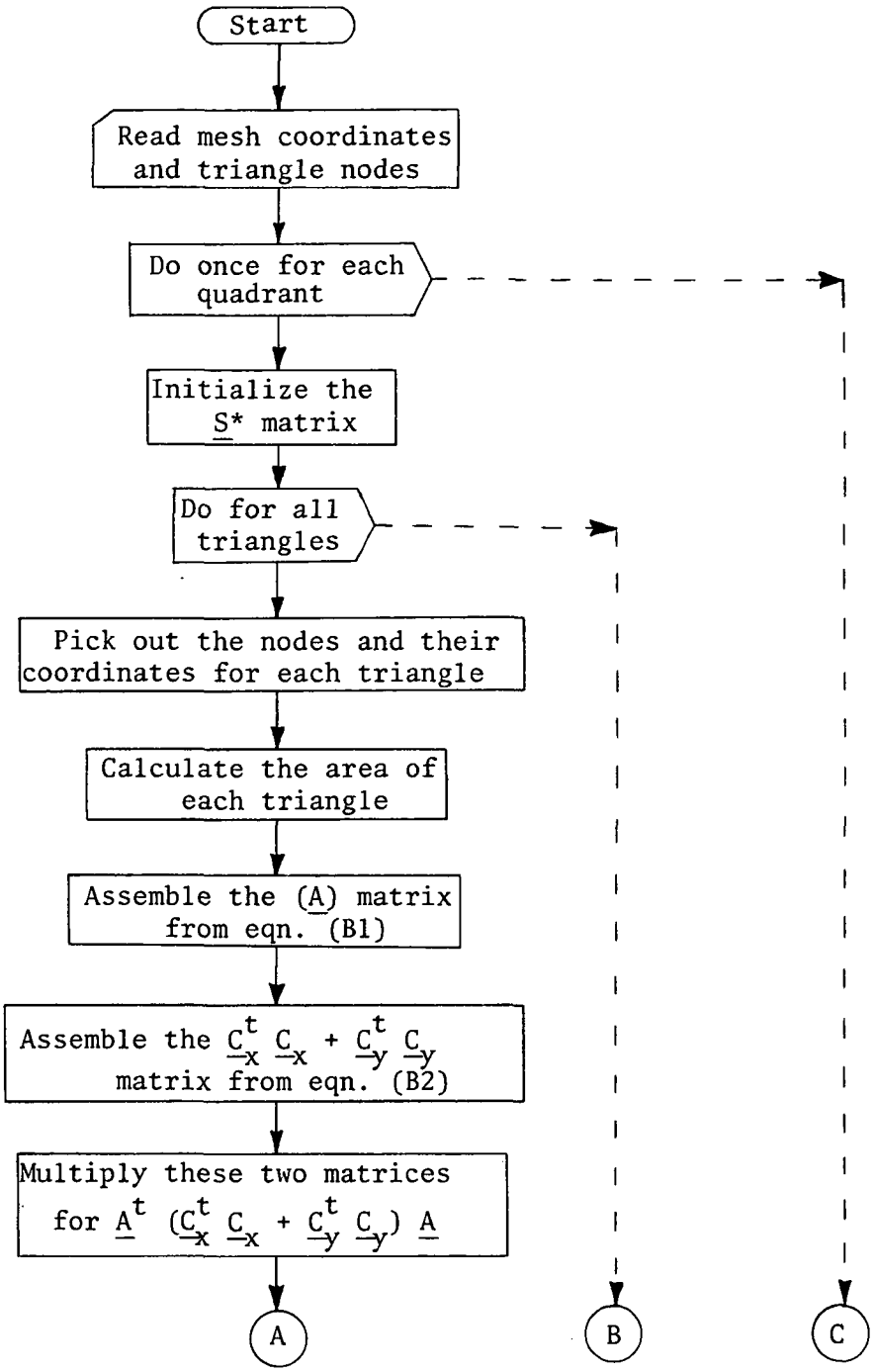

Fig. C2. Computational procedure for assembly of the constant matrix for stream functions.

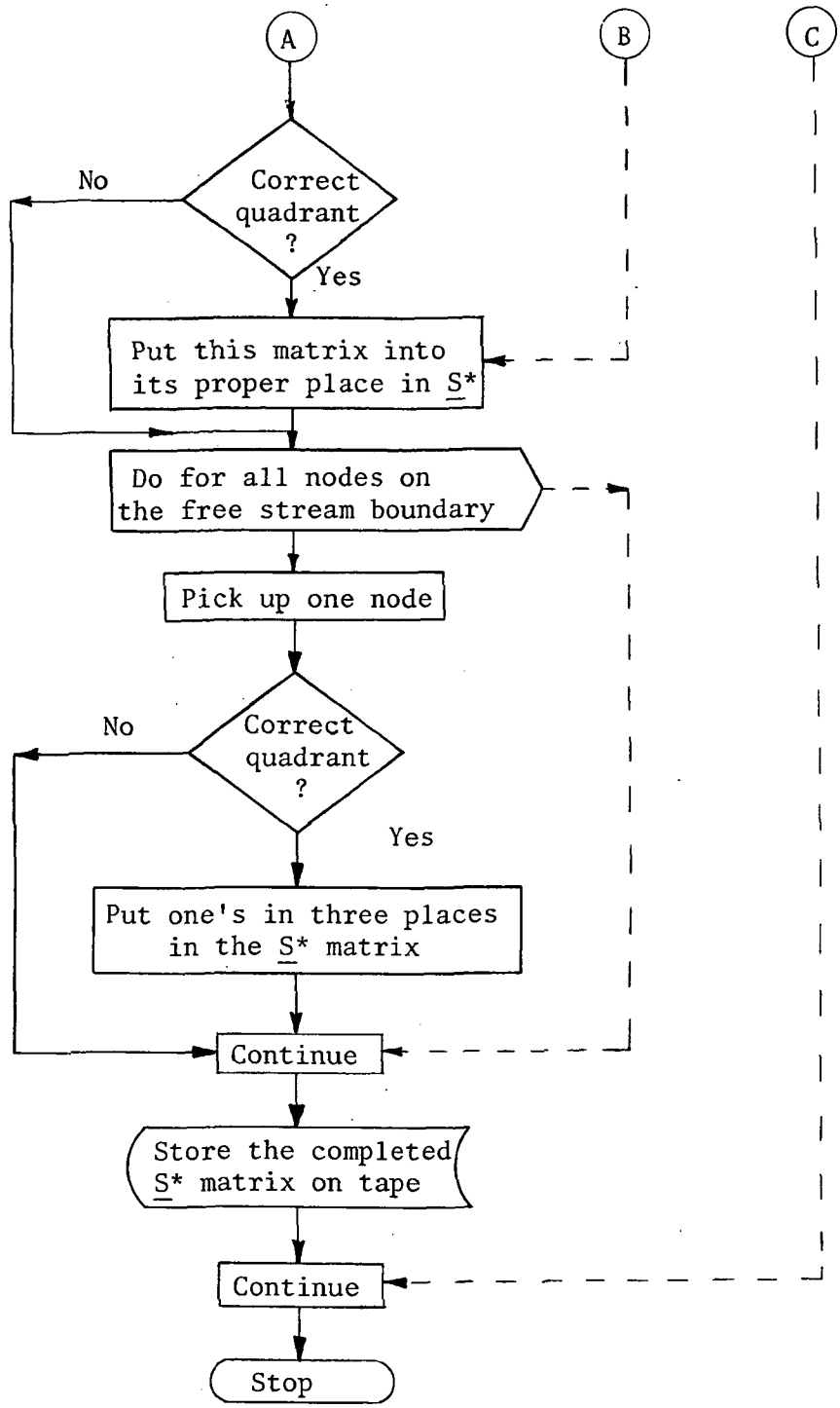

Fig. C2. Continued.

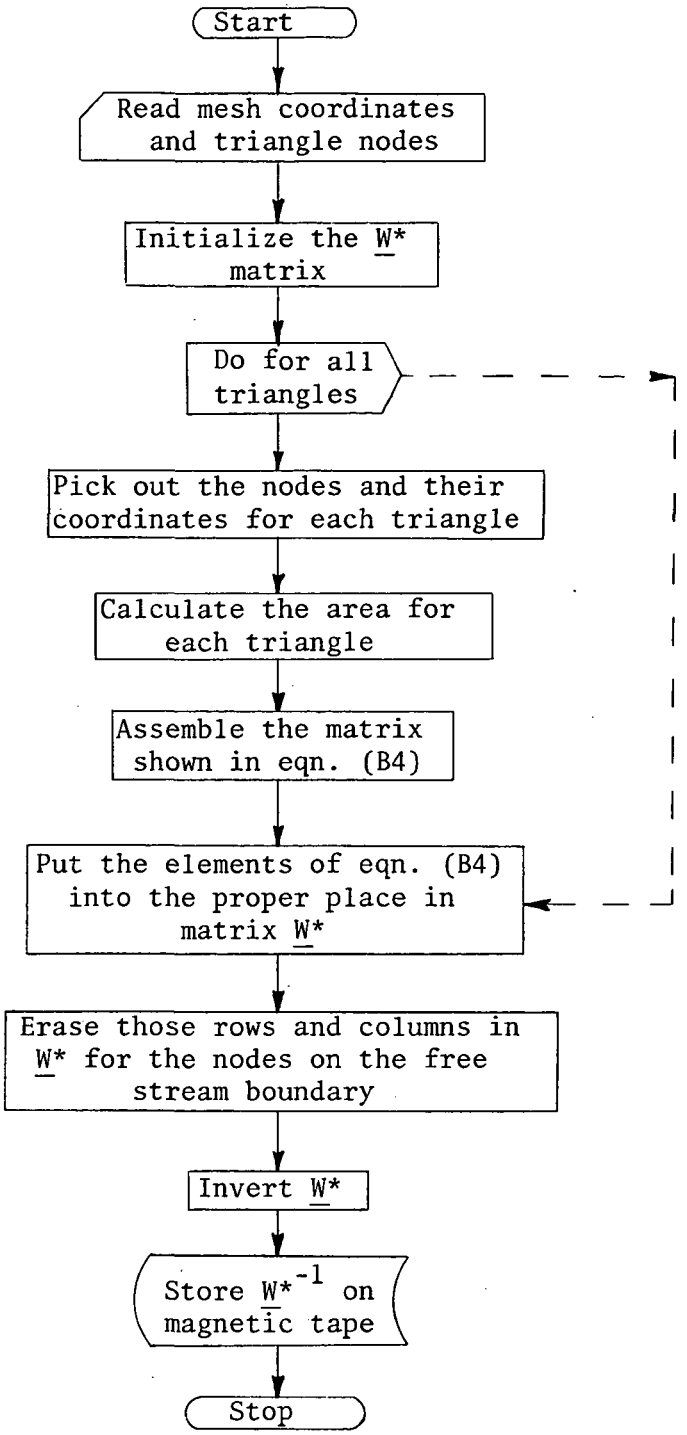

Fig. C3. Computational procedures for assembly and inversion of the constant matrix for vorticities.

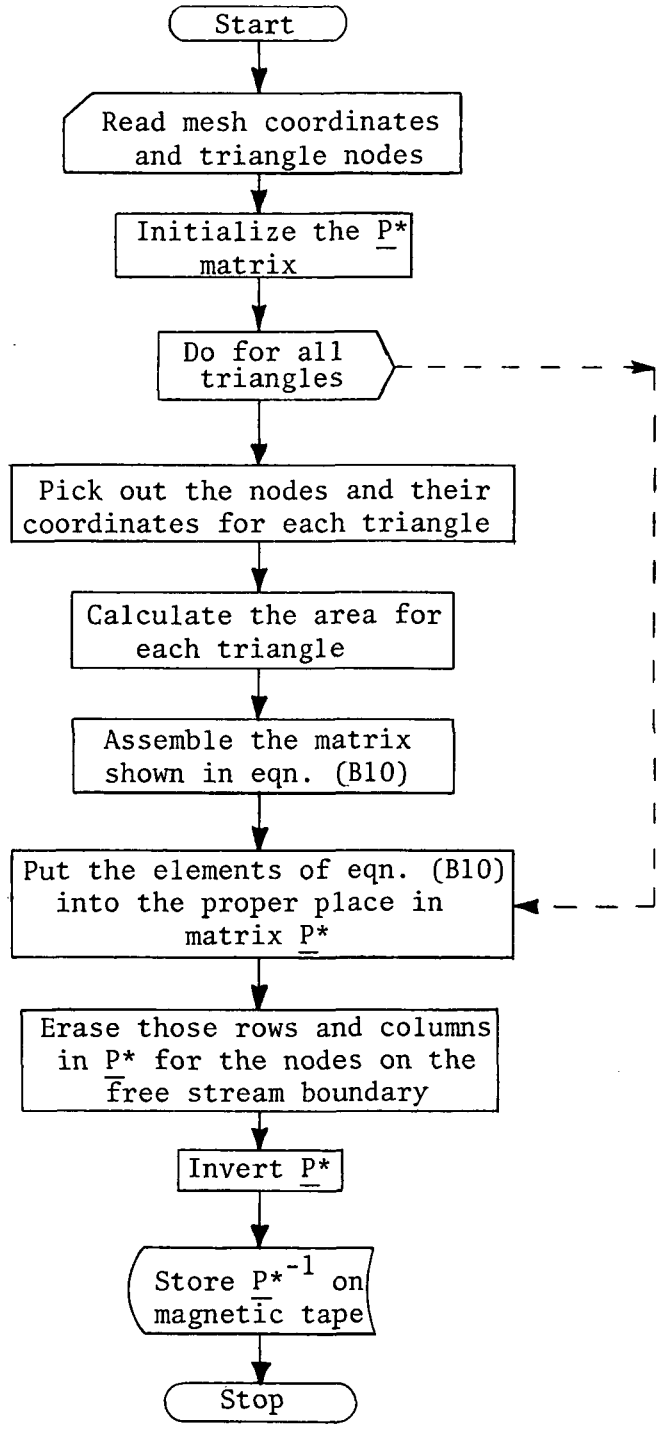

Fig. C4. Computational procedure for assembly and inversion of the constant matrix for pressures.

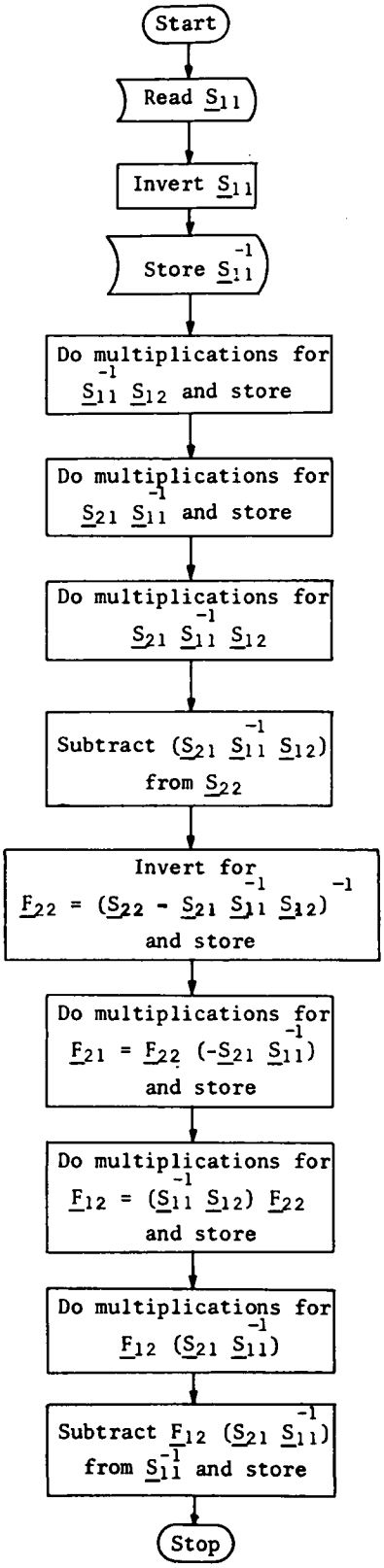

Fig. C5. Inverse routine for the stream function matrix.

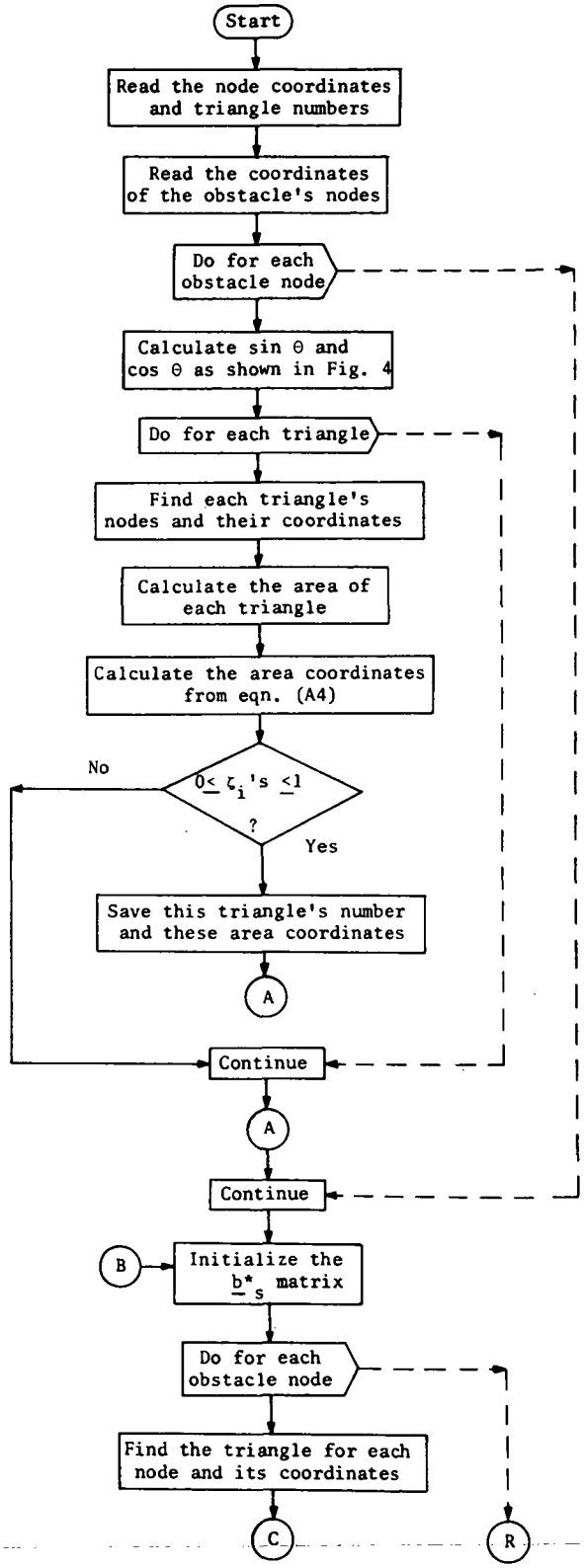

Fig. C6. Flow chart to obtain the final solutions.

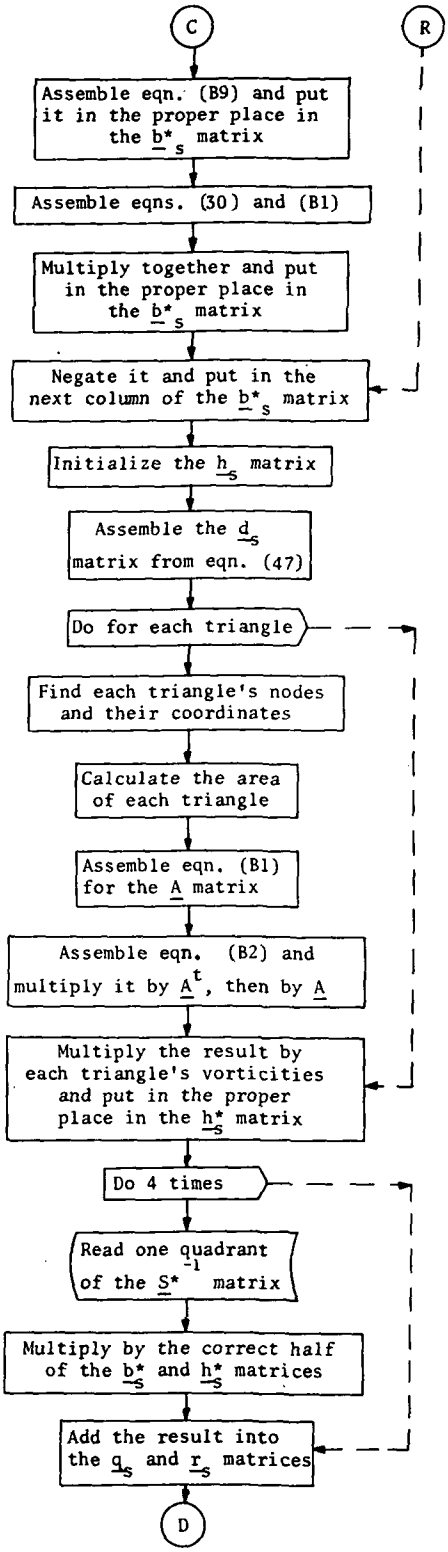

Fig. C6. Continued.

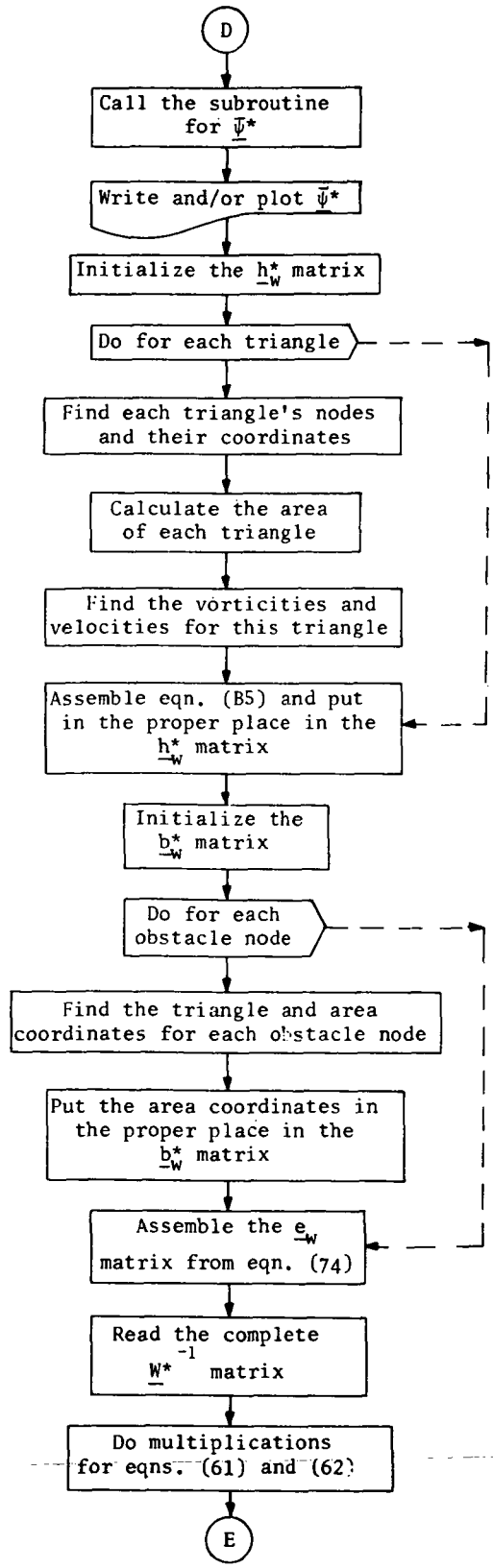

Fig. C6. Continued.

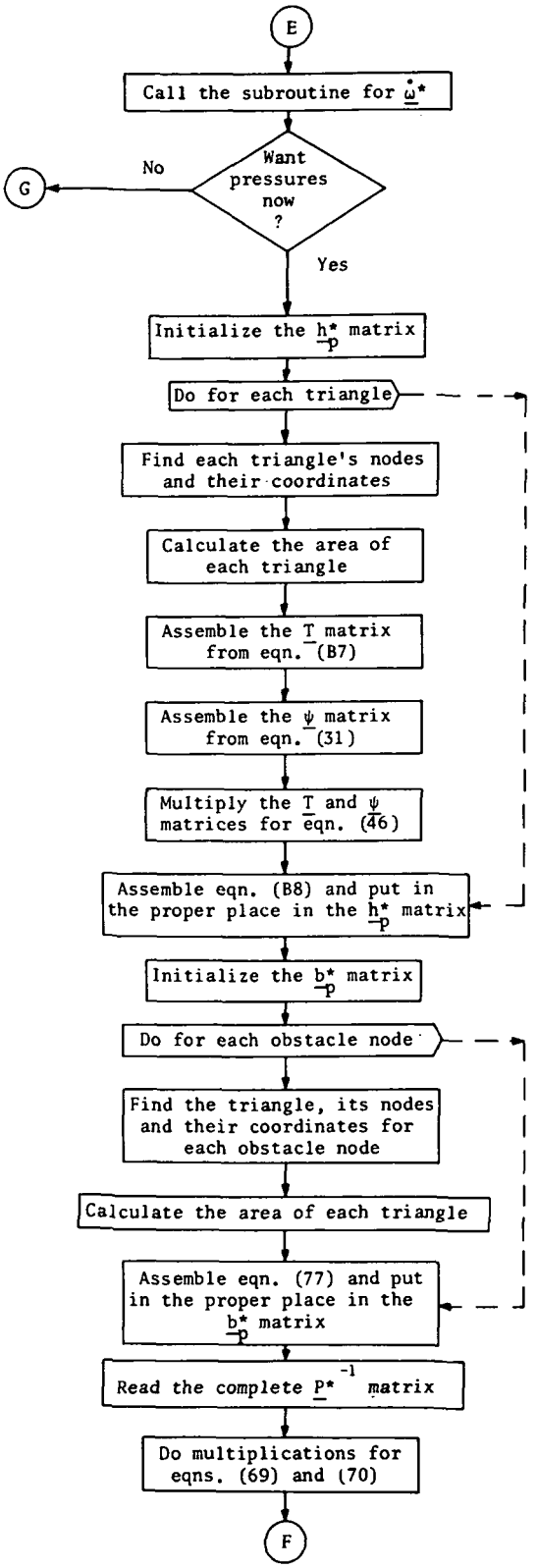

Fig. C6. Continued.

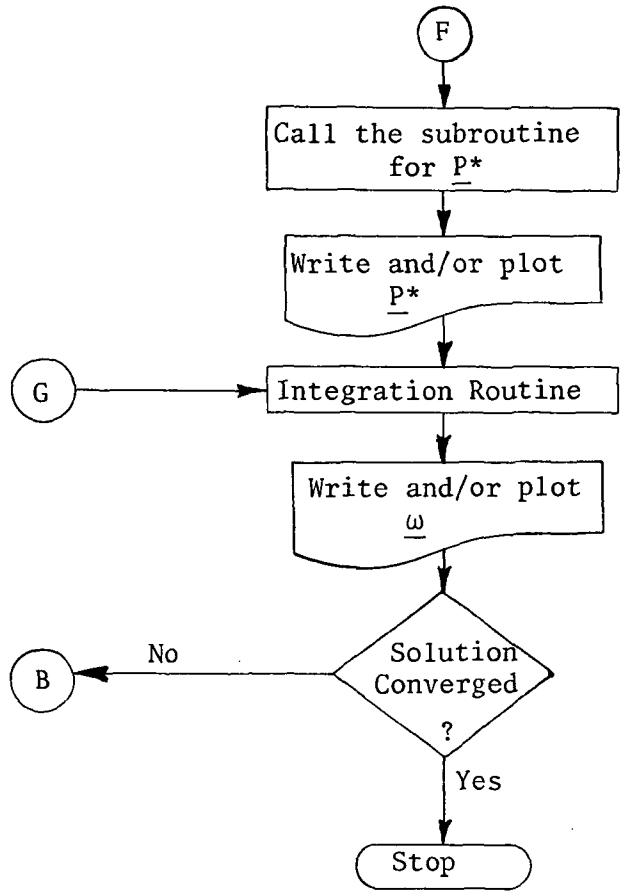

Fig. C6. Continued.

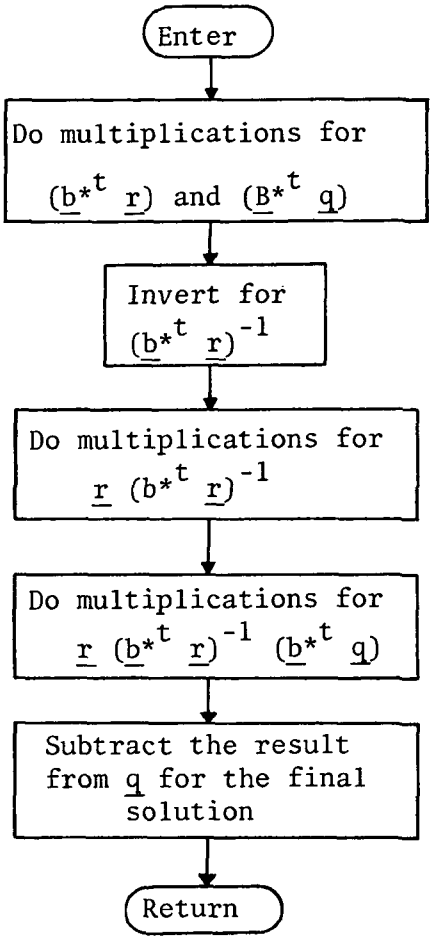

Fig. C7. Flow chart for the subroutine used in the final program shown in fig. C6.

REFERENCES

1. Son, J.S. and Hanratty, T.J.: Numerical Solution for the Flow Around a Cylinder at Reynolds Numbers of 40, 200, and 500. J. Fluid Mech., Vol. 35, Feb. 1969, p. 369.

2. Sykes, D.M.: The Supersonic and Low-Speed Flows Past Circular Cylinders of Finite Length Supported at One End. J. Fluid Mech., Vol. 12, Mar. 1962, p. 367.

3. Takami, H. and Keller, H.B.: Steady Two-Dimensional Viscous Flow of an Incompressible Fluid Past a Circular Cylinder. Phys. Fluids Suppl. II, 1969, pp. 51-56.

4. Okajima, A.: Numerical Solution for the Analysis of Unsteady Viscous Flow Around an Oscillating Cylinder. Recent Advances in Matrix Methods of Structural Analysis and Design, R.H. Gallagher, Y. Yamada, and J.T. Oden, Eds., The Univ. of Ala. Press, Ala., 1971, p. 809.

5. Achenbach, E.: Distribution of Local Pressure and Skin Friction Around a Circular Cylinder in Cross-Flow Up to Re = $5x10^6$. J. Fluid Mech., Vol. 34, Dec. 1968, p. 625.

6. Thoman, D.C. and Szewczyk,A.A.: Time-Dependent Viscous Flow Over a Circular Cylinder. Phys. Fluids Suppl. II, Vol. 12, No. 12, Dec. 1969, p. 76.

7. Dennis, S.C.R. and Staniforth, A.N.: A Numerical Method for Calculating the Initial Flow Past a Cylinder in a Viscous Fluid. Proc. of the Conf. on Numerical Methods in Fluid Dyn., held at the Univ. of Calif., Berkeley, Sep. 1970, M. Holt, ed., p. 343.

8. Schlichting, H.: Boundary Layer Theory. McGraw-Hill Book Co. Inc., New York, 1968.

9. Fromm, J.E.: A Method for Computing Nonsteady, Incompressible, Viscous Fluid Flows. Los Alamos Scientific Laboratory Report LA-2910, Sep. 1963.

10. Mikhlin, S.G.: Variational Methods in Mathematical Physics. The Macmillan Co., New York, 1964.

11. Cheng, S.I. and Rimon, Y.: Numerical Solution of a Uniform Flow over a Sphere at Intermediate Reynolds Numbers. Phys. Fluids, Vol. 12, No. 5, May 1969, p. 949.

12. Holand, I.: The Finite Element Method in Plane Stress Analysis. Finite Element Methods in Stress Analysis, I. Holand and K. Bell, eds., Tapir Book Co., Norway, 1969, p. 43.

13. Zienkiewicz, O.C. and Cheung, Y.K: The Finite Element Method in Structural and Continuum Mechanics. McGraw-Hill Publishing Company, Limited, Great Britain, 1967.

14. Kawaguti, M.: Numerical Solution of the Navier-Stokes Equations for the Flow Around a Circular Cylinder at Reynolds Number 40. J. Phys. Soc. Japan, Vol. 8, No. 6, 1953, p. 747.

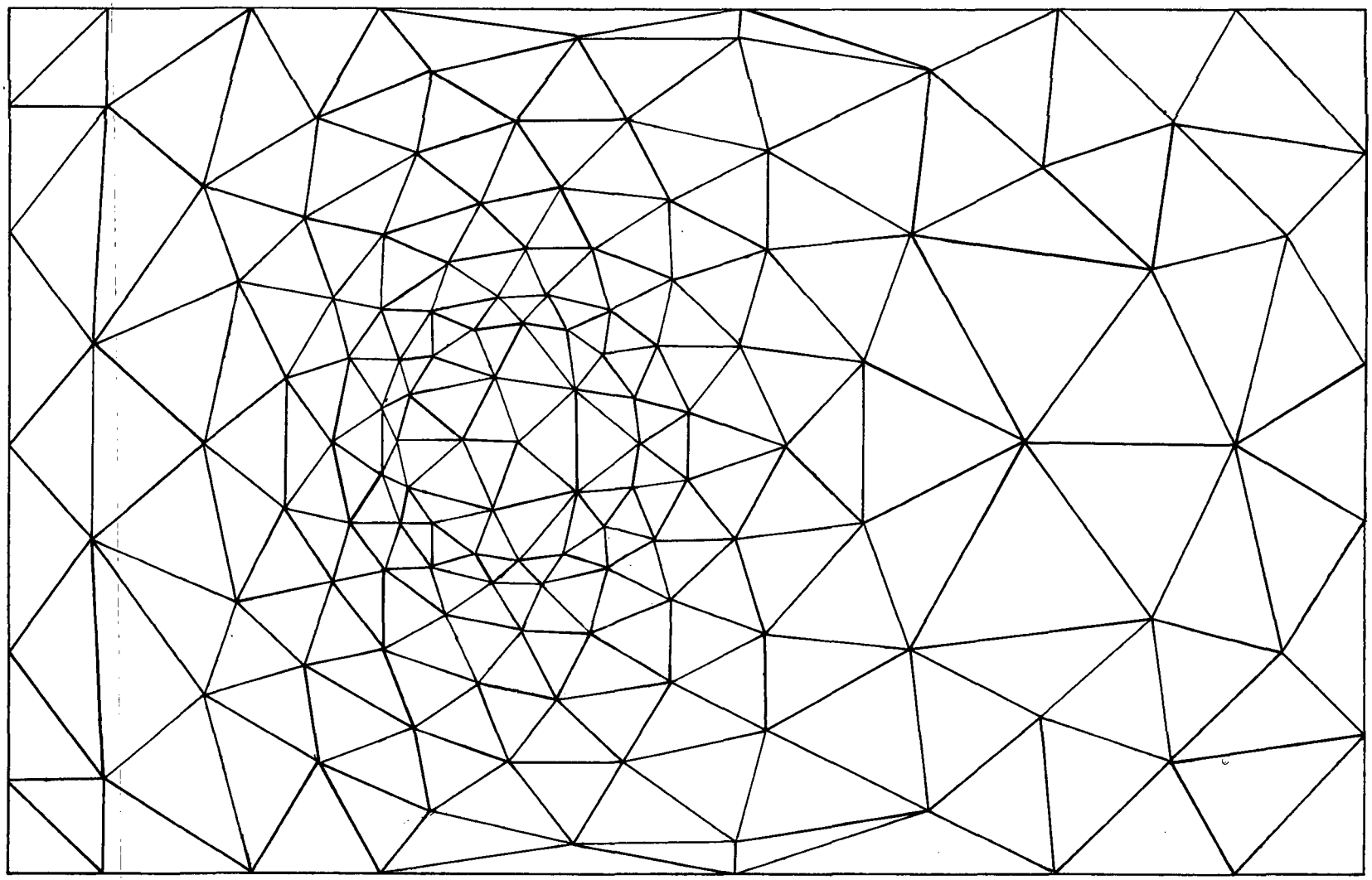

Fig. 1. Finite element mesh for circular cylinder calculations.

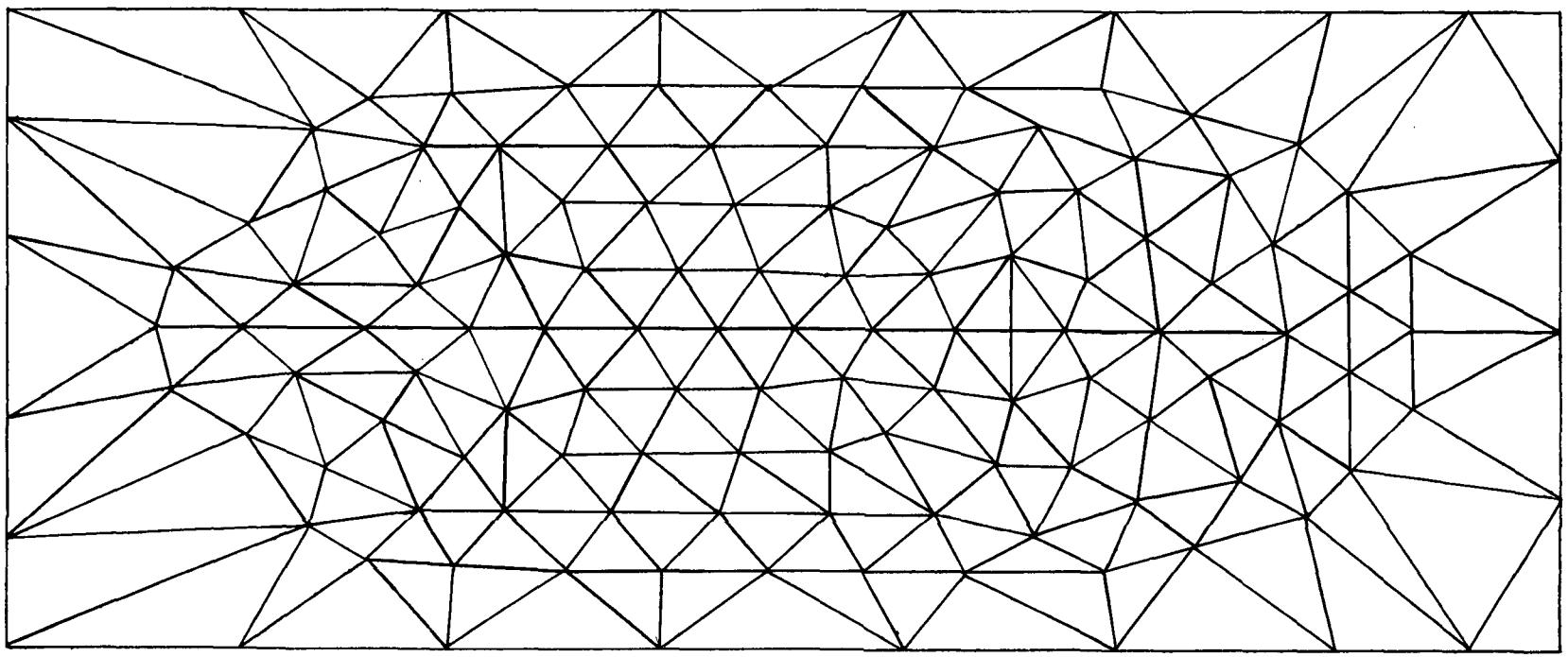

Figure 2. Finite element mesh for the pitching and plunging airfoil analysis.

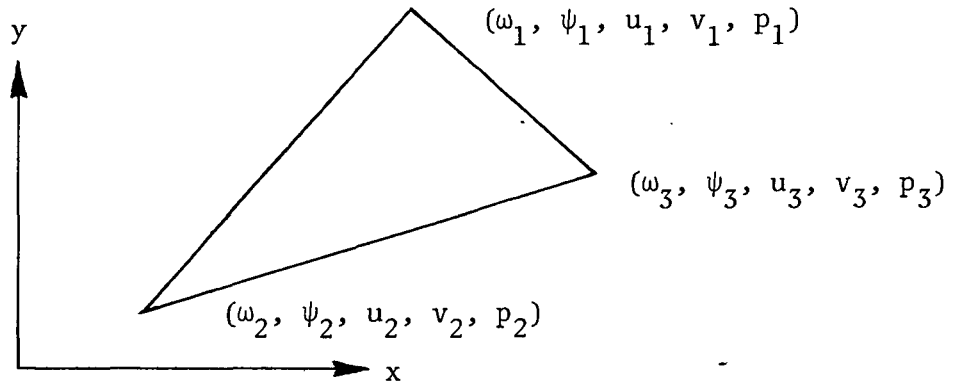

Fig. 3. A typical triangular grid element for the finite element analysis of the Navier-Stokes equations.

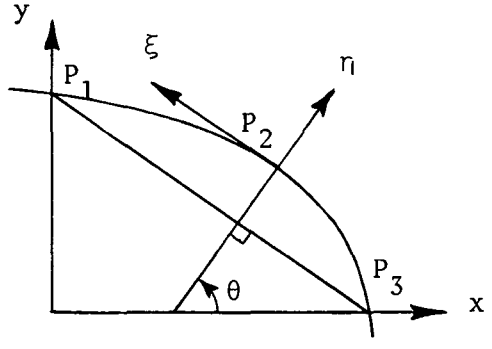

Fig. 4. Definition of the tangential and normal directions for any point on the obstacle. Sines and cosines for point P_2 are defined in terms of points P_1 and P_3.

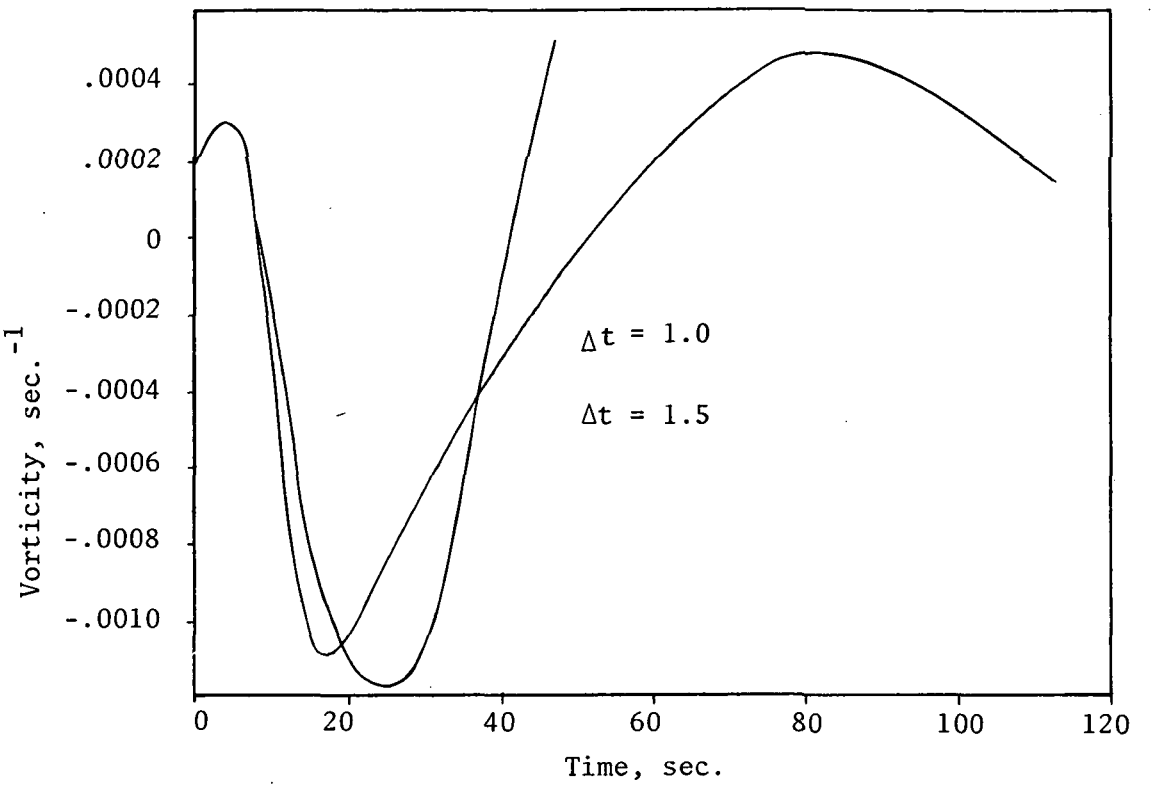

Fig. 5a. Stability of the numerical integration of the vorticity transport equation for a point upstream of the obstacle (Re = 40).

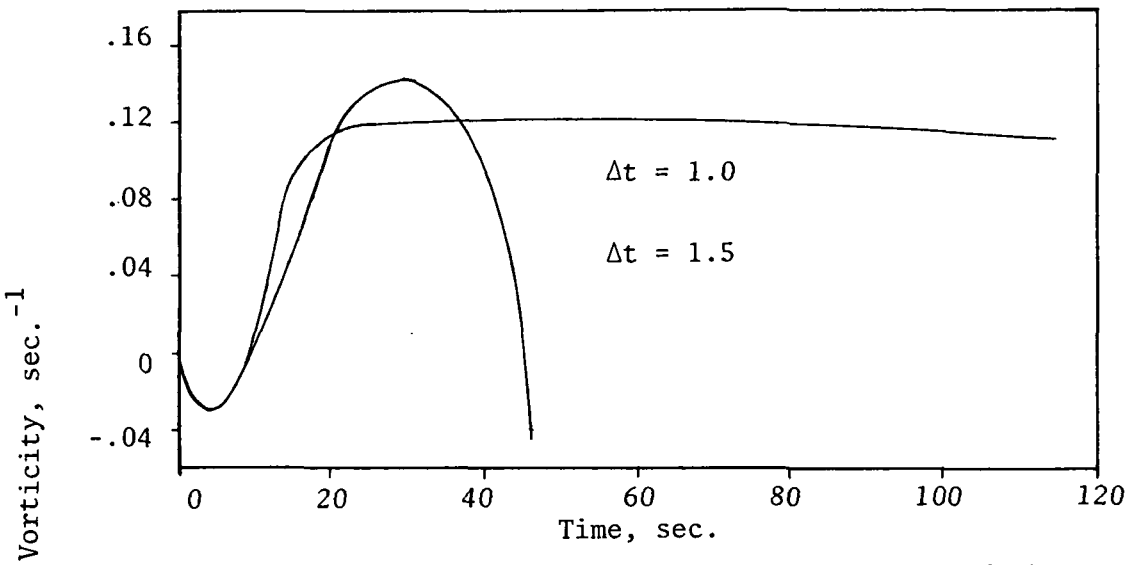

Fig. 5b. Stability of the numerical integration of the vorticity transport equation for a point near the obstacle (Re = 40).

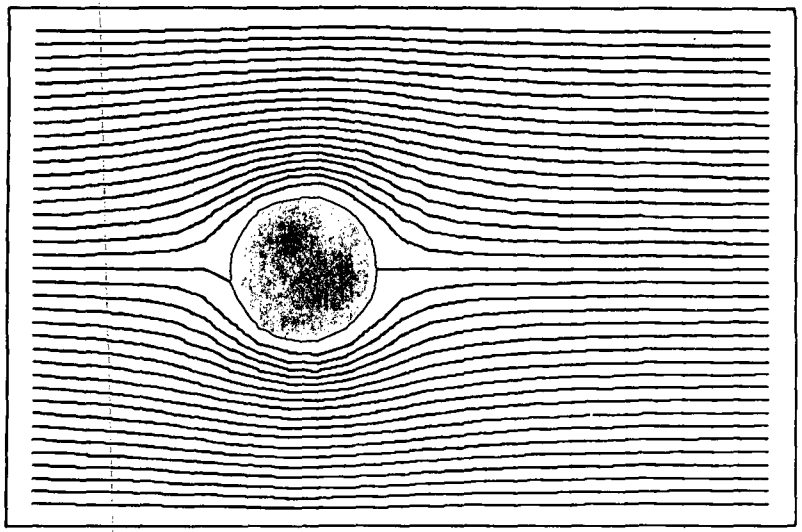

t = 15.

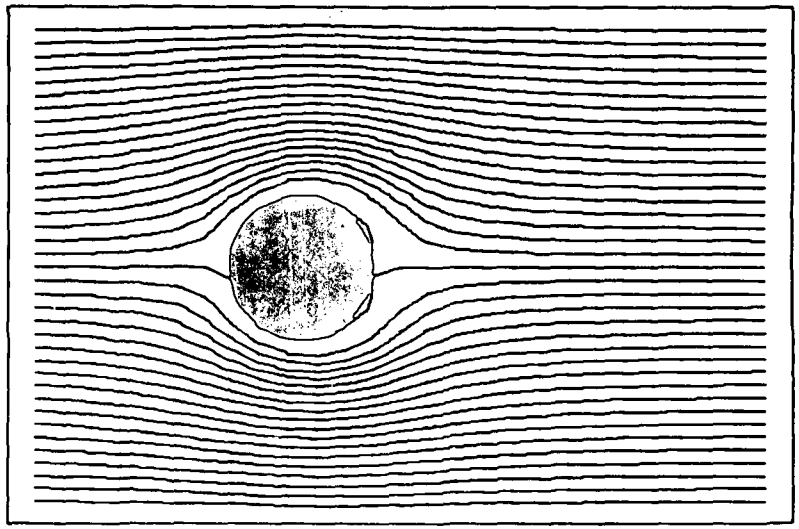

t = 30.

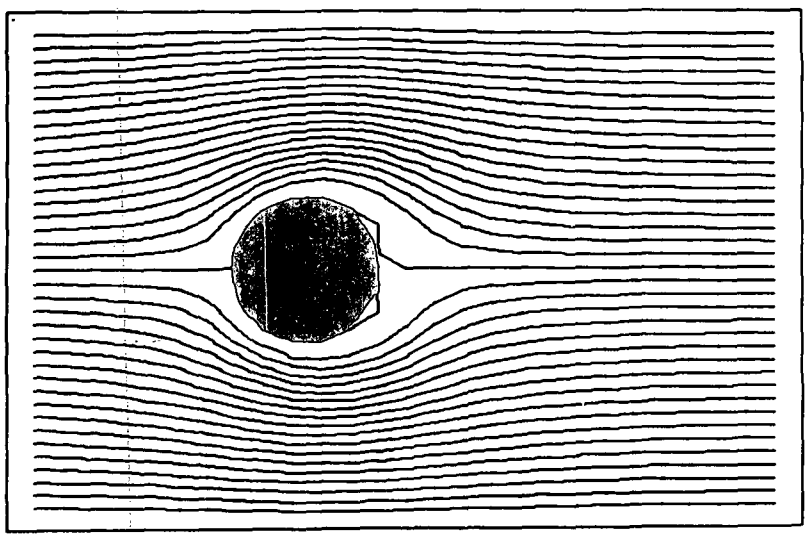

t = 45.

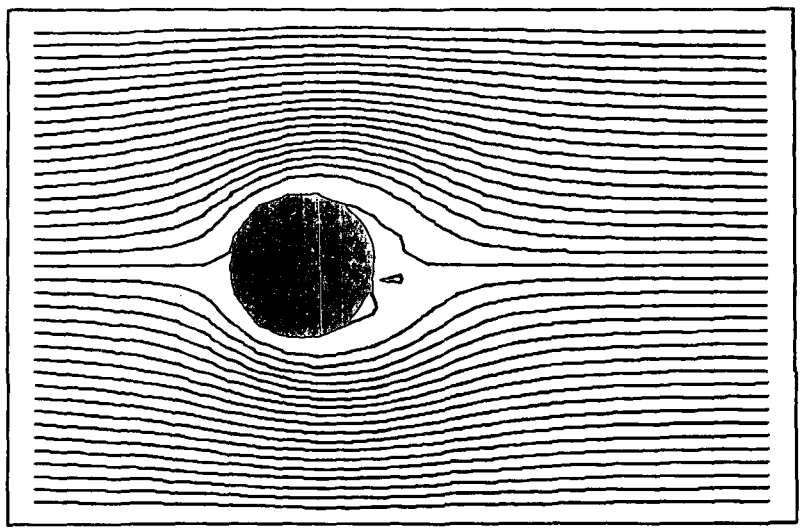

t = 60.

Fig. 6a. Stream lines around a circular cylinder (Re = 40).

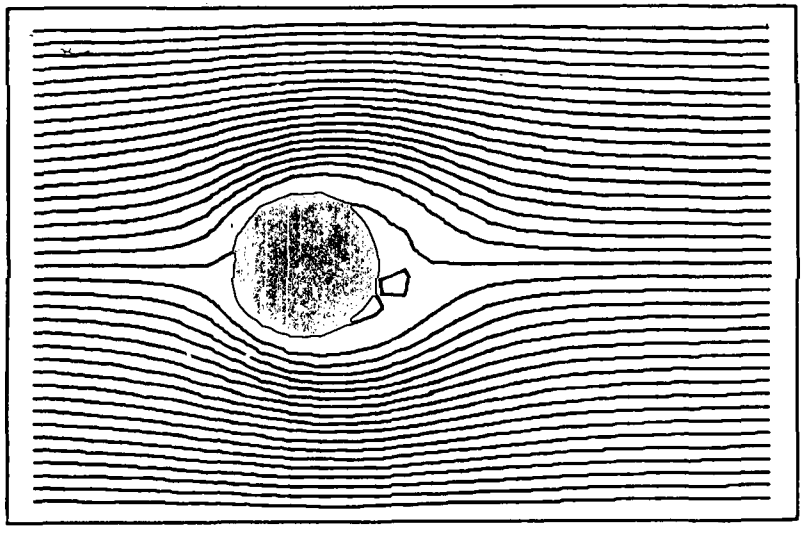

t = 66.

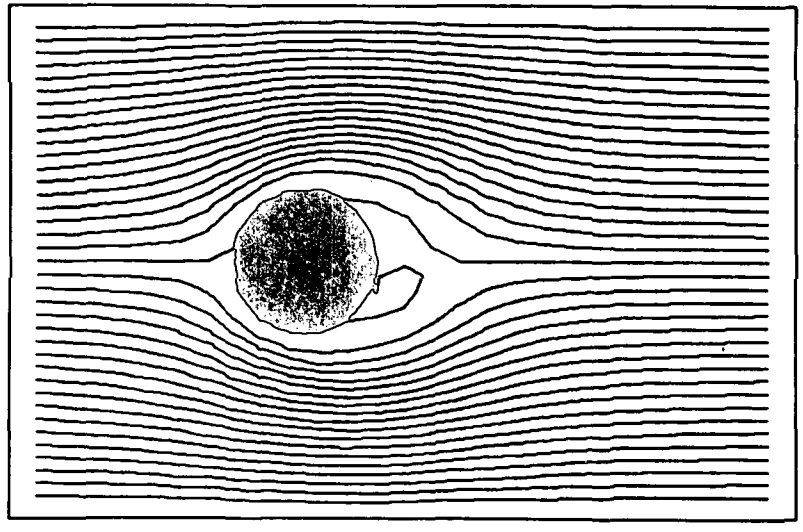

t = 80.

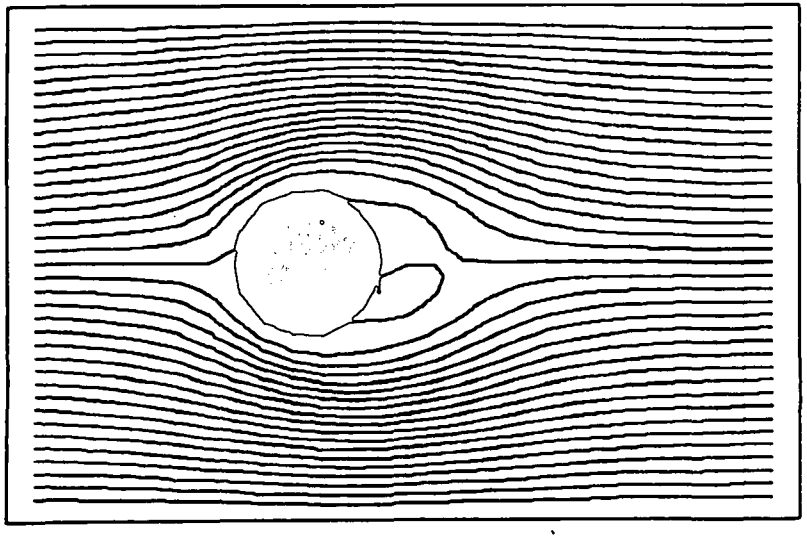

t = 95.

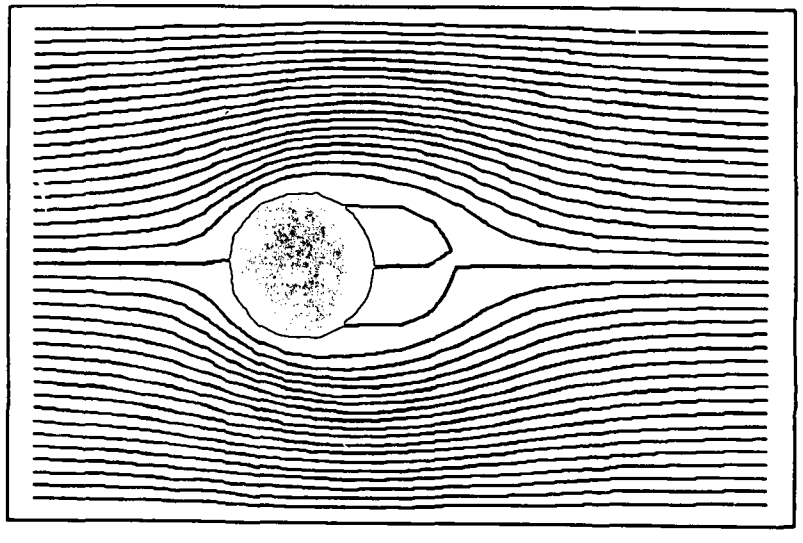

t = 110.

Fig. 6b. Stream lines around a circular cylinder (Re = 40).

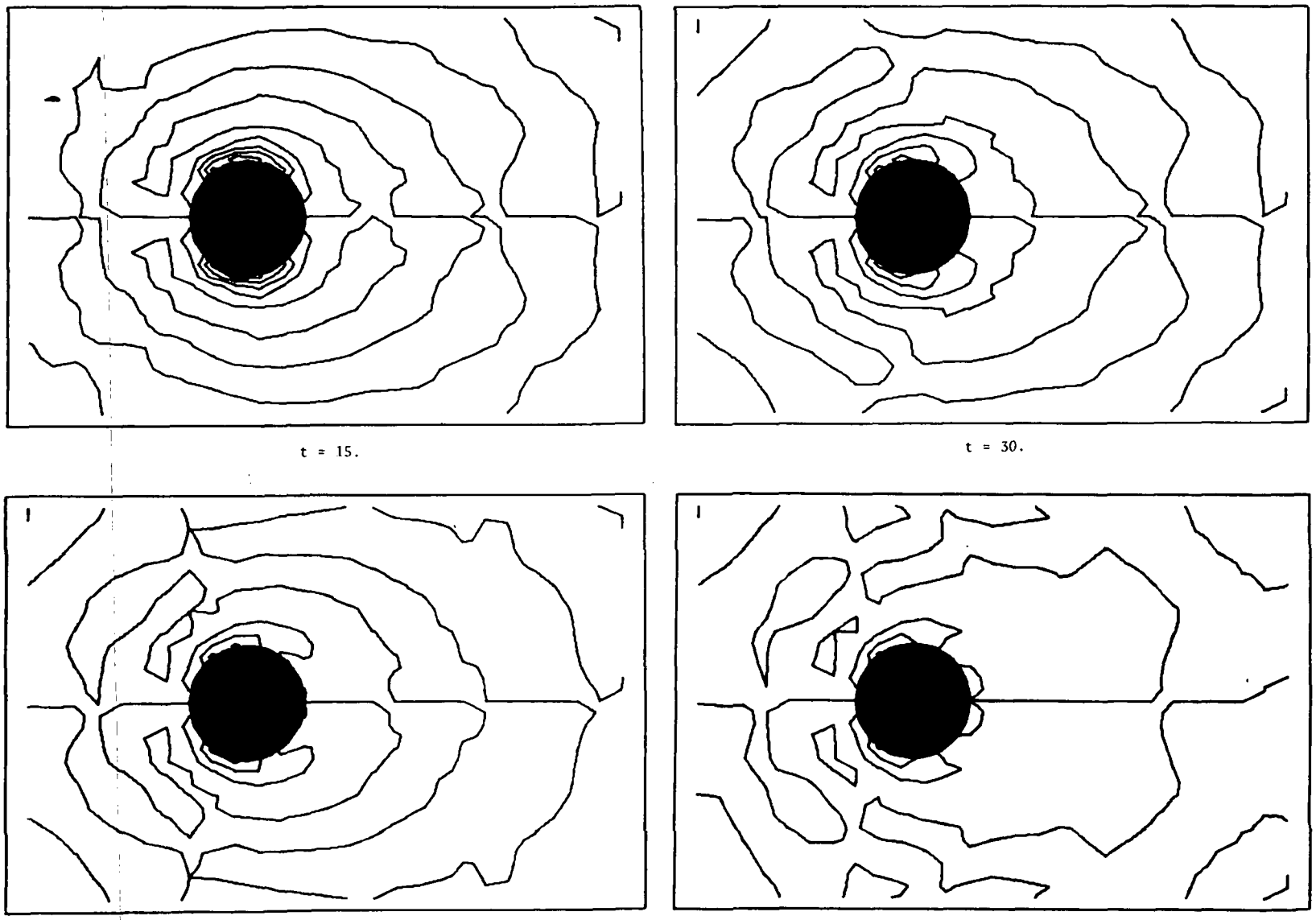

Fig. 7. Vorticity distribution around a circular cylinder (Re = 40).

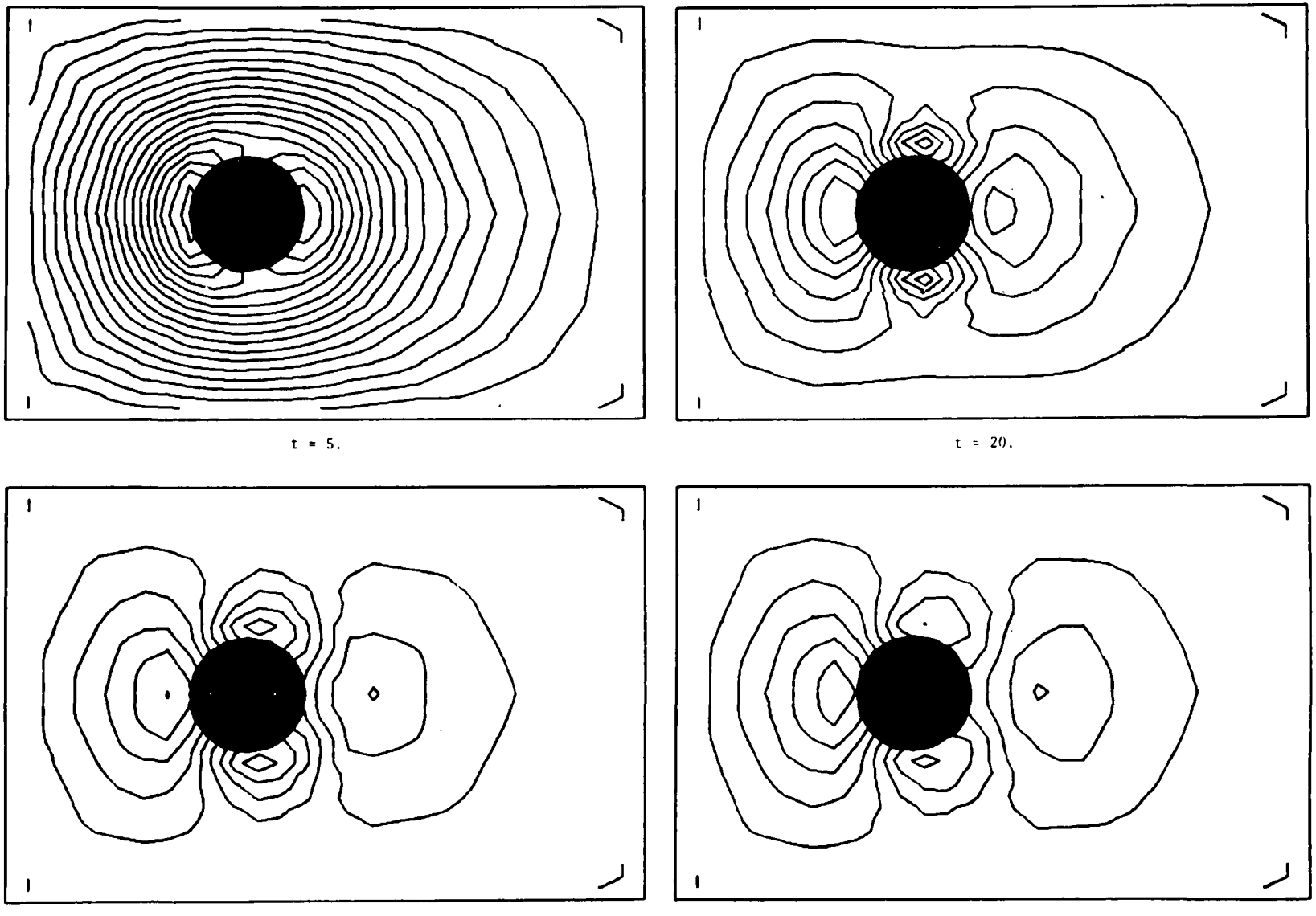

Fig. 8. Pressure distribution around a circular cylinder (Re = 40).

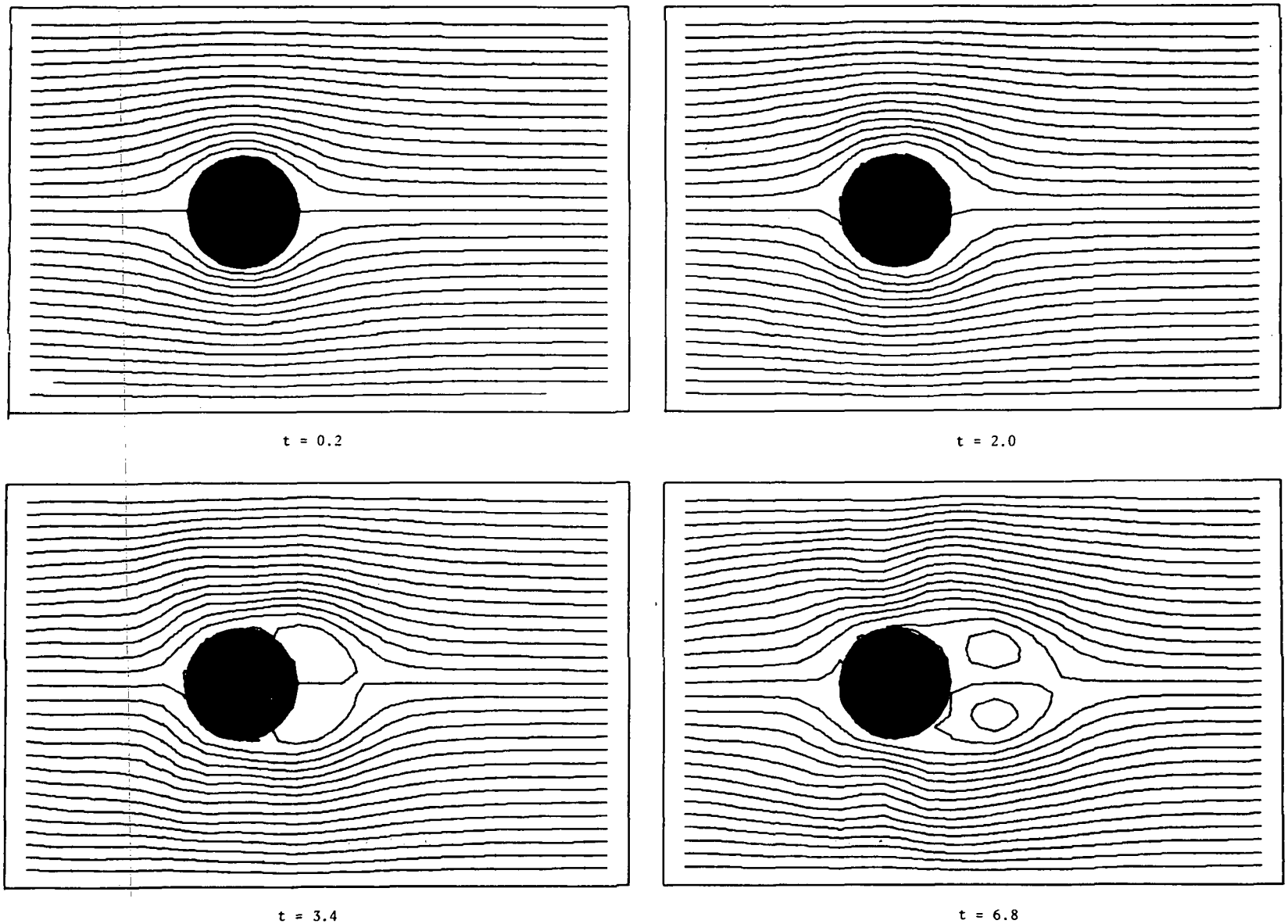

Fig. 9. Stream lines around a circular cylinder (Re = 10^3).

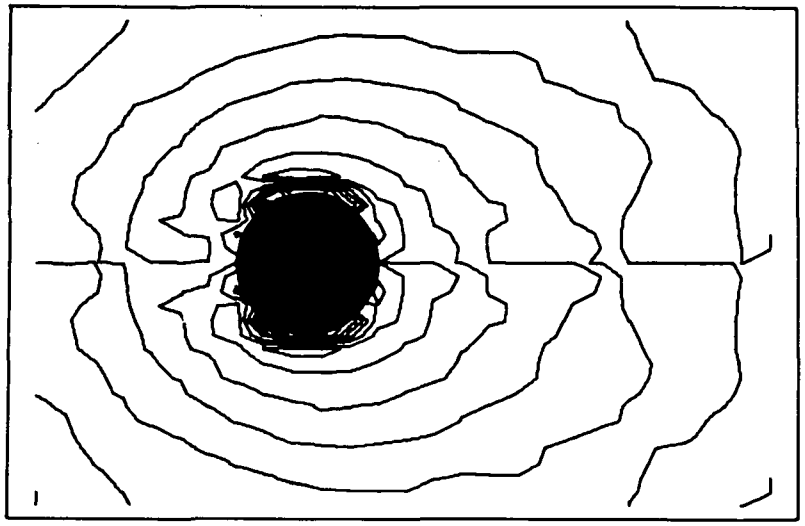

t = 0.2

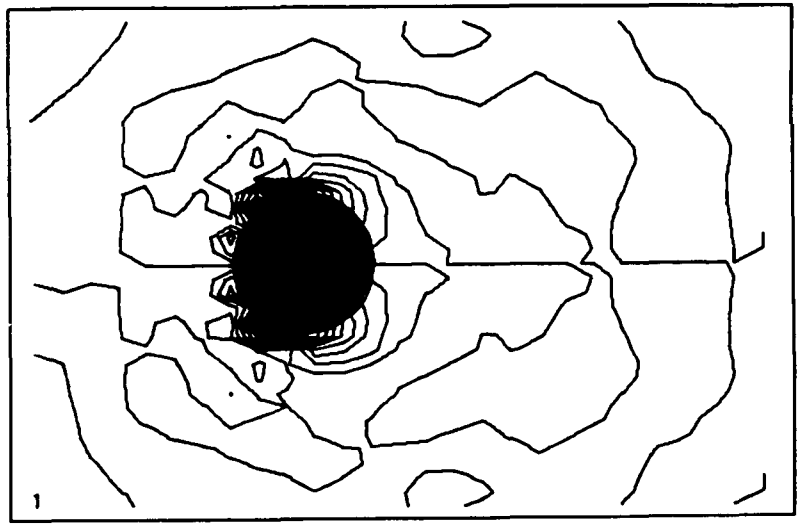

t = 2.0

t = 3.4

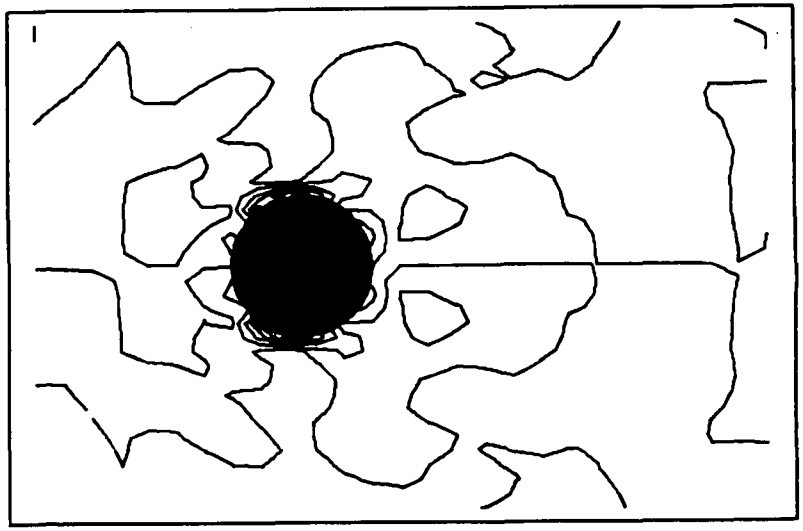

t = 6.8

Fig. 10a. Vorticity distribution around a circular cylinder (Re = 10^3).

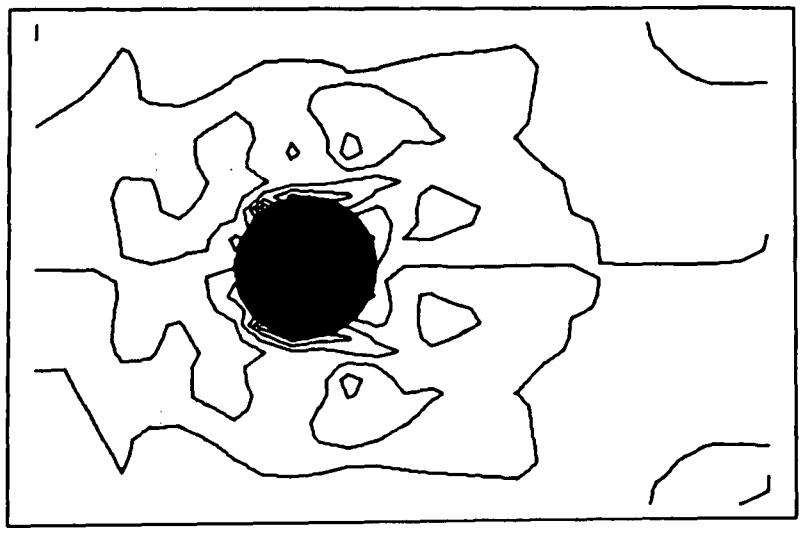

t = 8.0

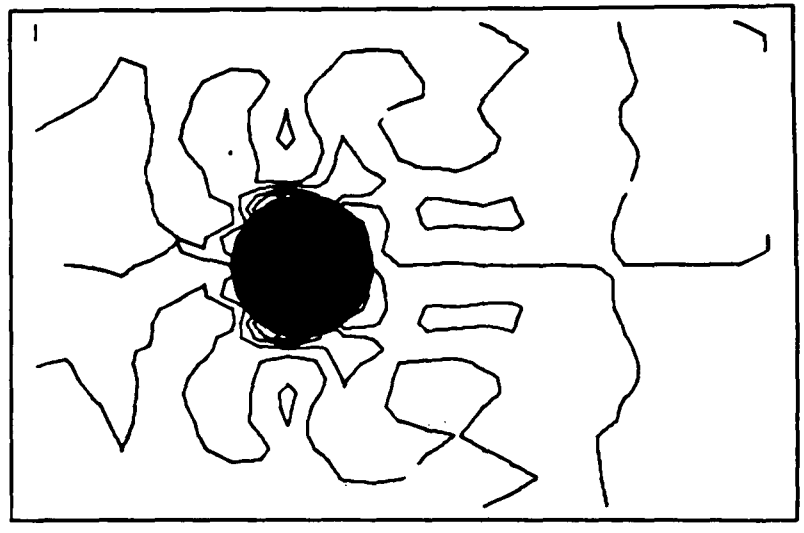

t = 9.5

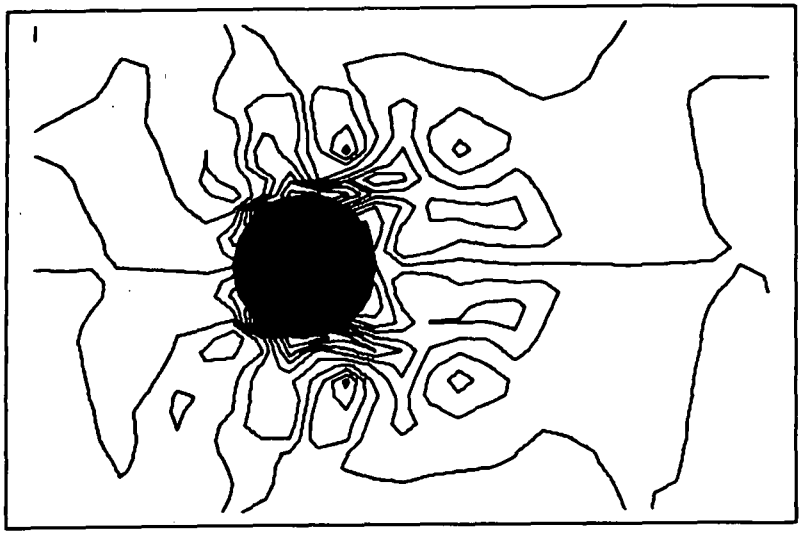

t = 10.5

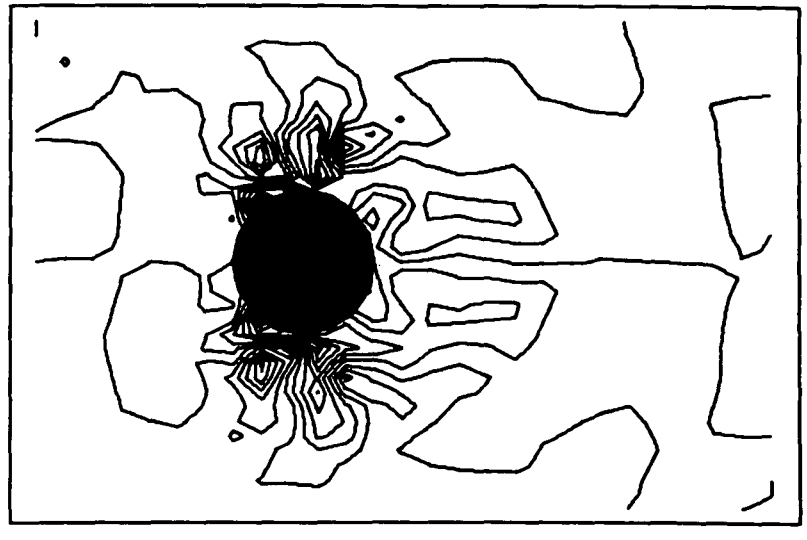

t = 11.5

Fig. 10b. Vorticity distribution around a circular cylinder (Re = 10^3).

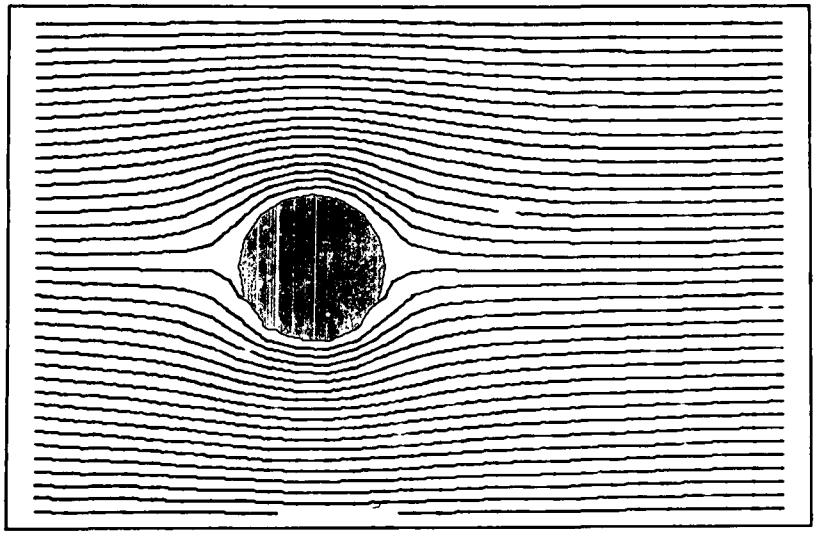

t = 0.04

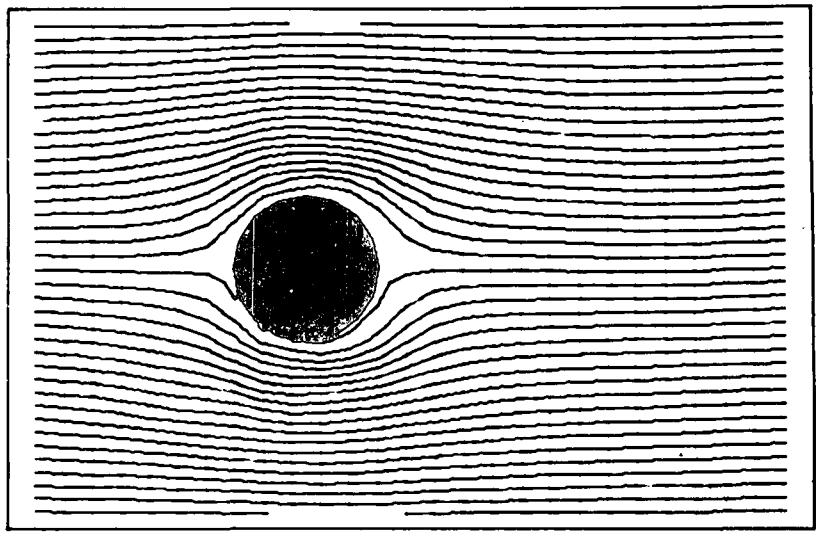

t = 0.14

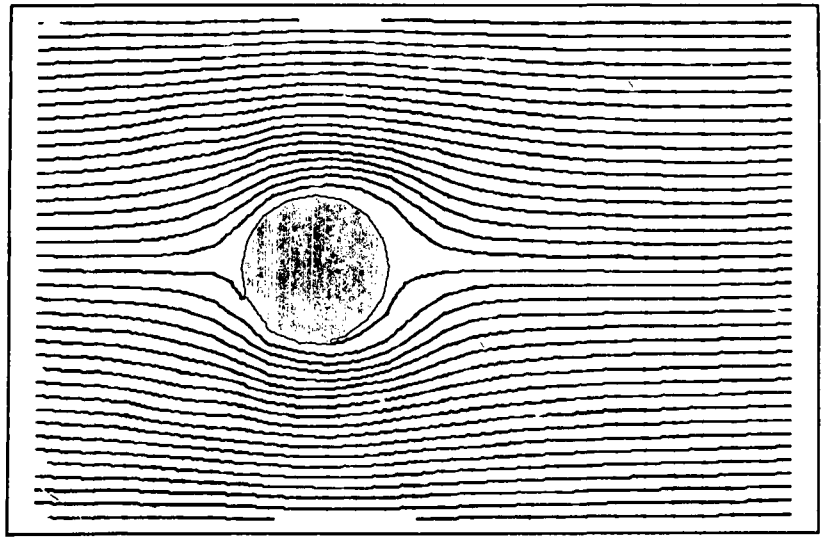

t = 0.17

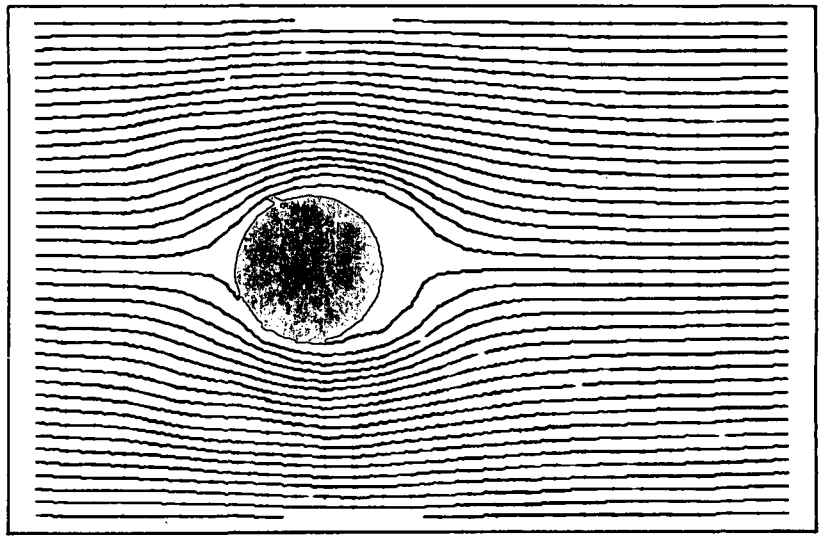

t = 0.24

Fig. 11a. Stream lines around a circular cylinder (Re = 10^4).

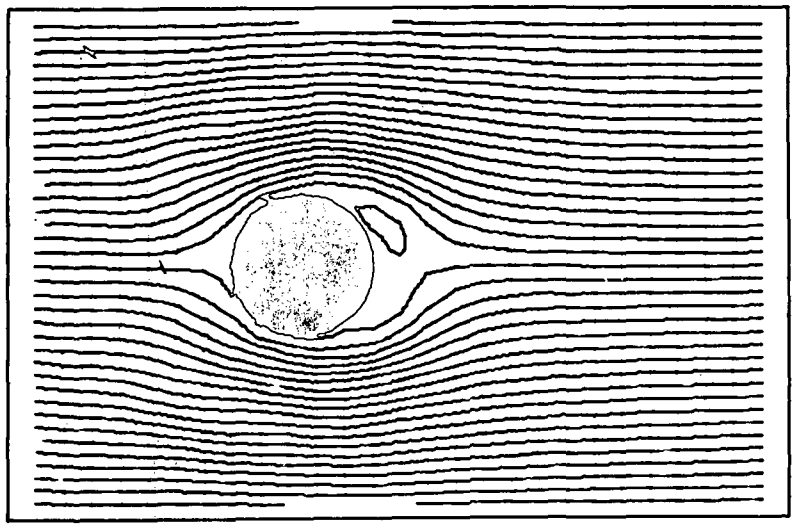

t = 0.27

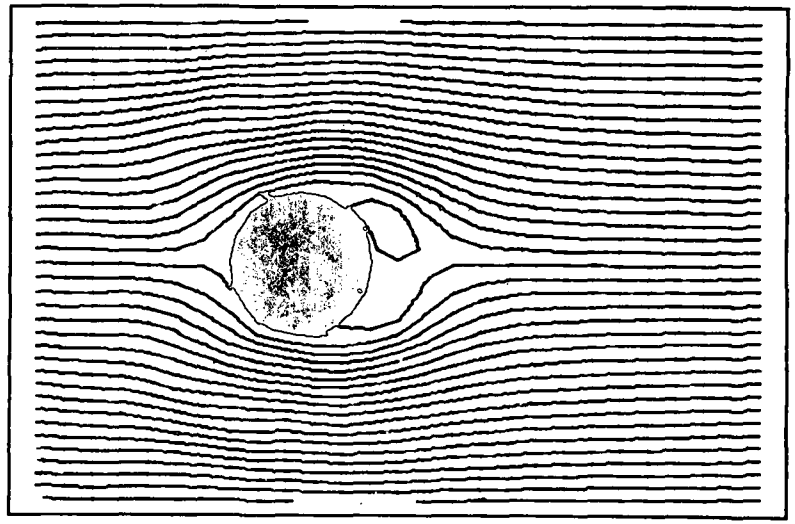

t = 0.30

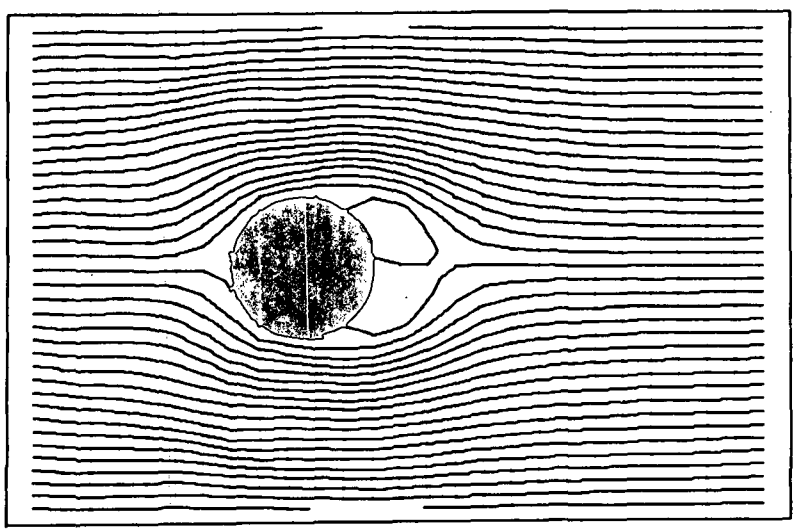

t = 0.34

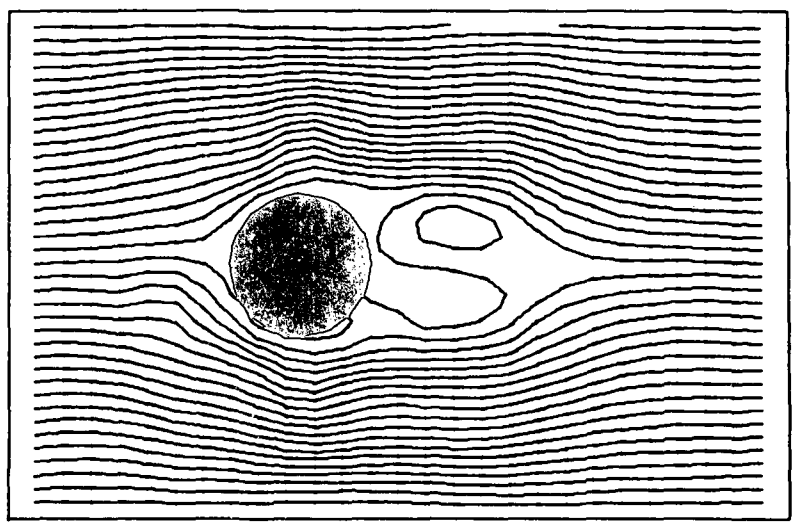

t = 0.80

Fig. 11b. Stream lines around a circular cylinder (Re = 10^4).

t = 0.04

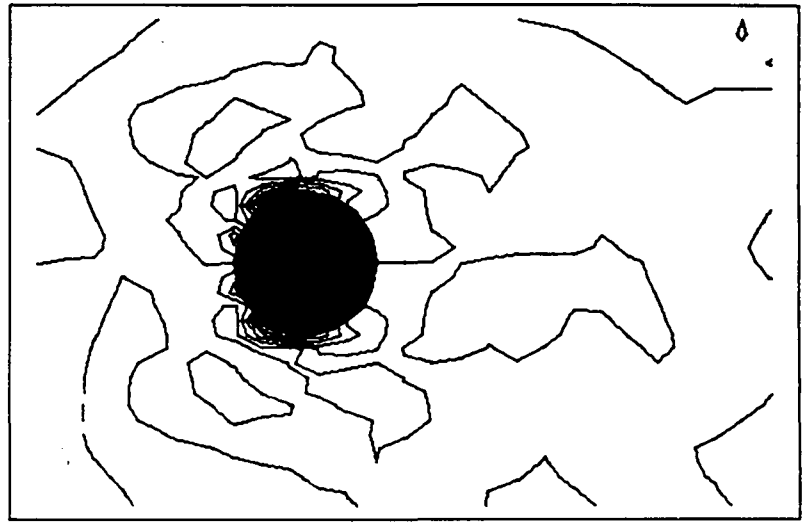

t = 0.17

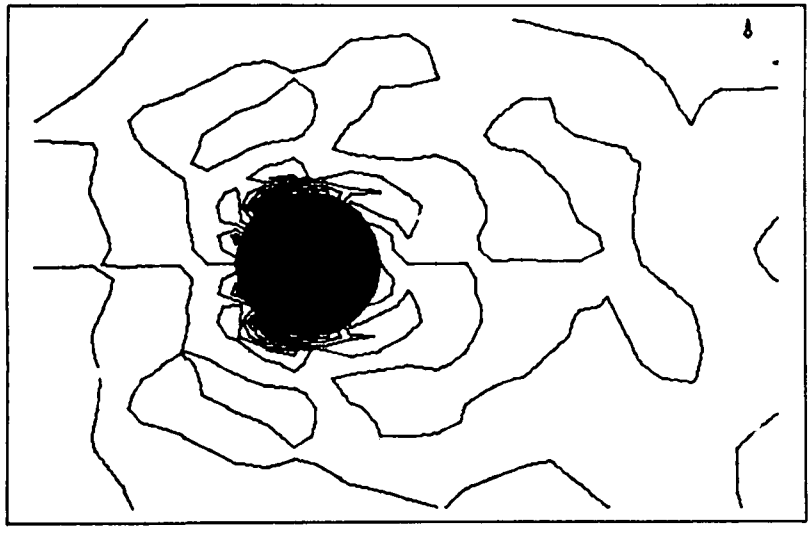

t = 0.27

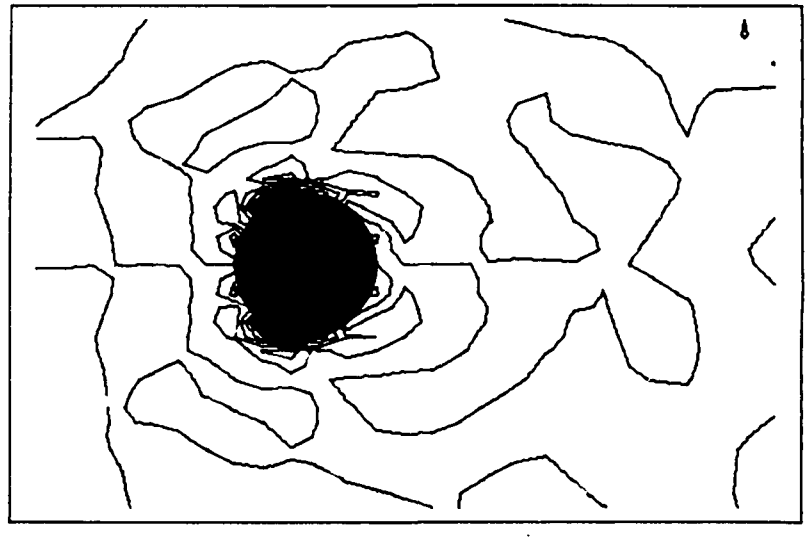

t = 0.30

Fig. 12a. Vorticity distribution around a circular cylinder (Re = 10^4).

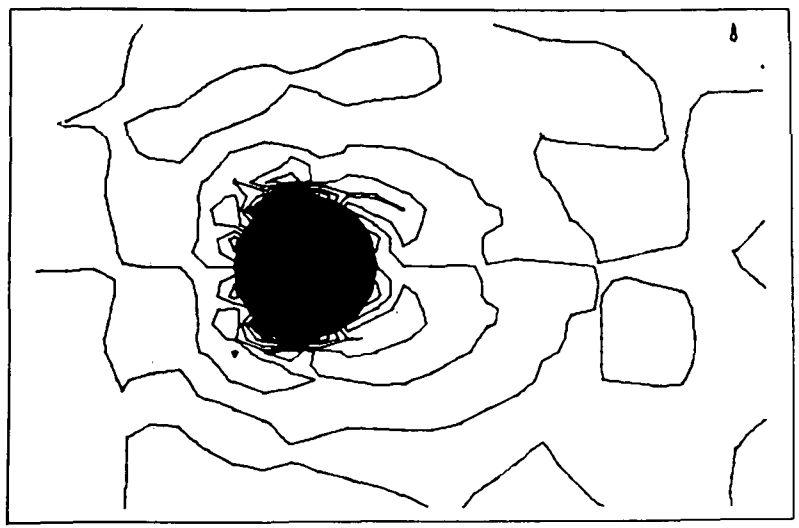

t = 0.34

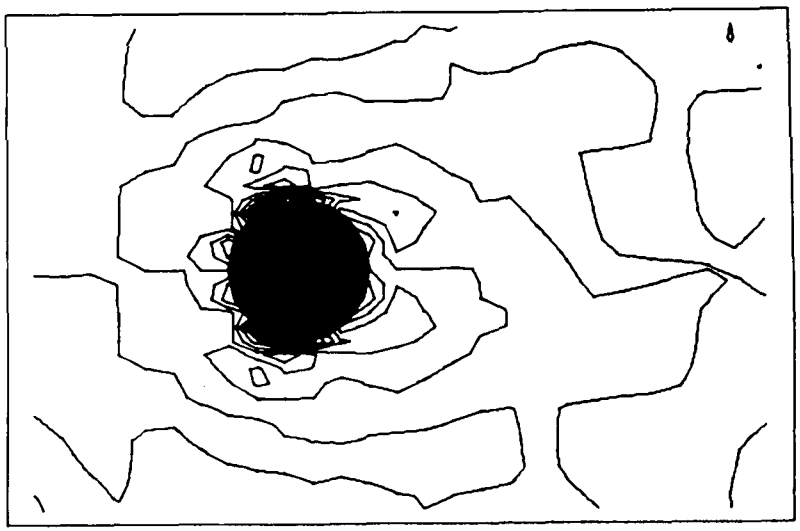

t = 0.40

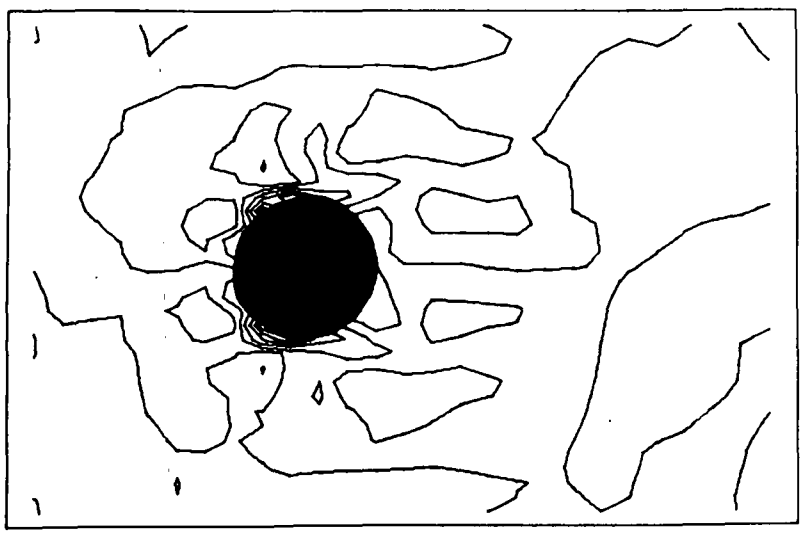

t = 0.80

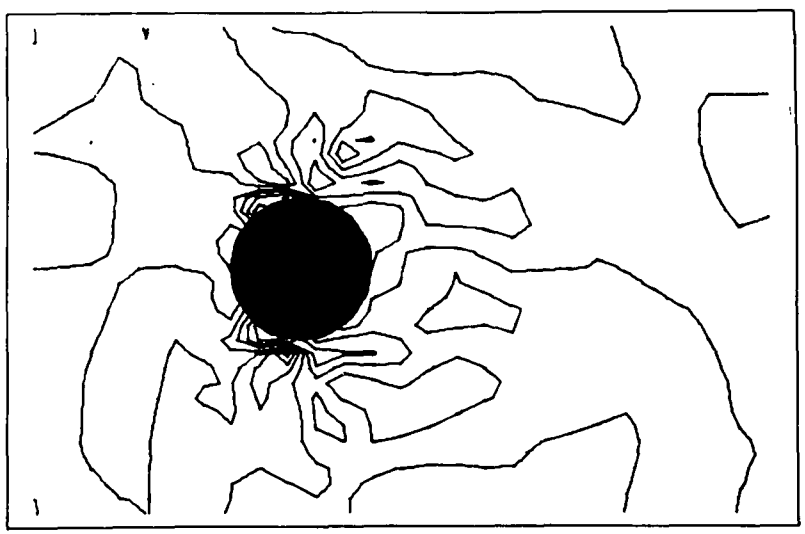

t = 1.10

Fig. 12b. Vorticity distribution around a circular cylinder (Re = 10^4).

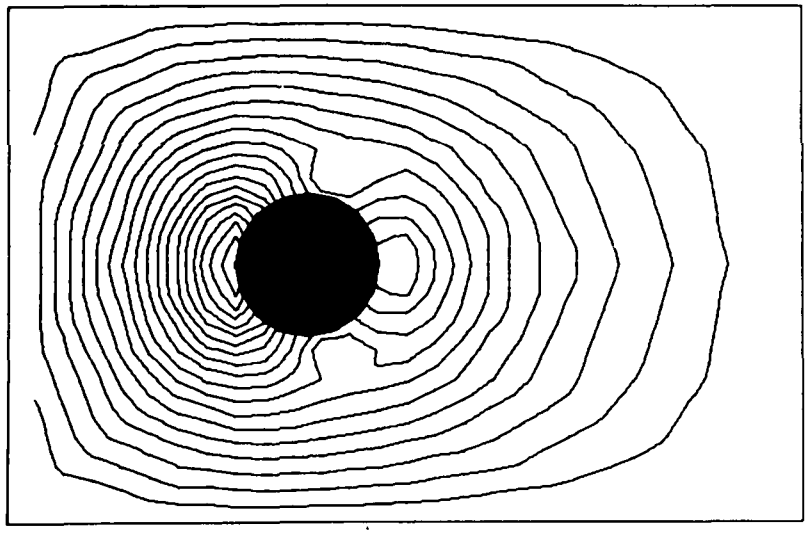

t = 0.1

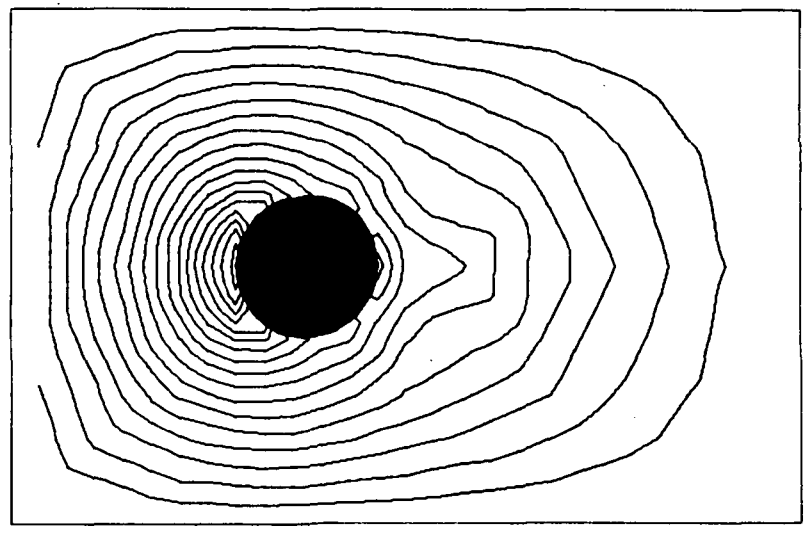

t = 0.3

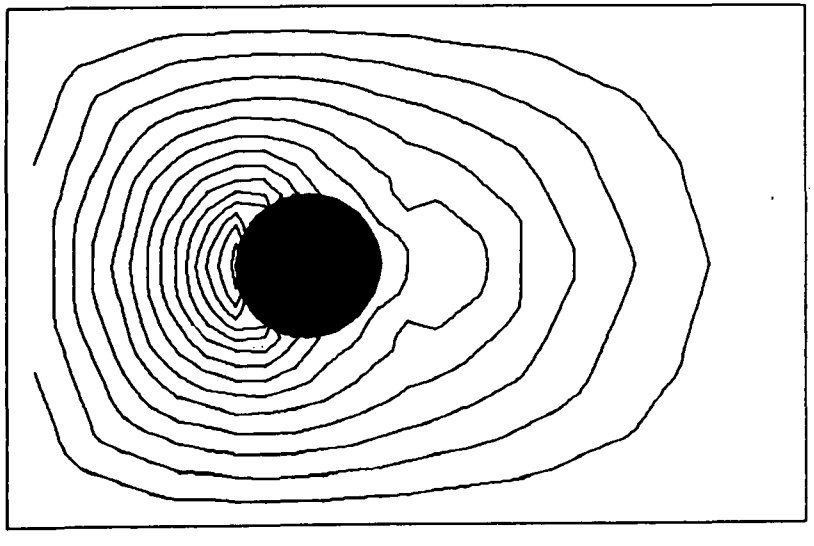

t = 0.4

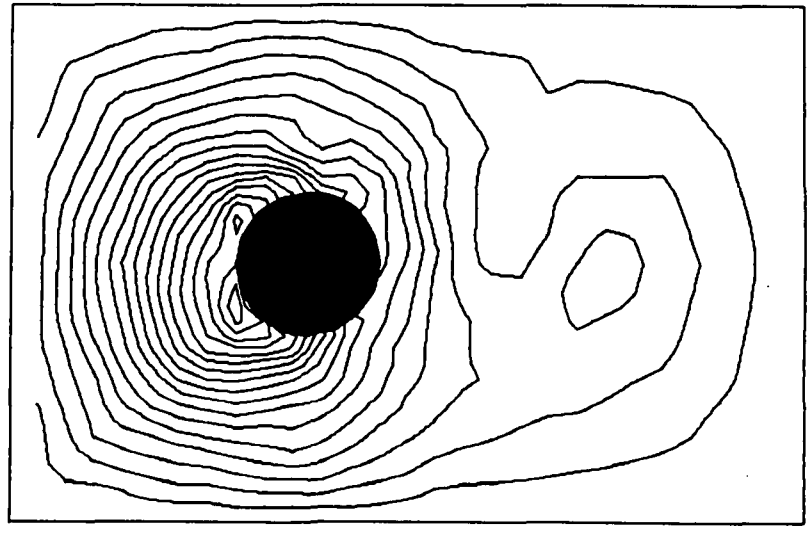

t = 1.1

Fig. 13. Pressure distribution around a circular cylinder (Re = 10^4).

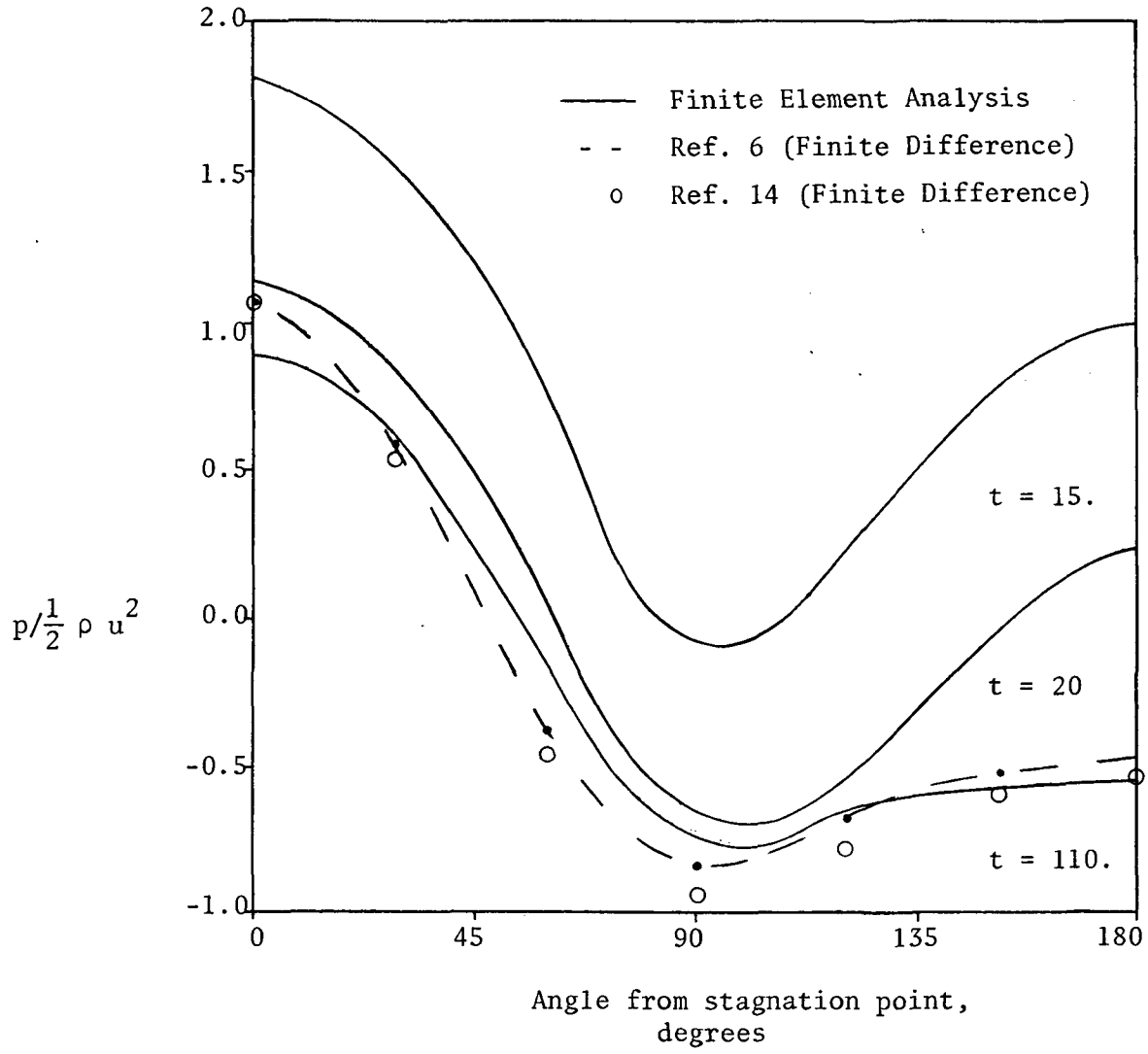

Fig. 14. Development of the surface pressure distribution on a circular cylinder (Re = 40).

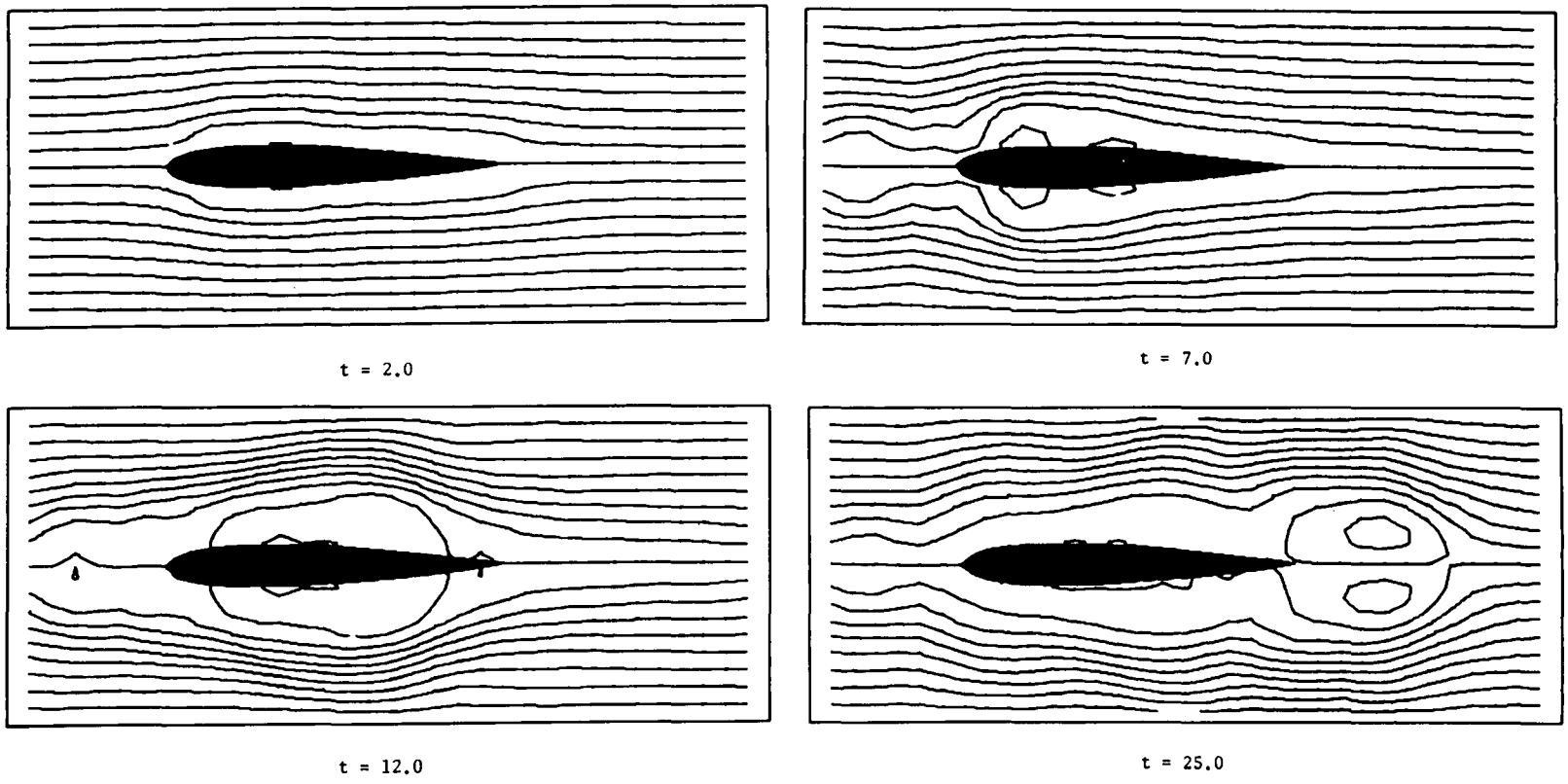

Fig. 15. Streamlines around a NACA 0012 airfoil at a 0° angle of attack (Re = 10^3)

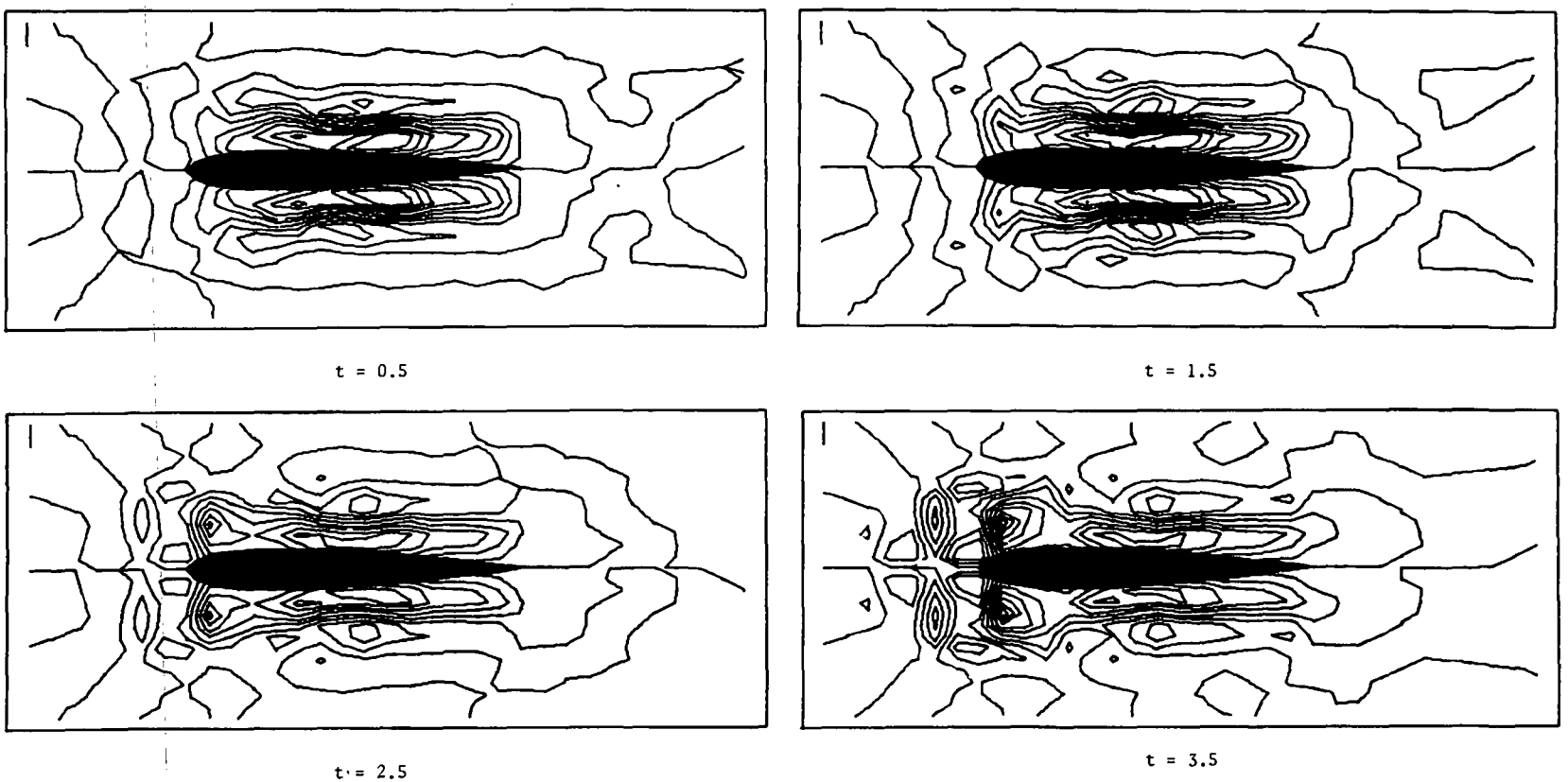

Fig. 16a. Vorticity distribution about a NACA 0012 airfoil at a 0° angle of attack (Re = 10^3)

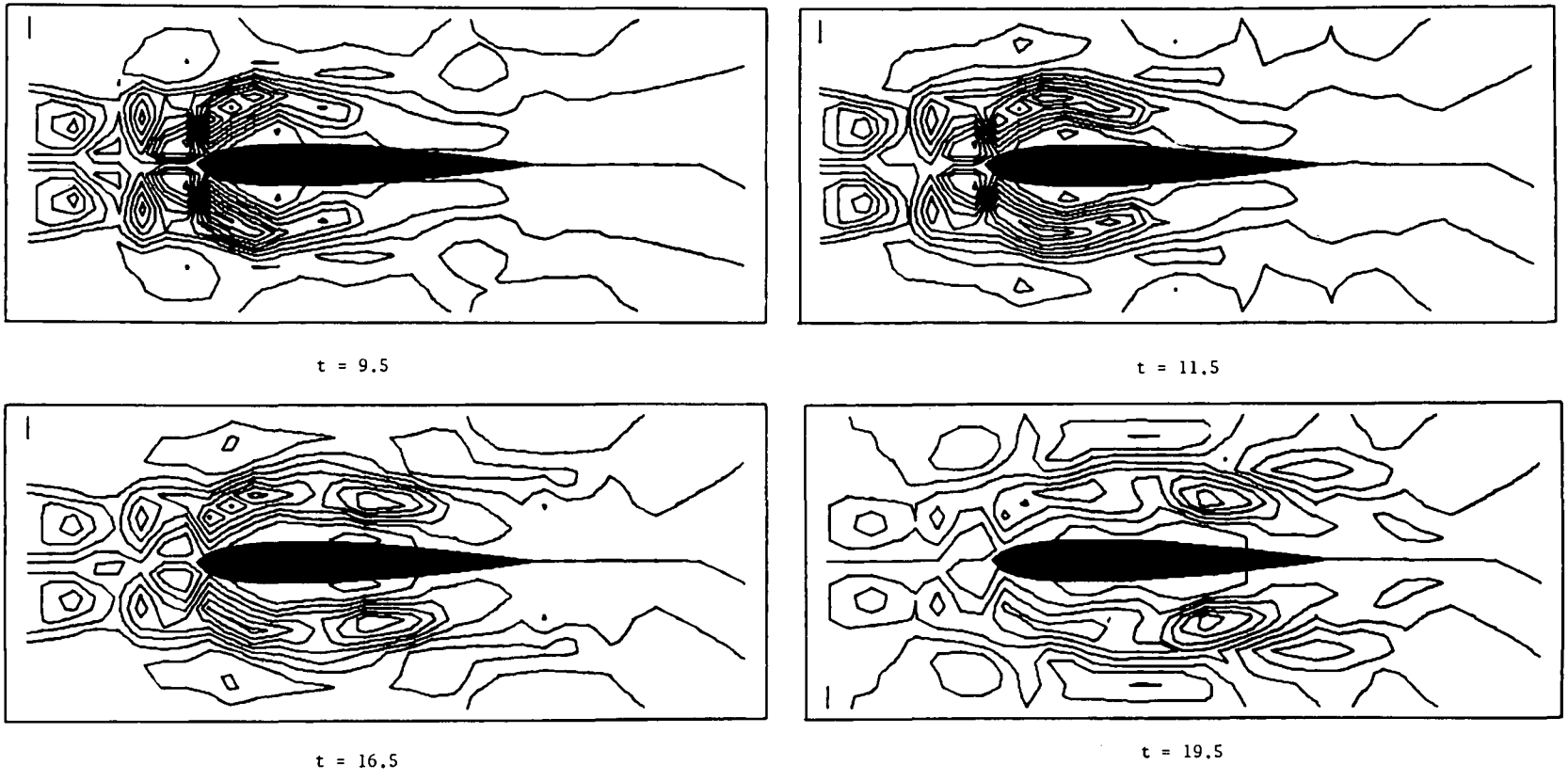

Fig. 16b. Vorticity distribution about a NACA 0012 airfoil at a 0° angle of attack (Re = 10^3)

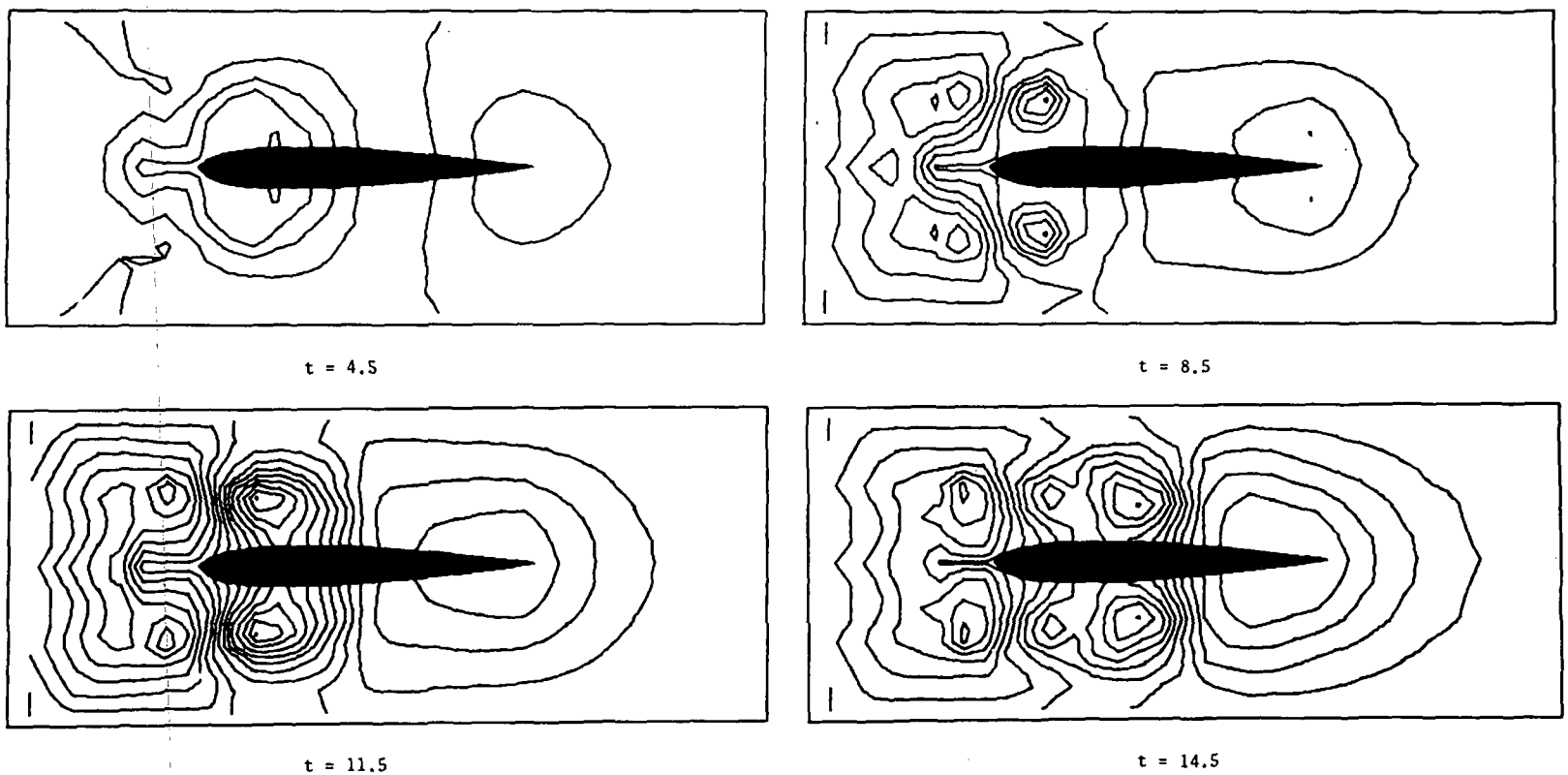

Fig. 17. Pressure distribution around a NACA 0012 airfoil at a 0° angle of attack (Re = 10^3)

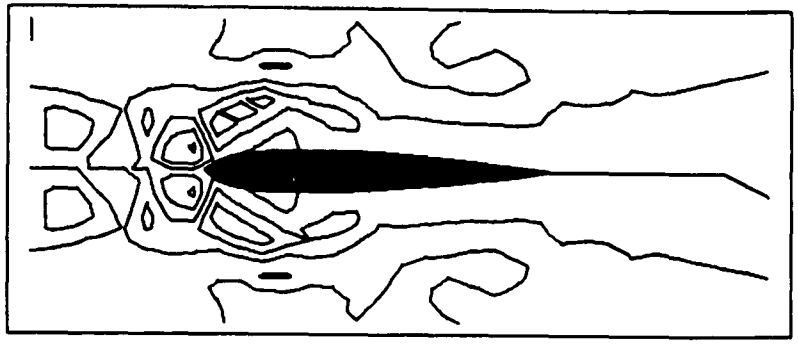

t = 0.090

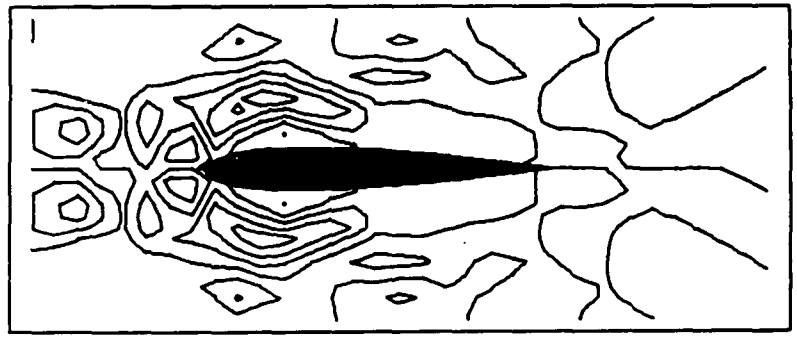

t = 0.130

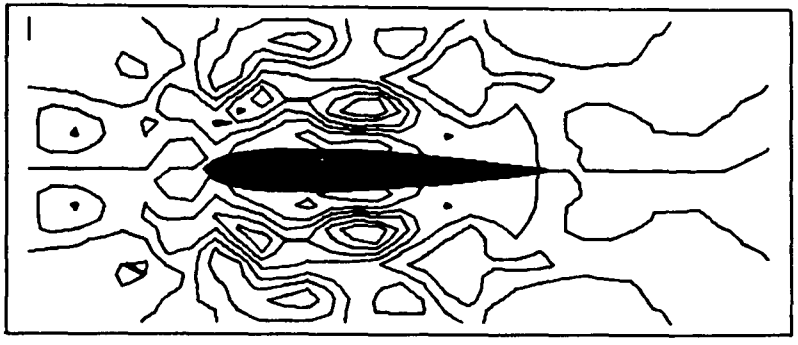

t = 0.190

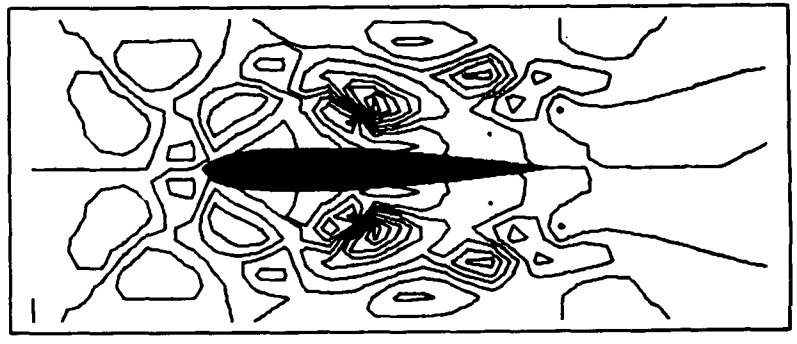

t = 0.215

Fig. 18. Vorticity distribution around a NACA 0012 airfoil at a 0° angle of attack (Re = 10^5).

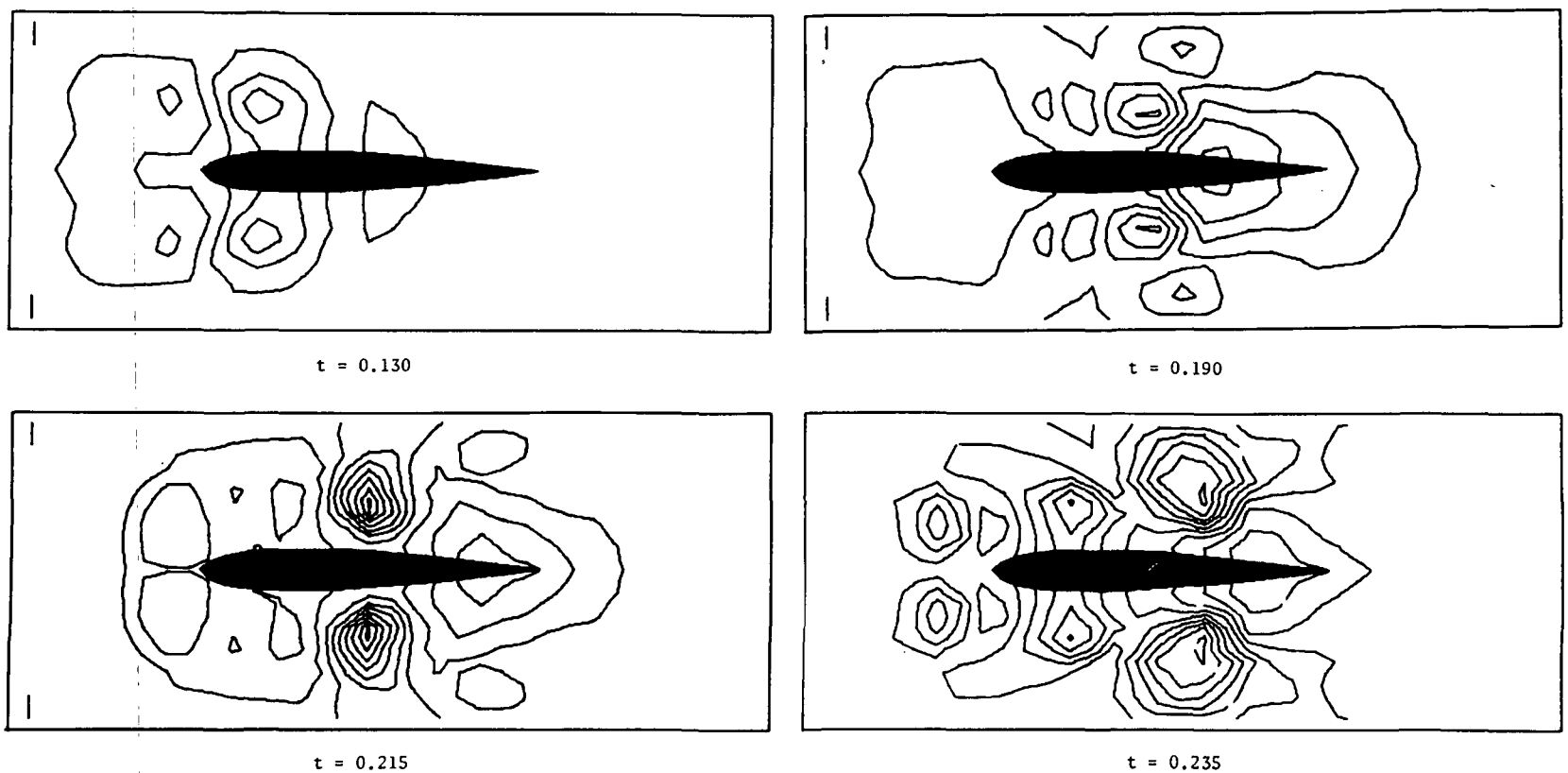

Fig. 19. Pressure distribution around a NACA 0012 airfoil at a 0° angle of attack (Re = 10^5).

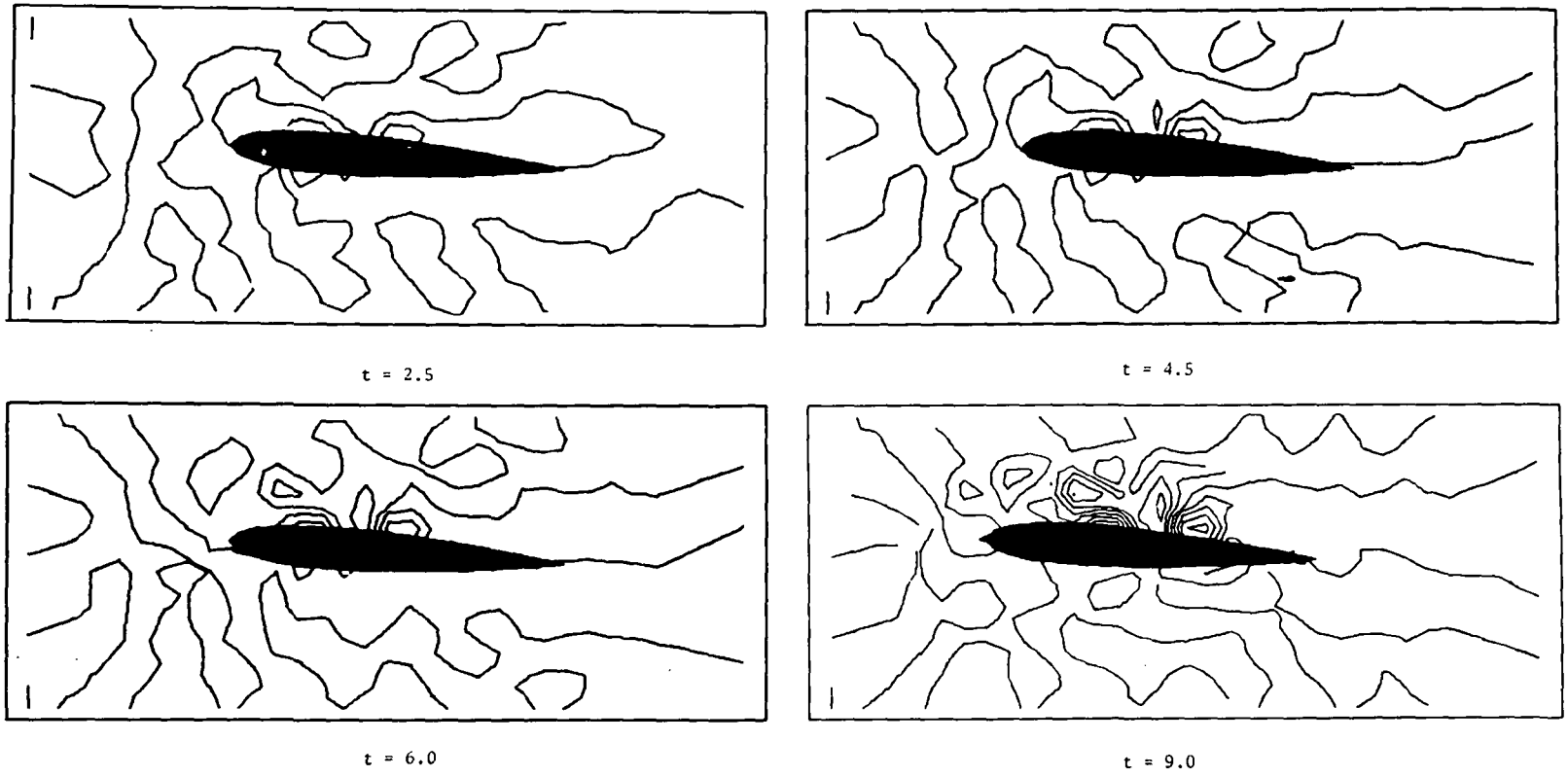

Fig. 20. Vorticity distribution about a NACA 0012 airfoil at a 4° angle of attack (Re = 10^3)

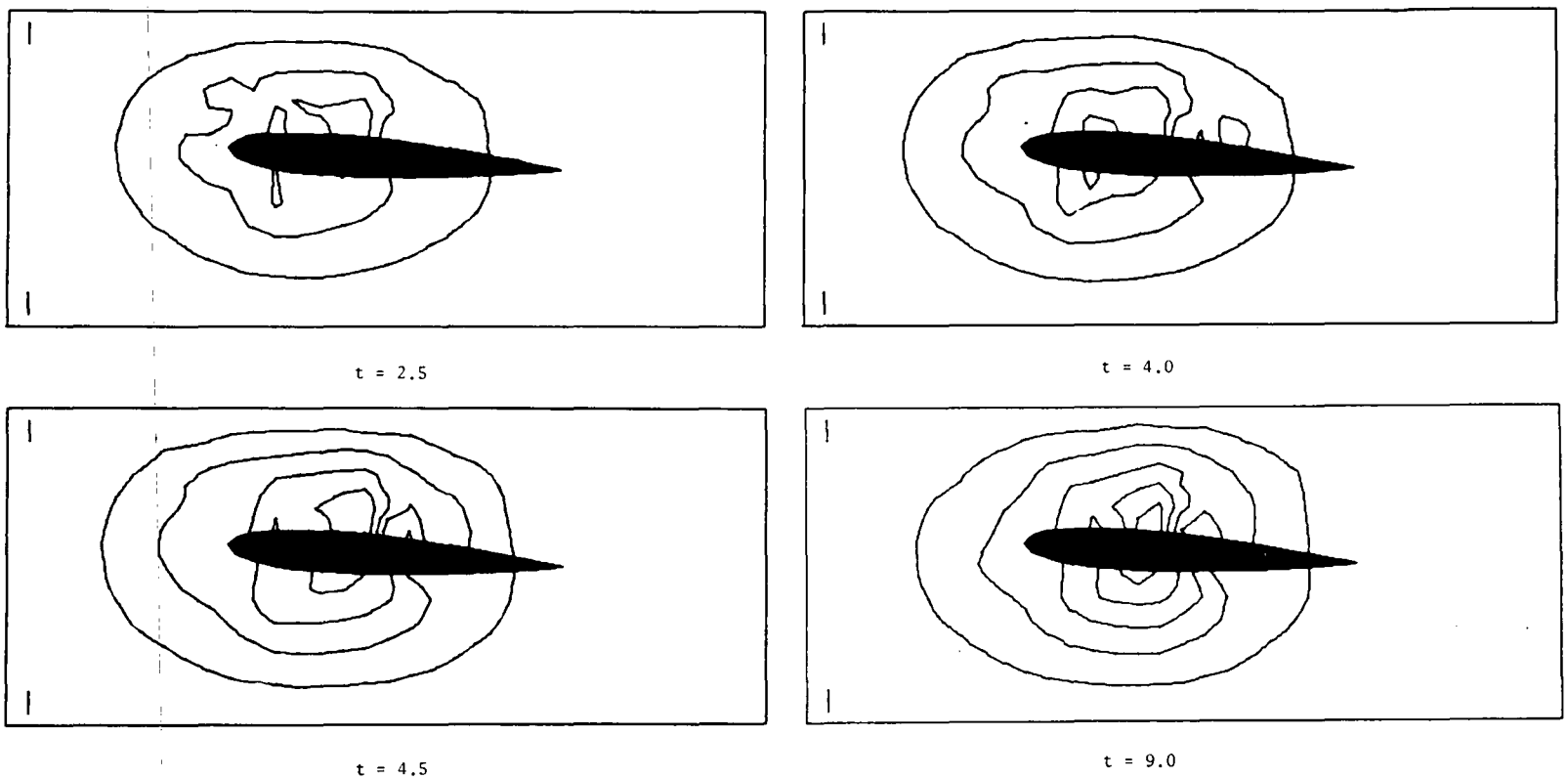

Fig. 21. Pressure distribution around a NACA 0012 airfoil at a 4° angle of attack (Re = 10^3)

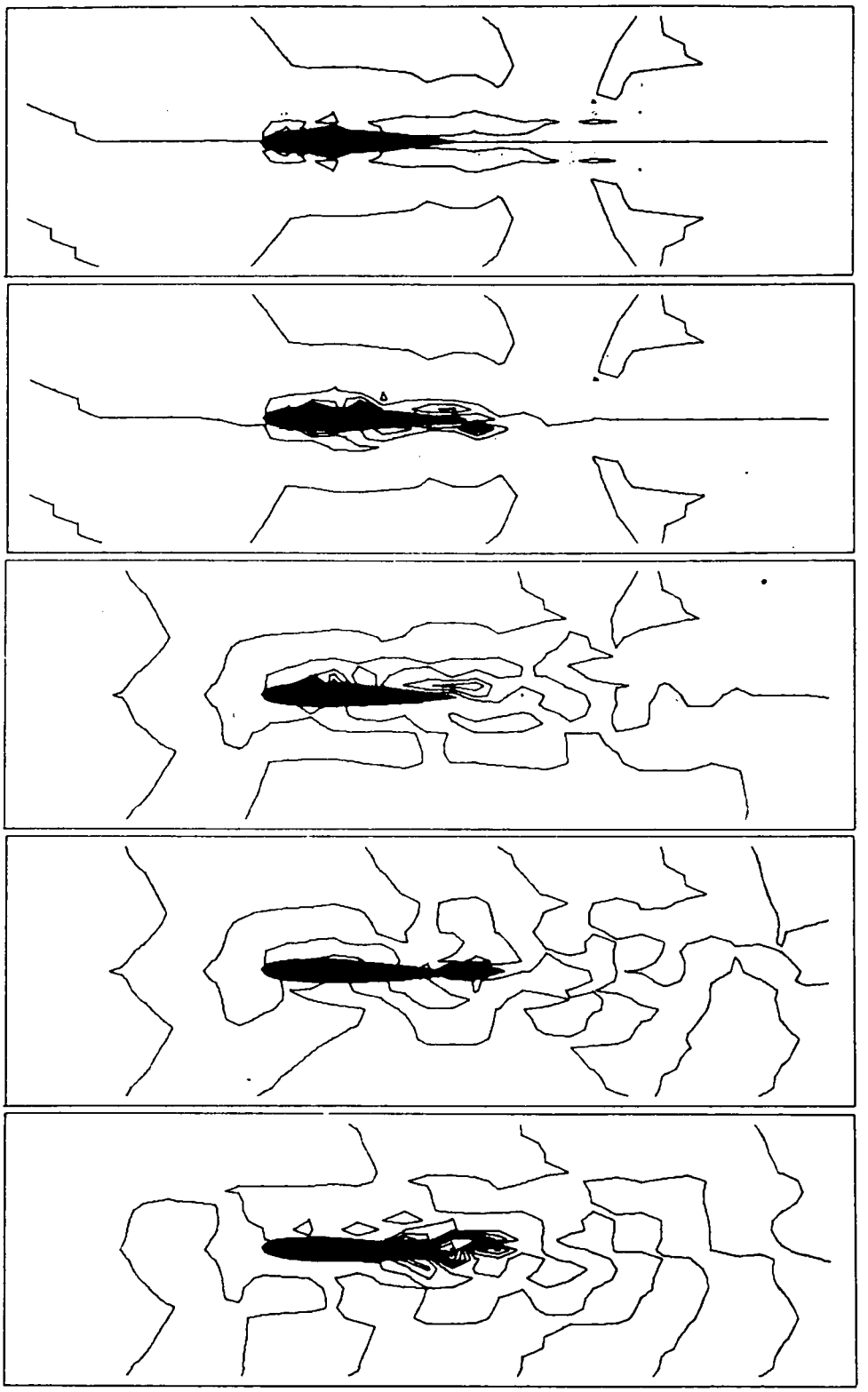

Fig. 22. Vorticity distribution about an oscillating NACA 0012 airfoil (Re = 10^3), (t = 0.01 - 0.05), ($\alpha = 0° - 2.5°$).

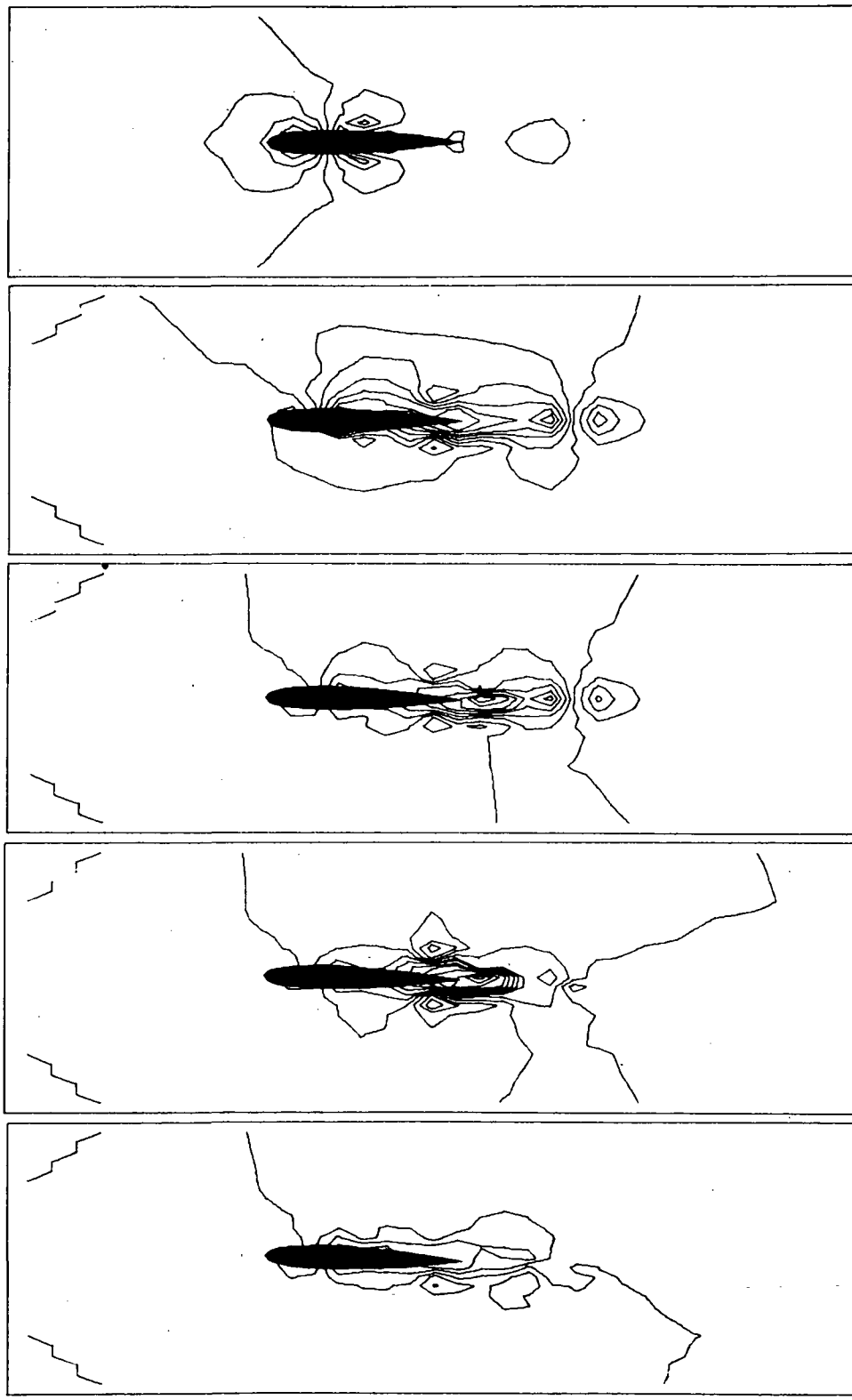

Fig. 23. Pressure distribution about an oscillating NACA 0012 airfoil (Re = 10^3), (t = 0.01 - 0.05), (α = 0° - 2.5°).

NATIONAL AERONAUTICS AND SPACE ADMINISTRATION
WASHINGTON, D.C. 20546

OFFICIAL BUSINESS
PENALTY FOR PRIVATE USE $300

SPECIAL FOURTH-CLASS RATE BOOK

POSTAGE AND FEES PAID
NATIONAL AERONAUTICS AND SPACE ADMINISTRATION
451

U.S.MAIL

POSTMASTER : If Undeliverable (Section 158 Postal Manual) Do Not Return

"The aeronautical and space activities of the United States shall be conducted so as to contribute . . . to the expansion of human knowledge of phenomena in the atmosphere and space. The Administration shall provide for the widest practicable and appropriate dissemination of information concerning its activities and the results thereof."

—NATIONAL AERONAUTICS AND SPACE ACT OF 1958

NASA SCIENTIFIC AND TECHNICAL PUBLICATIONS

TECHNICAL REPORTS: Scientific and technical information considered important, complete, and a lasting contribution to existing knowledge.

TECHNICAL NOTES: Information less broad in scope but nevertheless of importance as a contribution to existing knowledge.

TECHNICAL MEMORANDUMS: Information receiving limited distribution because of preliminary data, security classification, or other reasons. Also includes conference proceedings with either limited or unlimited distribution.

CONTRACTOR REPORTS: Scientific and technical information generated under a NASA contract or grant and considered an important contribution to existing knowledge.

TECHNICAL TRANSLATIONS: Information published in a foreign language considered to merit NASA distribution in English.

SPECIAL PUBLICATIONS: Information derived from or of value to NASA activities. Publications include final reports of major projects, monographs, data compilations, handbooks, sourcebooks, and special bibliographies.

TECHNOLOGY UTILIZATION PUBLICATIONS: Information on technology used by NASA that may be of particular interest in commercial and other non-aerospace applications. Publications include Tech Briefs, Technology Utilization Reports and Technology Surveys.

Details on the availability of these publications may be obtained from:

SCIENTIFIC AND TECHNICAL INFORMATION OFFICE

NATIONAL AERONAUTICS AND SPACE ADMINISTRATION

Washington, D.C. 20546